Breach detection using diffuse reflectance spectroscopy during spinal screw placement

Swamy, A.

DOI
10.4233/uuid:8c5055e3-477e-438c-b722-f55d2c3e41fc

Publication date
2021

Document Version
Final published version

Citation (APA)
Swamy, A. (2021). *Breach detection using diffuse reflectance spectroscopy during spinal screw placement*. [Dissertation (TU Delft), Delft University of Technology]. https://doi.org/10.4233/uuid:8c5055e3-477e-438c-b722-f55d2c3e41fc

Important note
To cite this publication, please use the final published version (if applicable).
Please check the document version above.

Propositions

belonging to the thesis
Breach detection using
diffuse reflectance spectroscopy
during spinal screw placement
by

Akash Swamy

1. Complications associated with pedicle screw misplacement during spine surgery are life threatening and should be corrected in more cases. *(Chapter 1)*

2. Fat fraction drops within 1 mm from the cortical bone boundary across a healthy spinal column. *This thesis*

3. A transition zone exists between cancellous and cortical bone, which can be identified using diffuse reflectance spectroscopy for breach detection. *This thesis*

4. A forward-looking diffuse reflectance spectroscopy probe inserted into vertebrae measures a drop in fat fraction just before coming in contact with the cortical bone boundary. *This thesis*

5. Positive results bias in clinical literature is unavoidable.

6. Successful spinal screw placement procedures require good craftsmanship.

7. Spinal screw fixation is similar to fixating a screw on a wall.

8. Without a valid clinical need, there is no problem to be solved.

9. For successful technology, reality must take precedence over public relations, for nature cannot be fooled. *(Richard P. Feynman)*

10. Pursuing an academic career in industry requires a lot of flexibility as research objectives change faster than Dutch weather forecasts. (*Saskia Camps)*

These propositions are regarded as opposable and defendable,
and have been approved as such by the promoters
Prof. dr. Benno Hendriks and Prof. dr. Jenny Dankelman

Breach detection using diffuse reflectance spectroscopy during spinal screw placement

Dissertation

for the purpose of obtaining the degree of doctor
at Delft University of Technology
by the authority of the Rector Magnificus, prof.dr.ir. T.H.J.J. van der Hagen,
chair of the Board for Doctorates
to be defended publicly on
27th, January, 2021 at 3 o' clock

by

Akash SWAMY

Master of Science in Biomedical Engineering,
Mechanical, Maritime and Materials Engineering,
Delft University of Technology, Delft, The Netherlands
born in Bangalore, India.

This dissertation has been approved by the promotors.

promotors: prof. dr. B.H.W. Hendriks and prof. dr. J. Dankelman

Composition of the doctoral committee:

Rector Magnificus,	chairperson
Prof. dr. B.H.W. Hendriks,	Technische Universiteit Delft (3mE), promoter
Prof. dr. J. Dankelman,	Technische Universiteit Delft (3mE), promoter
Independent members:	
Prof. dr. H.J. Sterenborg,	Netherlands Cancer Institute
Prof. dr. T.J.M. Ruers,	Netherlands Cancer Institute
Prof. dr. S. Stallinga,	Technische Universiteit Delft (TNW)
Prof. dr. ir. R. Dekker,	Technische Universiteit Delft (EWI)
Other members:	
Dr. A. Elmi-Terander,	Karolinska Institutet, Sweden

Keywords: diffuse reflectance spectroscopy, spinal screw placement, breach detection.

Printed by: Gildeprint.

Front & Back: Designed in collaboration with Nishant Dsouza. A figure adapted with permission from Neurosurgery journal.

SUMMARY

The intraoperative guidance and placement of spinal screws is a complex procedure. High technical expertise is required from the surgeons in order to achieve adequate fixation and ensure patient safety by preventing vascular and neurological injuries. The conventional screw placement techniques face several challenges. Surgeons heavily rely on experience-based judgement, tactile feedback and X-ray guidance. The consequences of which are reflected in clinical literature via high risks associated with complications, screw placement accuracy variability and radiation exposure. Moreover, cost savings in terms of improved patient outcomes such as patient recovery times and fewer revision surgeries are major incentives towards development and clinical adoption of better intraoperative guidance technologies.

The aim of this PhD work was to investigate the applicability of spectral sensing based technique namely Diffuse Reflectance Spectroscopy (DRS) for intraoperative instrument guidance and breach detection during pedicle screw placement procedures.

In order to investigate the application of DRS in pedicle screw placement procedures, the spectral and physiological differences between cancellous and cortical vertebral bone were studied (detailed in **Chapter 2** of this thesis). The tissue optical properties required for breach detection were determined based on experiments on cadaveric tissues. It was investigated whether optical properties extracted from the spectra namely fat, water, blood content along with photon scattering, can be used to distinguish between cancellous and cortical vertebral bone types. The DR spectra showed higher amount of fat, blood and photon scattering in cancellous bone than in cortical bone. Monte-Carlo (MC) simulations were then performed and a three-layered model was developed to study the fat content trend as the probe approached a cortical bone boundary during a simulated insertion. The simulation findings were used to validate a breach of an optical screw probe in a cadaveric setting. The MC simulations and experimental insertion of the optical screw probe showed a similar drop in fat content more than 1 mm before the optical probe came in contact with the cortical bone. It was shown that DRS at the instrument tip has the potential to detect breaches using fat content as an important discriminatory parameter.

Currently, MRI is one of the most accurate techniques used to measure fat concentration in tissues. Fat fraction being an important breach detection parameter found via the DRS technique was thus compared to a standardized Magnetic Resonance (MR) technique in **Chapter 3**. The accuracy of fat content measured invasively in cadaveric spines using DRS was compared to Proton density fat fraction (PDFF) derived via the MRI technique on the same specimens. Several insertions using a custom-made screw with integrated optical fibers were performed under cone beam computer tomography (CBCT). DR spectra were recorded at several positions along the probe trajectory during turn by turn insertions. DRS and MRI derived fat fractions were compared by spatially correlating the probe position within vertebral bodies on CBCT images with respect to

MRI images. It was found that DRS and MRI based fat fraction are highly correlated ($R^2 = 0.905$). Indicating that DRS sensing integrated into a surgical instrument can accurately measure fat content within vertebrae. However, PDFF measured non-invasively in clinical literature was found to vary based on age, gender, vertebral level and diseases.

In order to further understand the true variation of fat fraction across the spinal column, a more detailed analysis of the distribution of PDFF across intravertebral zones such as cancellous, pre-cortical zones and cortical bone boundary was defined and performed in **Chapter 4**. PDFF distributions of cortical bone was found to be different from that of cancellous bone across the spinal column. Furthermore, aggregate distributions of the intravertebral zones of the six cadavers showed a median drop in PDFF from cancellous bone to cortical bone. However, the variability in PDFF distributions within the intravertebral zones cannot be ignored.

In **Chapter 5**, the utility of DRS in a surgical setting during clinically relevant breach scenarios was investigated. The DRS integrated screw probe was tested on six cadavers in a surgical setting using typical breach scenarios encountered in clinical practice. DRS measurements were recorded at various positions along an insertion trajectory. The tissue type that the probe tip encountered were labelled based on information from CBCT images. For each breach direction, the DRS technique was able to accurately detect an impending breach defined as the entry into the pre-cortical zone (PCZ) and subsequently the cortical bone. Support Vector Machine (SVM) classification scheme showed a sensitivity of 98.1% and specificity of 98.9% in classifying cancellous from cortical bone based on the usage of fat fraction and collagen as input parameters. Thus, further underpinning the potential of DRS at the tip of the surgical instrument in detecting breaches in a preclinical setting.

The final step was to evaluate the reliability of the DRS derived measurements in a minimally invasive *in vivo* setting (see **Chapter 6**).The first *in vivo* investigation of DRS for breach detection was performed in a porcine model. The study adopted the minimally invasive workflow applied in clinical practice during pedicle screw placement procedures. To this end, DRS sensing was integrated into a Jamshidi needle by housing optical fibers into a kirschner wire (K-wire). The effect of probe handling conditions on the fat fraction measurements due tissue perfusion was also studied. A typical insertion along the anterior breach direction showed a drop in fat fraction as the probe tip transitioned from cancellous to cortical bone confirming previous investigations. Intraoperative probe pressure changes did not have a significant impact on the quality of fat fraction measurements as long as direct contact between probe tip and bone surface was achieved. Thus pointing towards that fat fraction being a reliable discriminatory parameter even in an *in vivo* setting where the presence of blood around the probe tip is inevitable.

Finally, in **Chapter 7** the main findings presented in this thesis are discussed in detail and put in a broader perspective. General conclusions are drawn and recommendations for future research are laid out.

SAMENVATTING

De intraoperatieve plaatsing van spinale schroeven is een complexe procedure. Een hoge technische expertise van de chirurgen is vereist om een adequate fixatie te bereiken en om de veiligheid van de patiënt te waarborgen ter voorkoming van vasculaire en neurologische letsels. De conventionele technieken voor het plaatsen van schroeven staan voor een aantal uitdagingen. Chirurgen vertrouwen sterk op ervaring, tactiele terugkoppeling en röntgensturing. De gevolgen hiervan zijn terug te vinden in de klinische literatuur als hoge risico's op complicaties, variaties in schroefplaatsingsnauwkeurigheid en blootstelling aan straling. Bovendien zijn kostenbesparingen in termen van verbeterde resultaten voor patiënten, zoals hersteltijden van patiënten en minder revisieoperaties, belangrijke stimulansen voor ontwikkeling en klinische adoptie van betere intraoperatieve begeleidingstechnologieën.

Het doel van deze studie was het onderzoeken van de toepasbaarheid van op optische spectrale detectie gebaseerde techniek, namelijk "Diffuse Reflectance Spectroscopy"(DRS) voor intraoperatieve instrumentgeleiding en breukdetectie tijdens pedikelschroefplaatsingsprocedures.

Om de toepassing van DRS in pedikelschroefplaatsingsprocedures te onderzoeken, werden de spectrale en fysiologische verschillen tussen poreus en corticaal wervelbot bestudeerd (gedetailleerd in **Hoofdstuk 2** van dit proefschrift). De optische eigenschappen van het weefsel die nodig zijn voor het detecteren van breuken werden bepaald op basis van experimenten op weefsel van kadavers. Verschillende eigenschappen die uit de spectra te herleiden zijn zoals vet, water, bloedgehalte en fotonverstrooiing, werden onderzocht of deze gebruikt kunnen worden om onderscheid te maken tussen poreuze en corticale wervelbottypen. De DR-spectra vertoonden meer vet, bloed en fotonverstrooiing in poreus bot dan in corticaal bot. Vervolgens werden Monte Carlo (MC) simulaties uitgevoerd en werd een drielaags model ontwikkeld om de trend van het vetgehalte te bestuderen toen de sonde tijdens een gesimuleerde insertie een corticale botgrens naderde. De bevindingen van de simulatie werden gebruikt om een door de optische schroef geïnduceerde doorbraak te valideren. De MC simulaties en het experimenteel inbrengen van de optische schroef toonden een vergelijkbare daling van het vetgehalte, meer dan 1 mm voordat de optische schroef in contact kwam met het corticale bot. Dit toonde aan dat DRS geïntegreerd in de tip van het instrument de mogelijkheid heeft om schroefbreuken op te sporen met vetgehalte als een belangrijke discriminerendeparameter.

Momenteel is MRI een van de meest nauwkeurige technieken om de vetconcentratie in weefsels te meten. Vetfractie, een belangrijke parameter bij DRS voor het detecteren van breuken, werd vergeleken met een gestandaardiseerde Magnetic Resonance (MR) techniek in **Hoofdstuk 3**. De nauwkeurigheid van het invasief gemeten vetgehalte in kadaverwervels met DRS werd vergeleken met de vetfractie van Proton-dichtheid (PDFF) afgeleid via de MRI-techniek op dezelfde wervels. Verschillende invoegingen met een

op maat gemaakte schroef met geïntegreerde optische vezels werden uitgevoerd onder cone beam computer tomography (CBCT). DR-spectra werden tijdens inserties op verschillende posities langs het sondetraject opgenomen. DRS en MRI afgeleide vetfracties werden vergeleken door de sondepositie binnen wervellichamen op CBCT afbeeldingen ruimtelijk te correleren met de MRI afbeeldingen. We vonden dat op DRS en MRI gebaseerde vetfractie sterk gecorreleerd is ($R^2 = 0,905$). Dit geeft aan dat DRS-detectie geïntegreerd in een chirurgisch instrument het vetgehalte in wervels nauwkeurig kan meten. Uit de klinische literatuur volgde verder dat niet-invasief gemeten PDFF blijkt te variëren met leeftijd, geslacht, wervelniveau en ziekten.

Om de ware variatie van vetfractie over de wervelkolom verder te begrijpen, werd een meer gedetailleerde analyse van de distributie van PDFF over intravertebrale zones zoals poreuze, pre-corticale zones en corticale botgrens uitgevoerd in **Hoofdstuk 4**. PDFF-distributies van corticaal bot bleken anders te zijn dan die van poreus bot over de wervelkolom. Bovendien vertoonden de totale verdelingen van de intravertebrale zones van de zes kadavers een mediane daling in PDFF van poreus bot naar corticaal bot. De variabiliteit in PDFF-distributies binnen de intravertebrale zones kan echter niet worden genegeerd.

In **Hoofdstuk 5** werd het nut van DRS in een chirurgische omgeving tijdens klinisch relevante doorbraak scenario's onderzocht. De DRS geintegreerde schroefsonde werd getest op zes kadavers in een chirurgische omgeving aan de hand van typische doorbraakscenario's die in de klinische praktijk voorkomen. DRS-metingen werden geregistreerd op verschillende posities langs een inbrengtraject. Het weefseltype dat de sondetip tegenkwam, werd gelabeld op basis van informatie uit CBCT afbeeldingen. Voor elke breukrichting was de DRS techniek in staat om een dreigende breuk, gedefinieerd als het bereiken van de pre-corticale zone (PCZ) en vervolgens het corticale bot, nauwkeurig te detecteren. Support Vector Machine (SVM) classificatieschema toonde een gevoeligheid van 98.1% en een specificiteit van 98.9% bij het classificeren van poreus van corticaal bot op basis van het gebruik van vetfractie en collageen als invoerparameters. Zo wordt de toevoegde waarde van DRS aan de punt van het chirurgische instrument verder ondersteund voor het detecteren van breuken in een preklinische setting.

De laatste stap was het evalueren van de betrouwbaarheid van de uit DRS afgeleide metingen in minimaal invasieve *in vivo* situaties (zie **Hoofdstuk 6**). Het eerste *in vivo* onderzoek naar DRS voor breukdetectie werd uitgevoerd in een varkensmodel. De studie heeft de minimaal invasieve workflow gebruikt die in de klinische praktijk wordt toegepast tijdens de plaatsing van pedikelschroeven. Daartoe werd DRS-detectie geïntegreerd in een Jamshidi-naald door optische vezels in een Kirschner-draad (K-draad) aan te brengen. Het effect van sondemanipulatie op de vetfractiemetingen als gevolg van weefselperfusie werd ook bestudeerd. Een typische insertie langs de anterieure breukrichting toonde een daling van de vetfractie op het moment dat de sondepunt overging van poreus naar corticaal bot, hetgeen door eerdere onderzoeken werden bevestigd. Intraoperatieve veranderingen in de sondedruk hadden geen significante invloed op de kwaliteit van de vetfractiemetingen, zolang direct contact tussen de sondepunt en het botoppervlak aanwezig was. Dit wijst erop dat vetfractie een betrouwbare discriminerende parameter is, zelfs in een *in vivo* situatie waar de aanwezigheid van bloed rond de sondepunt onvermijdelijk is.

Ten slotte worden in **Hoofdstuk 7** de belangrijkste bevindingen in dit proefschrift in detail besproken en in een breder perspectief geplaatst. Er worden algemene conclusies getrokken en er worden aanbevelingen gedaan voor toekomstig onderzoek.

The history of every major Galactic civilization tends to pass through three distinct and recognizable phases, those of Survival, Enquiry and Sophistication, otherwise known as the How, Why and Where phases. For instance, the first phase is characterized by the question: How can we eat?, the second by the question: Why do we eat?, and the third by the question: Where shall we have lunch?

The Hitchhiker's Guide to the Galaxy

CONTENTS

1

INTRODUCTION: EXPLORING THE CLINICAL PROBLEM OF INTRAOPERATIVE PEDICLE SCREW GUIDANCE DURING SPINAL FUSION SURGERY

Pedicle screw placement is a critical step in spinal fusion surgery. The close proximity of vital neural and vascular structures and the added variability in patient and spinal region dependent morphology makes the misalignment of one or more pedicle screws to have direct effect on the surgical outcome. To this end, conventional imaging and non-imaging based systems and devices currently used in clinical practice for intraoperative pedicle screw guidance were explored via clinical literature and surgeons opinions. Life and cost savings in terms improved outcome, reduced patient recovery times and revision surgeries are major incentives towards development and clinical adoption of better breach detection technologies. Optical-based technique namely Diffuse Reflectance Spectroscopy might be suited as a breach detection tool in order to mitigate some of the challenges for safe guidance during intraoperative pedicle screw placement.

1

1.1. SPINE ANATOMY

The human spine is an integrated complex of bones, nerves, muscles, tendons and ligaments. The vertebrae are the bony building blocks of the spine. There are 24 individual bones that interlock with each other to form the spinal column. These are divided into 5 regions namely cervical, thoracic, lumbar, sacral and coccyx as shown in figure 1.1. Each

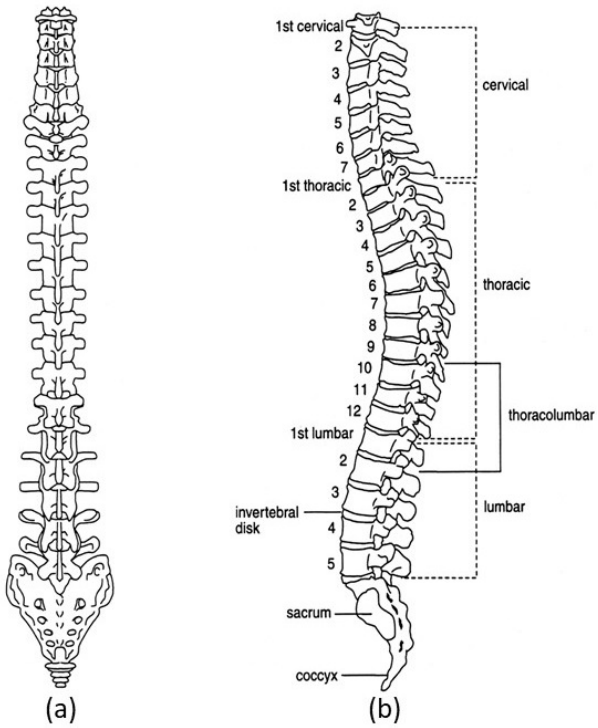

Figure 1.1: Spine anatomy.(a) Anterior/posterior(A/P) view, (b) lateral view. Figure adapted from [1].

vertebrae consists of three main parts namely the body, vertebral arch and the processes. Each vertebral arch is made up of two supporting pedicles and one lamina as shown in the axial view of figure 1.2a. The hollow spinal canal contains the spinal cord, fat, ligaments and blood vessels. Under each of the pedicles, a pair of spinal nerves exits the spinal cord and passes through the intervertebral foramen to branch out to the rest of the body as shown in figure 1.2a and figure 1.2b.

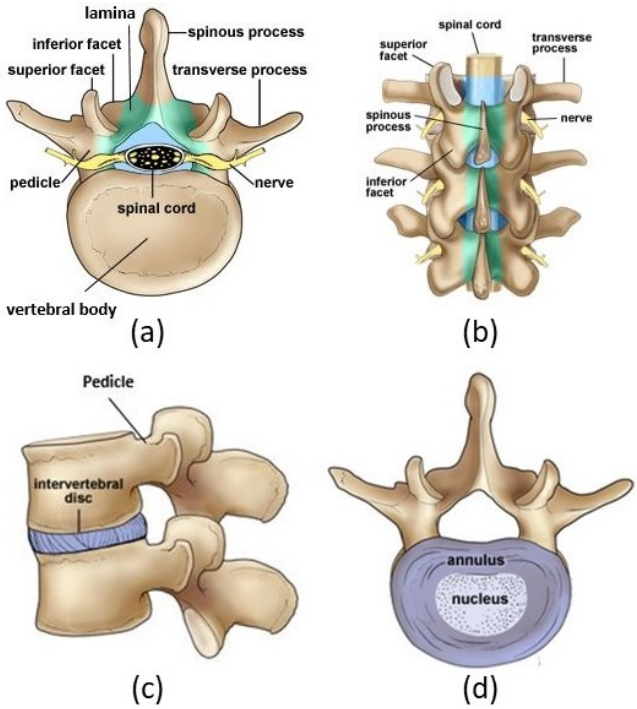

Figure 1.2: Various views depicting the spine anatomy. (a) axial view. (b) posterior view. (c) lateral view. (d) axial view with intervertebral disc. Illustration used with permission of MayfieldClinic.com. All rights reserved. No reuse permitted.

INTERVERTEBRAL DISC

Each vertebrae is separated and cushioned by an inter-vertebral disc (IVD) as illustrated in 1.2c. The disc consists of an outer fibrous ring called the anulus fibrosus, which surrounds an inner gel-like center, namely the nucleus pulposus as depicted in 1.2d. They have three extremely important functions which fundamentally ensure proper functioning of the spine. They help provide mobility to the spine by preventing the bones from rubbing against each other; they act as shock absorbers which function like coiled springs to bear the necessary dynamic loads during various activities; and they also act like spacers, to help maintain a constant gap between vertebrae and to allow the branching out of the nerves as shown in 1.2 b and c [2].

1.2. SPINE FUSION SURGERY

Spinal fusion surgery involves a surgical technique in which two or more vertebrae are fused together using screws and rods (spinal instrumentation) and bone graft material [3]. Spinal fusion is performed to eliminate any relative motion between the affected vertebrae in order to reduce pain indications and to improve the stability of the spine. After complete fusion of the vertebrae, the role of the spinal instrumentation gradually

decreases but is not removed unless the patient experiences discomfort or other complications. This concept of load sharing between the spinal column and the instrumentation and its importance in maintaining stability has been studied extensively in several biomechanical studies [4–6].

Spinal instrumentation is also required for the correction of deformity due to conditions like scoliosis or kyphosis. In these cases, the screws and rods are inserted and used to reduce the amount of curvature. Compressive and distractive forces are applied via the instrumentation in order to get a suitable correction of the spine [7].

There are several indications for the need of spinal fusion surgery namely:

- Spondylosis, a degenerative osteoarthritis of the joints between the centers of the spinal vertebrae and intervertebral foramen.
- Spondylolisthesis, a condition in which one vertebrae slips forward relative to the vertebrae above or below it.
- Instability and pain caused due to excessive motion between vertebrae.
- Bulging or herniated disc, which can cause compression of the spinal nerves (see figure 1.3).
- Spinal deformities such as Scoliosis or Kyphosis (see figure 1.4a).
- Trauma to the vertebrae

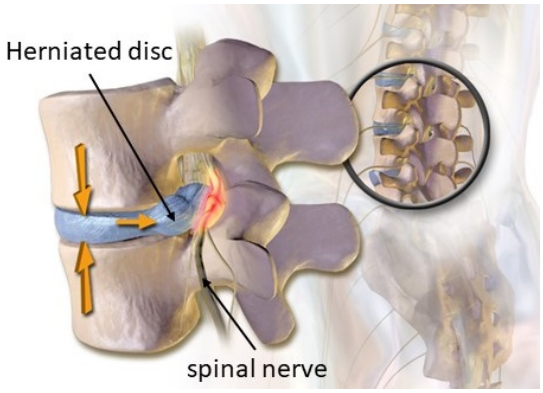

Figure 1.3: Bulging of disc impinging on a spinal nerve. Figure adapted from [8].

Spinal fusion surgery is performed in two main steps. The first step is to perform the necessary decompression due to diseases mentioned above such as herniated disc, Spondylolisthesis etc. This step usually involves dissection or removal of the intervertebral disc in question and followed by placement of bone graft material in the particular segment of the spine. The second step involves installing the spine instrumentation (pedicle screws and rods) for adequate spinal fusion.

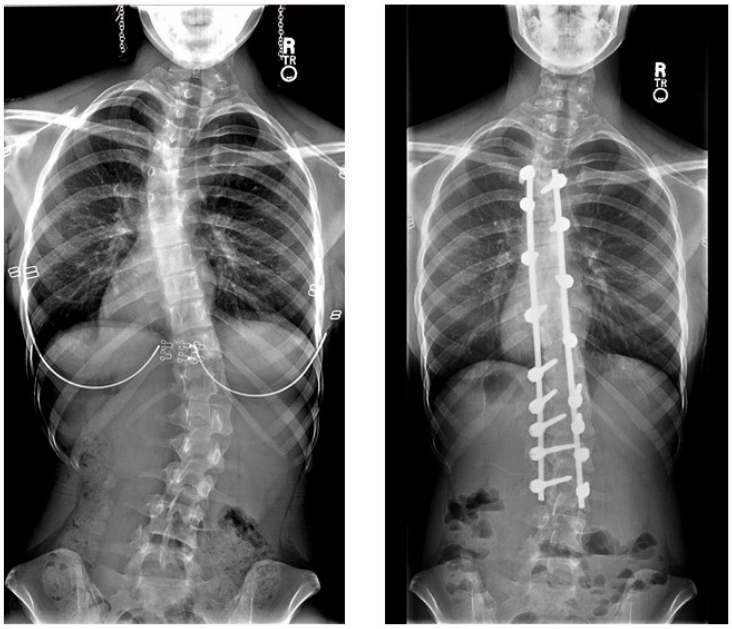

Figure 1.4: Anterior/Posterior radiographs of a patient showing (a) Scoliosis deformity of the spine, (b) curve corrected with pedicle screws and rods placed. Figure adapted from [9].

In case of spinal deformity cases such as scoliosis and kyphosis, spine instrumentation is first installed which serves as an anchor for the application of corrective and distractive maneuvers in order to correct the deformity (figure 1.4b). In the second step, all instrumented vertebrae are usually fused to prevent movement of the particular segment and thereby control the progression of the curve deformity [10, 11].

1.2.1. MANUAL FREE HAND TECHNIQUE OF PEDICLE SCREW PLACEMENT

The traditional approach of placing pedicle screws is the free hand technique. The surgeon relies on the appreciation of various anatomical landmarks at each level across the spinal column. In order to avoid improper placement of screws, the surgeon relies on experience based judgement and tactile feedback to differentiate between the less resistive cancellous bone and the stiffer cortical bone surrounding the pedicle, spinal canal and the sidewalls [12–14].

A drill or an awl is used to create a hole at the entry site as shown in figure 1.5. A pedicle probe/finder is then inserted to cannulate and prepare the hole. At this step of the procedure the neural or vascular risk is high. Thus, integrity of the tract is assessed using a feeler or a ball tipped probe after hole creation. A screw tap is then optionally inserted to prepare the hole further followed by the larger pedicle screw as shown in figure 1.5. The screw location is confirmed using anterior/ posterior (AP) and/or lateral fluoroscopy images of the vertebra.

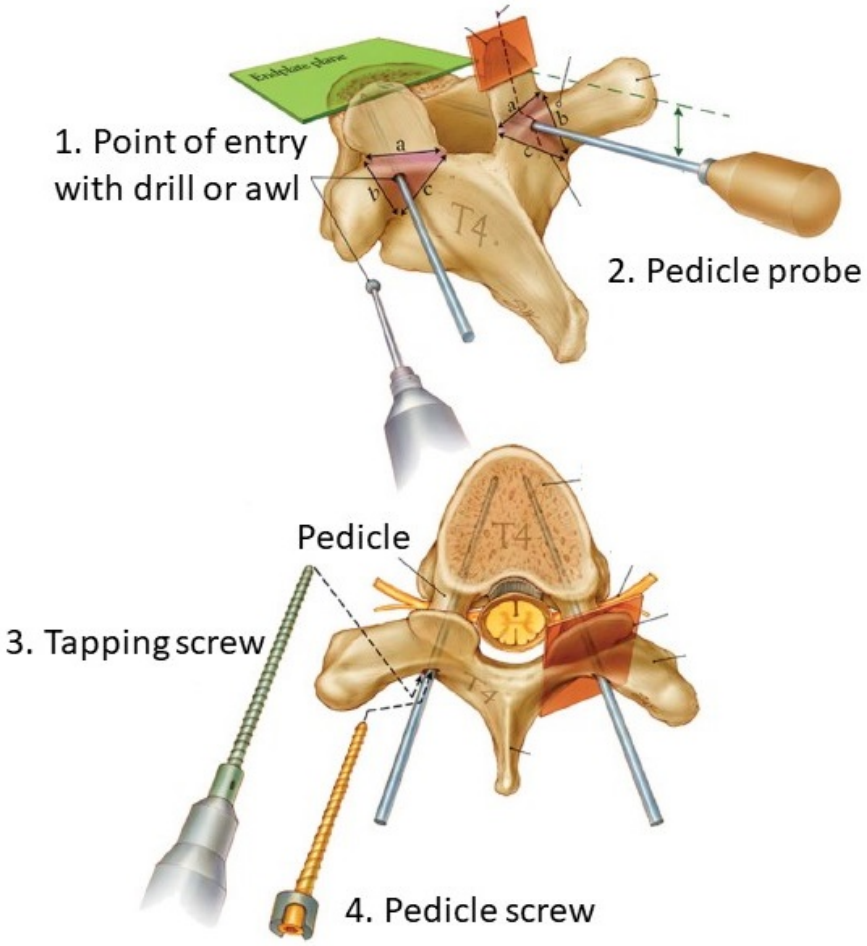

Figure 1.5: Surgical workflow of free-hand surgery. Figure adapted with permission from Parker et al. [13].

1.3. CHALLENGES IN PEDICLE SCREW PLACEMENT SURGICAL PROCEDURE

The procedure for pedicle screw placement is known to be highly complex and technically demanding with a long learning curve [14, 15]. There is a limited visibility of spinal anatomical landmarks during surgery which makes it important to gain a sound understanding of the spine anatomy that are hidden from direct view. Adding to the complexity are the limited sizes of the pedicles. The inner diameter of the pedicles can be as small as 2 millimeters [16]. Moreover, the close proximity of vital neural and vascular structures and the added variability in patient and region dependent morphology contribute significantly to the difficulties in accurate placement. The implication of perforation of vertebral wall due to improperly placed screws could lead to inadequate fixation

and place the neural and vascular structures at risk.

Accuracy rates of pedicle screw placement reported in literature vary widely. A meta-analysis study by Gelalis et al. [17] found the accuracy rate of the free-hand technique to vary between 69 - 94 %. The study also found that screws placed using the free-hand technique had a higher probability of screws perforating the cortex medially which increases the risk of a neurological injury. Moreover, malpositioned screws without clinical symptoms can be linked directly to screw loosening [18], which can result in improper fusion leading to spinal instability. In the worst case scenario a revision surgery might have to be performed.

Additionally, due to the increasing aging population and pressure on healthcare systems, pedicle screw placement procedures performed using minimally invasive approaches are rapidly increasing. The known advantages of minimally invasive surgeries (MIS) include reduced blood loss, shorter hospital stays and decreased surgical site infections [19]. Since MIS are performed through series of small incisions, they add an additional layer of complexity to the procedure due to limited visibility of anatomical landmarks. Schizas et al. [20] found a screw perforation rate of 23% (or accuracy rate of 77 %) based on 60 screws placed using an MIS approach and concluded that the procedure is technically demanding and has to be performed with extreme care.

The screw placement accuracy is also found to be correlated to surgeons' experience. Samdani et al. [21] showed a trend toward decreased rate of breaches for the most experienced surgeons especially while preventing medial breaches which have a higher possibility of neurological damage.

A systematic review of 35,630 pedicle screws by Gautschi et al. [22] provides an exhaustive analysis of the clinically relevant complications related to pedicle screw placement. Mean incidence of neurological complications reported are low and found in the range of 0 - 2% per pedicle screw. Complications were related to nerve root or spinal cord injury, dural lesions, vascular injury, cerebrospinal fluid leak, visceral injury, pedicle fracture, screw pullout, screw breakage and late spinal instability [22–24]. Figure 1.6a illustrates a case of new-onset radiculopathy due to a medially misplaced screw. It was confirmed that the complication was screw related because the symptoms disappeared after screw replacement [22]. Overall, it can be concluded that neurological complications associated with pedicle screw placement is rare but a serious complication[23].

An important distintion highlighted was between clinically significant complications and asymptomatic screw-related complications. As several malpositioned screws might lead to no complications. Figure 1.6b shows a screw breaching anteriorly and in close proximity with an illiac vessel without any symptoms reported. Moreover, there is also found to be a significant variability of opinion among surgeons regarding which malpositioned screws should be removed or revised in an asymptomatic patient [25]. Therefore, the true estimation of screw -related complication rate is extremely difficult. Complication rates are also susceptible to underreporting due to authors's medicolegal concerns.

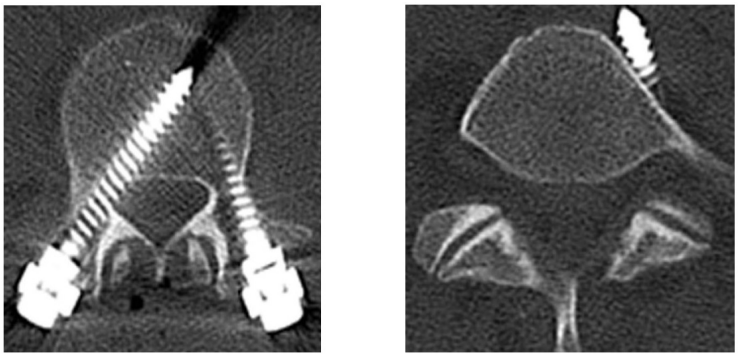

(a) (b)

Figure 1.6: (a) CT scan showing an axial view of a right medially misplaced screw in L-4, which caused new on-set radiculopathy. Symptoms disappeared after screw replacement. (b) L-5 screw exceeding ventral cortex of vertebral body with close proximity to illiac vessel. Figure used with permission from [22].

1.3.1. SURGEONS' OPINIONS

Surgeons personal opinions via questionnaires and interviews serve as an additional source of information regarding the clinical relevance of PSP.

Patel et al. [26] investigated the current practice of pedicle screw surgery in UK and Ireland via a questionnaire study. Accordingly, he received responses from a total of 67 surgeons who comprised of neuro, orthopedic and spine surgeons. The results are depicted in Figure 1.7. The results indicate that most surgeons would prefer a simple device to aid PSP due to the technically demanding nature of the procedure. The most common sources of error stated were the perforation of the lateral vertebral body wall and risking impingement of the descending nerve root, loss of fixation due to osteoporotic bone and difficulty in identifying landmarks in revision surgery.

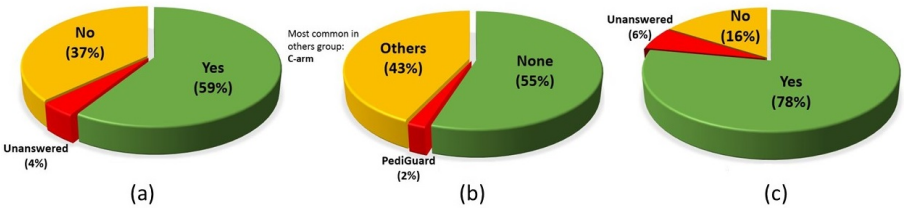

Figure 1.7: Survey questionnaire results from Patel et al. [26]: (a) Do you think there is a need for a simple device to aid PSP ? (b) What spinal systems do you currently use to aid PSP? (c) Have you experienced any problems with PSP in patients?

However, the outcomes of these surveys should be interpreted with caution due to the inevitable biases associated with questionnaires.

Given the challenges of pedicle screw placement expressed in literature and via surgeons opinions, clinical need for intraoperative breach detection and guidance systems seems valid. Hence, various intraoperative guidance systems have been developed in order to harness the developments of modern technology.

1.3.2. CONVENTIONAL IMAGING-BASED GUIDANCE TECHNIQUES

2D fluoroscopy-guided technique: Intraoperative fluoroscopy relies on serial X-rays to allow surgeons to track a screw's trajectory in real time. Fluoroscopy often utilizes an image intensifier system to take Anterior-Posterior(AP) and lateral images (figure. 1.8) of the vertebral levels. Following a treatment procedure such as decompression, the screw placement procedure is performed involving entry point selection, pedicle hole preparation, serial images which guide the surgeon's screw placement trajectory [14].

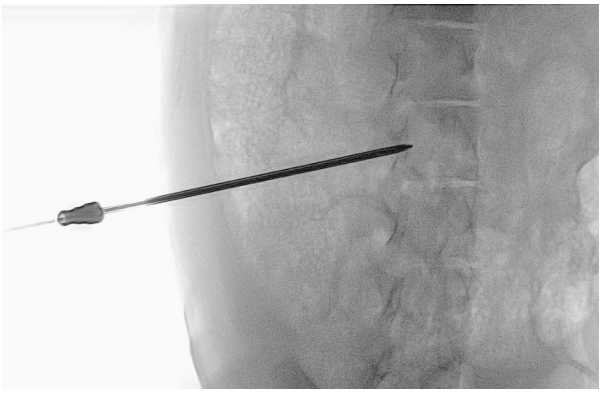

Figure 1.8: Lateral fluoroscopic views confirmng final screw position.

Apart from using the open approach, fluoroscopy is often performed minimally invasively. A skin incision of approx. 25-mm long is made. Sequential dilation of the entry point is performed using a tubular dilator. For the remainder of the procedure a surgical microscope is used for visualization of the entry site. Various instruments are then used to perform the treatment procedure such as decompression of the central canal. Interbody fusion of the vertebra is carried out using bone graft placement. With adequate fluoroscopic images, a Jamshidi needle is gradually introduced and tapped by a mallet to advance into and reach the cancellous bone of the vertebral body [27]. A guidewire namely the Kirschner wire (K-wire) is then inserted over which the hole is further prepared using a tap before the screw placement is finally performed. In case of MIS procedures, intra operative 2D fluoroscopy images are a necessity for following, tracking and confirming screw trajectories.

The main advantage of this approach is the real-time image acquisition and visualization of the screw trajectory. As a result, the increased accuracy rates using this technique are reflected in litearture [14, 28]. Moreover, since intraoperative fluoroscopy allows the surgeon to perform the surgery using the minimally invasive approach, several additional benefits can be derived such as less collateral tissue damage, reduced blood loss, reduced surgical site infections and faster recovery times [29].

However, the radiation exposure on the patient and more importantly on the surgeon cannot be underestimated. Rampersaud et al. [30] found that spine surgeon who perform fluoroscopy-guided pedicle screw insertion experience a 10 to 12 fold increase in radiation dosage compared to other musculoskeletal extremity procedures. Study by Haque et al. [31] estimated that spine surgeons beginning their career at the age of 30

would exceed the recommended life time limit in less than 10 years. Adding to the concern is that surgeons performing MIS procedures would acquire increased fluoroscopy shots due to limited visualization [32]. Increase in operation times relative to the free-hand technique with increased incidences of surgical site infections is also a point of concern [14].

3D Computer-assisted technique The 3D computer-assisted surgical (3D CAS) technique uses a computer model which uses Computer Tomography (CT) images and generates a 3D model of the spine anatomy. With the help of optical cameras and markers placed on the patient, surgical instruments are tracked in real-time as shown in figure 1.9. This information is then used to plan screw entry site and adjust the trajectory of the screws intra-operatively [11, 14, 33].

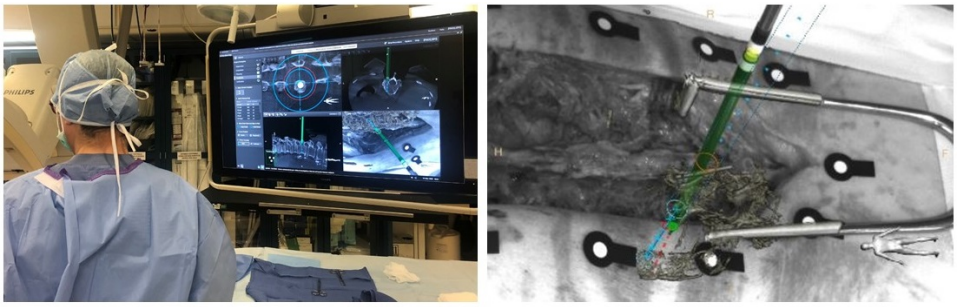

(a) (b)

Figure 1.9: (a) Surgeon viewing the screen showing various views of the surgical area.(b) Information used to perform pedicle screw path planning.

The accuracy of PSP has been shown to have improved using the 3D CAS technique due to increased visualization and enhanced intra-operative path planning capabilities [34]. Another advantage is the lower radiation exposure especially to the surgeon and OR staff, due to fewer intraoperative image acquisitions needed as compared to the 2D fluoroscopy technique [35].

One of the most prominent criticisms of the 3D CAS technique are associated with the workflow interruptions and additional operation time. Another possible disadvantage is the high initial costs associated with the purchase and installation of these systems.

ULTRASOUND IMAGING-BASED GUIDANCE DEVICE

Ultrasound based guidance for determining the best screw trajectory has been investigated in an academic setting [36–38]. These researchers have used A-mode and B-mode imaging transducers at various low (1-3 MHz) and high (20 MHz) frequency ranges to generate cross-sectional images from within the pedicle. Sideways and forward looking probes were designed. However, high acoustic impedance of bone relative to vasculature and soft tissue serves as a major fundamental limitation for reliable ultrasonic guided pedicle screw insertion technique from entering into the clinic.

1.3.3. NON IMAGING-BASED GUIDANCE DEVICES

ELECTRICAL CONDUCTIVITY-BASED MEASUREMENT TECHNIQUE

Central to this technique is the PediGuard probe device which is a flagship product developed by SpineGuard ® [39]. The PediGuard probe measures the electrical conductivity of different tissue types such as cancellous, cortical bone and blood using an electromagnetic field sensor described by Bolger et al. [40] . By measuring the differences in electrical conductivity between these tissues, cortical breaches can be anticipated by warning the surgeon via an audio and/or LED-based feedback. The device has been adopted in clinical practice and shown to increase pedicle screw placement accuracy (especially in thoracic area), reduce insertion time and radiation in scoliosis surgery [41, 42].

However, an independent assessment performed by Guillen et al. [43] noted that the PediGuard probe is sensitive to the amount of pressure applied to the probe which altered the frequency of the audio feedback, thereby significantly limiting the interpretability by the surgeon. Chaput et al. [42] also found that due to the relaxing of steady probe pressure by the surgeon, allowed blood to reach the tip leading to false positive results during breach detection.

NEURO AND ELECTRPHYSIOLOGICAL MONITORING TECHNIQUES

Electromyography (EMG) a non-imaging technique has been shown to be useful in detecting and avoiding potential complications during spinal screw placement [44, 45]. However, it has also known to have a relatively low sensitivity for pedicle screw malposition detection [46, 47]. Such a technique can often indicate a presence of a nerve injury after they have occurred thus not helping in mitigating the risk of injury [15]. Moreover, factors such as anaesthetic relaxants, differences in patient anatomy, lack of consensus on stimulation thresholds, all contribute towards the unreliability of technique for breach detection. Finally, the high costs associated with the employment of trained personnel required during surgery for interpreting the signals is also a concern.

1.4. CLINICAL NEED FOR A BREACH DETECTION TOOL

The greatest risk of improper hole preparation and screw placement is spinal instability (due to improper fusion) and screw-related complications. Such complications can place the neural and vascular structures at serious risk and thereby negatively impact the surgical outcome. Therefore, guidance systems and technologies discussed in the previous section have been developed to improve upon the free-hand approach of pedicle screw placement which relies on tactile feedback and experience-based judgement to distinguish between the softer cancellous bone and the stiffer cortical bone.

The development and commercialization of new pedicle screw guidance technologies into the clinic are highly dependent on market size and the cost savings associated with them [15]. The rise of aging population and a trend towards accepting elderly patients with complex medical histories have led to an increase in spinal fusion surgeries [48, 49]. Moreover, cost savings for the hospital in terms of improved outcome, reduced recovery times and revision surgeries are major incentives towards development and clinical adoption of better technologies for breach detection [50].

Another possible optical-based technique that has the potential of being a cost- effective solution in reducing risk of improper screw placement is diffuse reflectance spectroscopy (DRS).

1.4.1. DIFFUSE REFLECTANCE SPECTROSCOPY AS A BREACH DETECTION TOOL

DRS is an optical spectroscopy technique in which a broad-band white light source is used to illuminate the tissue sample via an optical fiber as shown in figure 1.10. The diffusely reflected light after undergoing absorption and scattering events is collected by another fiber. The spectral information derived from the locally probed tissue can be translated into clinically relevant parameters using two broad approaches. One approach is to use machine learning models to correlate raw measured spectra from a tissue type directly to clinically relevant parameters. Such mathematical models include support vector machines, principal component analysis, artificial neural networks etc.

Another approach is to apply an analytical model based on diffusion theory to estimate optical properties of the locally probed tissue such as absorption and scattering coefficients [51, 52]. A priori knowledge of the wavelength dependent absorption spectra of the individual chromophores present in the sample can then be used to extract relevant physiological information such as concentration of blood (%) fat(%), water(%) and scattering (cm^{-1}) within the locally probed sample.

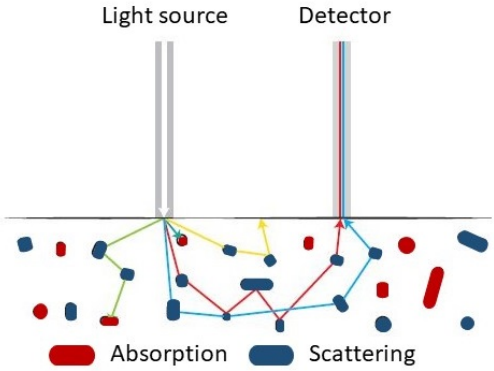

Figure 1.10: Schematic representation of photon scattering and absorption in tissue. The transmitting fiber emits broad-band white light, the right fiber collects photons and transports them to the spectrometer.

Over the years, DRS has been used for tissue characterization in various clinical applications such as liver tumor detection, nerve detection for regional anesthesia procedures and for lung biopsy guidance [53–55]. From a hardware perspective, the value of DRS lies in its integrability into the existing surgical tool sets due to the low form factor of optical fibers used to transmit and receive light, thus maintaining surgical workflows. It also allows for data acquisition and visualization of the spectra per second which makes it promising for intra-operative decision making and guidance. Lastly, the use of harmless non-ionizing radiation belonging to the visible and near-infrared wavelength window makes the technique safe in the clinical environment.

1.5. GOAL AND OUTLINE OF THE THESIS

The intraoperative guidance of spinal screws, is a complex procedure which demands high technical expertise from surgeons in order to achieve adequate fixation and ensure patient safety by preventing vascular and neurological injuries. The conventional screw placement techniques face several challenges. Surgeons heavily rely on experience-based judgement, tactile feedback and X-ray guidance. The consequences of which are reflected in clinical literature via high risks associated with complications, screw placement accuracy variability and radiation exposure. Moreover, cost savings in terms of improved patient outcomes such as patient recovery times and fewer revision surgeries are major incentives towards development and clinical adoption of better intraoperative guidance technologies.

*The **goal of this PhD work** is to investigate the applicability of DRS for breach detection during pedicle screw placement procedures using pre-clinical studies.*

In order to investigate the application DRS in pedicle screw placement procedures, the tissue optical properties required for breach detection is determined based on *ex vivo* swine and cadaveric tissues in **Chapter 2**. First, it is investigated whether optical properties extracted from the spectra namely fat, water, blood content along with photon scattering, can be used to distinguish between cancellous and cortical vertebral bone types. Monte-Carlo (MC) simulations are then performed to study the fat content trend as the probe approached a cortical bone boundary. The simulation findings are used to validate a breach of an optical screw probe in a cadaveric setting.

In **Chapter 3**, fat content measured invasively using DRS are compared to Proton density fat fraction (PDFF) derived via the MRI technique on the same specimens. Several insertions using a custom-made screw with integrated optical fibers are performed under cone beam computer tomography (CBCT). DR spectra are recorded at several positions along the probe trajectory during the turn by turn insertion. DRS and MRI derived fat fractions are compared by spatially correlating the probe position within vertebral bodies on CBCT images with respect to MRI images.

MR images are then used to non-invasively determine the distribution of PDFF across the spinal column based on the various intravertebral zones defined such as cancellous, pre-cortical and cortical zones (**Chapter 4**).

In **Chapter 5**, the DRS integrated screw probe are tested on six cadavers in a surgical setting using typical breach scenarios encountered in clinical practice. DRS measurements are recorded at various positions along an insertion trajectory. The tissue type that probe tip encountered are labelled based on information from CBCT images.

The first *in vivo* investigation of DRS for breach detection is performed in a porcine model **Chapter 6**. The study also adopts the minimally invasive workflow applied in clinical practice during pedicle screw placement procedures. To this end, DRS sensing is integrated into a Jamshidi needle using an optical K-wire. The effect of probe handling conditions on the fat fraction measurements due tissue perfusion is also studied.

Finally, in **Chapter 7** the main findings presented in this thesis are discussed in detail and put in a broader perspective. General conclusions are drawn and recommendations for future research are laid out.

1

REFERENCES

[1] "Side View and Back View of a Normal Spine," Dec 2015. [Online; accessed 08. June. 2020].

[2] A. Voloshin and J. Wosk, "An in vivo study of low back pain and shock absorption in the human locomotor system," *Journal of biomechanics*, vol. 15, no. 1, pp. 21–27, 1982.

[3] K. Yone, T. Sakou, Y. Kawauchi, M. Yamaguchi, and M. Yanase, "Indication of fusion for lumbar spinal stenosis in elderly patients and its significance," *Spine*, vol. 21, no. 2, pp. 242–248, 1996.

[4] W.-K. Chou, A. Chien, and J.-L. Wang, "Pullout strength of thoracic pedicle screws improved with cortical bone ratio: a cadaveric study," *Journal of orthopaedic science*, vol. 19, no. 6, pp. 900–906, 2014.

[5] J. C. Dick, T. A. Zdeblick, B. D. Bartel, and D. N. Kunz, "Mechanical evaluation of cross-link designs in rigid pedicle screw systems," *Spine*, vol. 22, no. 4, pp. 370–375, 1997.

[6] G. Lynn, D. P. Mukherjee, R. N. Kruse, K. K. Sadasivan, and J. A. Albright, "Mechanical stability of thoracolumbar pedicle screw fixation: the effect of crosslinks," *Spine*, vol. 22, no. 14, pp. 1568–1572, 1997.

[7] C. L. Hamill, L. G. Lenke, K. H. Bridwell, M. P. Chapman, K. Blanke, and C. Baldus, "The use of pedicle screw fixation to improve correction in the lumbar spine of patients with idiopathic scoliosis: is it warranted?," *Spine*, vol. 21, no. 10, pp. 1241–1249, 1996.

[8] "Medical gallery of Blausen Medical 2014," Aug 2014. [Online; accessed 08. June. 2020].

[9] "X-ray of U.S. girl, age 16 years 10 months, with post-operative scoliosis. Front, standing, clothed.," Feb 2010. [Online; accessed 08. June. 2020].

[10] C. T. Price, J. F. Connolly, A. C. Carantzas, and I. Ilyas, "Comparison of bone grafts for posterior spinal fusion in adolescent idiopathic scoliosis," *Spine*, vol. 28, no. 8, pp. 793–798, 2003.

[11] A. C. Bourgeois, A. R. Faulkner, A. S. Pasciak, and Y. C. Bradley, "The evolution of image-guided lumbosacral spine surgery," *Annals of translational medicine*, vol. 3, no. 5, 2015.

[12] Y. J. Kim, L. G. Lenke, K. H. Bridwell, Y. S. Cho, and K. D. Riew, "Free hand pedicle screw placement in the thoracic spine: is it safe?," *Spine*, vol. 29, no. 3, pp. 333–342, 2004.

[13] S. L. Parker, M. J. McGirt, S. H. Farber, A. G. Amin, A.-M. Rick, I. Suk, A. Bydon, D. M. Sciubba, J.-P. Wolinsky, Z. L. Gokaslan, *et al.*, "Accuracy of free-hand pedicle screws in the thoracic and lumbar spine: analysis of 6816 consecutive screws," *Neurosurgery*, vol. 68, no. 1, pp. 170–178, 2011.

[14] V. Puvanesarajah, J. A. Liauw, S.-f. Lo, I. A. Lina, and T. F. Witham, "Techniques and accuracy of thoracolumbar pedicle screw placement," *World journal of orthopedics*, vol. 5, no. 2, p. 112, 2014.

[15] A. Manbachi, R. S. Cobbold, and H. J. Ginsberg, "Guided pedicle screw insertion: techniques and training," *The Spine Journal*, vol. 14, no. 1, pp. 165–179, 2014.

[16] M. Yusof, L. Ming, and M. Abdullah, "Computed tomographic measurement of cervical pedicles for transpedicular fixation in a malay population," *Journal of Orthopaedic Surgery*, vol. 15, no. 2, pp. 187–190, 2007.

[17] I. D. Gelalis, N. K. Paschos, E. E. Pakos, A. N. Politis, C. M. Arnaoutoglou, A. C. Karageorgos, A. Ploumis, and T. A. Xenakis, "Accuracy of pedicle screw placement: a systematic review of prospective in vivo studies comparing free hand, fluoroscopy guidance and navigation techniques," *European Spine Journal*, vol. 21, no. 2, pp. 247–255, 2012.

[18] G. Li, G. Lv, P. Passias, M. Kozanek, U. S. Metkar, Z. Liu, K. B. Wood, L. Rehak, and Y. Deng, "Complications associated with thoracic pedicle screws in spinal deformity," *European Spine Journal*, vol. 19, no. 9, pp. 1576–1584, 2010.

[19] M. Vazan, J. Gempt, B. Meyer, N. Buchmann, and Y.-M. Ryang, "Minimally invasive transforaminal lumbar interbody fusion versus open transforaminal lumbar interbody fusion: a technical description and review of the literature," *Acta neurochirurgica*, vol. 159, no. 6, pp. 1137–1146, 2017.

[20] C. Schizas, J. Michel, V. Kosmopoulos, and N. Theumann, "Computer tomography assessment of pedicle screw insertion in percutaneous posterior transpedicular stabilization," *European Spine Journal*, vol. 16, no. 5, pp. 613–617, 2007.

[21] A. F. Samdani, A. Ranade, D. M. Sciubba, P. J. Cahill, M. D. Antonacci, D. H. Clements, and R. R. Betz, "Accuracy of free-hand placement of thoracic pedicle screws in adolescent idiopathic scoliosis: how much of a difference does surgeon experience make?," *European Spine Journal*, vol. 19, no. 1, pp. 91–95, 2010.

[22] O. P. Gautschi, B. Schatlo, K. Schaller, and E. Tessitore, "Clinically relevant complications related to pedicle screw placement in thoracolumbar surgery and their management: a literature review of 35,630 pedicle screws," *Neurosurgical focus*, vol. 31, no. 4, p. E8, 2011.

[23] J. E. Lopera, C. S. Restrepo, A. Gonzales, C. K. Trimmer, and F. Arko, "Aortoiliac vascular injuries after misplacement of fixation screws," *Journal of Trauma and Acute Care Surgery*, vol. 69, no. 4, pp. 870–875, 2010.

[24] J. E. Lonstein, F. Denis, J. H. Perra, M. R. Pinto, M. D. Smith, and R. B. Winter, "Complications associated with pedicle screws," *JBJS*, vol. 81, no. 11, pp. 1519–28, 1999.

[25] L. V. Floccari, A. N. Larson, C. H. Crawford, C. G. Ledonio, D. W. Polly, L. Y. Carreon, and L. Blakemore, "Which malpositioned pedicle screws should be revised?," *Journal of Pediatric Orthopaedics*, vol. 38, no. 2, pp. 110–115, 2018.

[26] P. S. Patel, *Screw fixation of implants to the spine*. PhD thesis, University of Birmingham, 2010.

[27] M.-C. Kim, H.-T. Chung, J.-L. Cho, D.-J. Kim, and N.-S. Chung, "Factors affecting the accurate placement of percutaneous pedicle screws during minimally invasive transforaminal lumbar interbody fusion," *European spine journal*, vol. 20, no. 10, p. 1635, 2011.

[28] A. Mason, R. Paulsen, J. M. Babuska, S. Rajpal, S. Burneikiene, E. L. Nelson, and A. T. Villavicencio, "The accuracy of pedicle screw placement using intraoperative image guidance systems: A systematic review," *Journal of Neurosurgery: Spine*, vol. 20, no. 2, pp. 196–203, 2014.

[29] J. Del Castillo-Calcáneo, R. Navarro-Ramirez, M. Gimenez-Gigon, J. Adjei, A. Damolla, J. Nakhla, R. N. Hernandez, and R. Hartl, "Principles and fundamentals of minimally invasive spine surgery," *World Neurosurgery*, vol. 119, pp. 465–471, 2018.

[30] Y. R. Rampersaud, K. T. Foley, A. C. Shen, S. Williams, and M. Solomito, "Radiation exposure to the spine surgeon during fluoroscopically assisted pedicle screw insertion," *Spine*, vol. 25, no. 20, pp. 2637–2645, 2000.

[31] M. U. Haque, H. L. Shufflebarger, M. O'Brien, and A. Macagno, "Radiation exposure during pedicle screw placement in adolescent idiopathic scoliosis: is fluoroscopy safe?," *Spine*, vol. 31, no. 21, pp. 2516–2520, 2006.

[32] R. K. Bindal, S. Glaze, M. Ognoskie, V. Tunner, R. Malone, and S. Ghosh, "Surgeon and patient radiation exposure in minimally invasive transforaminal lumbar interbody fusion," *Journal of Neurosurgery: Spine*, vol. 9, no. 6, pp. 570–573, 2008.

[33] A. Elmi-Terander, H. Skulason, M. Söderman, J. Racadio, R. Homan, D. Babic, N. van der Vaart, and R. Nachabe, "Surgical navigation technology based on augmented reality and integrated 3d intraoperative imaging: a spine cadaveric feasibility and accuracy study," *Spine*, vol. 41, no. 21, p. E1303, 2016.

[34] R. Verma, S. Krishan, K. Haendlmayer, and A. Mohsen, "Functional outcome of computer-assisted spinal pedicle screw placement: a systematic review and meta-analysis of 23 studies including 5,992 pedicle screws," *European Spine Journal*, vol. 19, no. 3, pp. 370–375, 2010.

[35] F. T. Gebhard, M. D. Kraus, E. Schneider, U. C. Liener, L. Kinzl, and M. Arand, "Does computer-assisted spine surgery reduce intraoperative radiation doses?," *Spine*, vol. 31, no. 17, pp. 2024–2027, 2006.

[36] S. R. Kantelhardt, C. H. Bock, J. Larsen, V. Bockermann, W. Schillinger, V. Rohde, and A. Giese, "Intraosseous ultrasound in the placement of pedicle screws in the lumbar spine," *Spine*, vol. 34, no. 4, pp. 400–407, 2009.

[37] A.-H. Aly, H. J. Ginsberg, and R. S. Cobbold, "On ultrasound imaging for guided screw insertion in spinal fusion surgery," *Ultrasound in medicine & biology*, vol. 37, no. 4, pp. 651–664, 2011.

[38] A. Manbachi, *Towards Ultrasound-guided Spinal Fusion Surgery*. Springer, 2016.

[39] M. Senn, *DSG Technology*, (accessed May, 2020). https://www.spineguard.com/dynamic-surgical-guidance-technology/.

[40] C. Bolger, C. Carozzo, T. Roger, L. McEvoy, J. Nagaria, G. Vanacker, and M. Bourlion, "A preliminary study of reliability of impedance measurement to detect iatrogenic initial pedicle perforation (in the porcine model)," *European Spine Journal*, vol. 15, no. 3, pp. 316–320, 2006.

[41] Y.-S. Bai, Y.-F. Niu, Z.-Q. Chen, X.-D. Zhu, L. K. P. Gabriel, H. K. Wong, and M. Li, "Comparison of the pedicle screws placement between electronic conductivity device and normal pedicle finder in posterior surgery of scoliosis," *Clinical Spine Surgery*, vol. 26, no. 6, pp. 316–320, 2013.

[42] C. D. Chaput, K. George, A. F. Samdani, J. I. Williams, J. Gaughan, and R. R. Betz, "Reduction in radiation (fluoroscopy) while maintaining safe placement of pedicle screws during lumbar spine fusion," *Spine*, vol. 37, no. 21, pp. E1305–E1309, 2012.

[43] P. T. Guillen, R. G. KnoPPeR, J. KRoGeR, N. D. Wycliffe, O. A. Danisa, and W. K. Cheng, "Independent assessment of a new pedicle probe and its ability to detect pedicle breach: a cadaveric study," *Journal of Neurosurgery: Spine*, vol. 21, no. 5, pp. 821–825, 2014.

[44] T. N. Pajewski, V. Arlet, and L. H. Phillips, "Current approach on spinal cord monitoring: the point of view of the neurologist, the anesthesiologist and the spine surgeon," *European Spine Journal*, vol. 16, no. 2, pp. 115–129, 2007.

[45] M. F. Duffy, J. H. Phillips, D. R. Knapp, and J. A. Herrera-Soto, "Usefulness of electromyography compared to computed tomography scans in pedicle screw placement," *Spine*, vol. 35, no. 2, pp. E43–E48, 2010.

[46] C.-H. Lee, H.-W. Kim, H. R. Kim, C.-Y. Lee, J.-H. Kim, and F. Sala, "Can triggered electromyography thresholds assure accurate pedicle screw placements? a systematic review and meta-analysis of diagnostic test accuracy," *Clinical Neurophysiology*, vol. 126, no. 10, pp. 2019–2025, 2015.

[47] R. M. Ajiboye, S. D. Zoller, A. D'Oro, Z. D. Burke, W. Sheppard, C. Wang, Z. Buser, J. C. Wang, and S. Pourtaheri, "The utility of intraoperative neuromonitoring for lumbar pedicle screw placement is questionable: A review of 9957 cases," *Spine*, vol. 42, no. 13, p. 1006, 2017.

[48] S. T. Kha, H. Ilyas, J. E. Tanenbaum, E. C. Benzel, M. P. Steinmetz, and T. E. Mroz, "Trends in lumbar fusion surgery among octogenarians: A nationwide inpatient sample study from 2004 to 2013," *Global spine journal*, vol. 8, no. 6, pp. 593–599, 2018.

[49] K. Kobayashi, K. Ando, Y. Nishida, N. Ishiguro, and S. Imagama, "Epidemiological trends in spine surgery over 10 years in a multicenter database," *European Spine Journal*, vol. 27, no. 8, pp. 1698–1703, 2018.

[50] N. Dea, C. G. Fisher, J. Batke, J. Strelzow, D. Mendelsohn, S. J. Paquette, B. K. Kwon, M. D. Boyd, M. F. Dvorak, and J. T. Street, "Economic evaluation comparing intraoperative cone beam ct-based navigation and conventional fluoroscopy for the placement of spinal pedicle screws: a patient-level data cost-effectiveness analysis," *The Spine Journal*, vol. 16, no. 1, pp. 23–31, 2016.

[51] R. Nachabe, B. H. Hendriks, A. E. Desjardins, M. van der Voort, M. B. van der Mark, and H. J. Sterenborg, "Estimation of lipid and water concentrations in scattering media with diffuse optical spectroscopy from 900 to 1600 nm," *Journal of biomedical optics*, vol. 15, no. 3, p. 037015, 2010.

[52] R. Nachabé, B. H. Hendriks, M. van der Voort, A. E. Desjardins, and H. J. Sterenborg, "Estimation of biological chromophores using diffuse optical spectroscopy: benefit of extending the uv-vis wavelength range to include 1000 to 1600 nm," *Biomedical optics express*, vol. 1, no. 5, pp. 1432–1442, 2010.

[53] D. Evers, R. Nachabe, D. Hompes, F. Van Coevorden, G. Lucassen, B. Hendriks, M.-L. van Velthuysen, J. Wesseling, and T. Ruers, "Optical sensing for tumor detection in the liver," *European Journal of Surgical Oncology (EJSO)*, vol. 39, no. 1, pp. 68–75, 2013.

[54] B. H. Hendriks, A. J. Balthasar, G. W. Lucassen, M. van der Voort, M. Mueller, V. V. Pully, T. M. Bydlon, C. Reich, A. T. van Keersop, J. Kortsmit, *et al.*, "Nerve detection with optical spectroscopy for regional anesthesia procedures," *Journal of translational medicine*, vol. 13, no. 1, p. 380, 2015.

[55] J. W. Spliethoff, W. Prevoo, M. A. Meier, J. de Jong, H. M. Klomp, D. J. Evers, H. J. Sterenborg, G. W. Lucassen, B. H. Hendriks, and T. J. Ruers, "Real-time in vivo tissue characterization with diffuse reflectance spectroscopy during transthoracic lung biopsy: a clinical feasibility study," *Clinical cancer research*, vol. 22, no. 2, pp. 357–365, 2016.

2

Investigation of Diffuse Reflectance Spectroscopy for Detection of Cortical Breaches in Spinal Fusion Surgery

Safe and accurate placement of screws remains a critical issue in open and minimally invasive spine surgery. We propose to use diffuse reflectance (DR) spectroscopy as a sensing technology at the tip of a surgical instrument to ensure a safe path of the instrument through the cancellous bone of the vertebrae. This approach could potentially reduce the rate of cortical bone breaches, thereby resulting in fewer neural and vascular injuries during spinal fusion surgery. In our study, DR spectra in the wavelength ranges of 400 to 1600 nm were acquired from cancellous and cortical bone from three human cadavers. First, it was investigated whether these spectra can be used to distinguish between the two bone types based on fat, water, and blood content along with photon scattering. Subsequently, the penetration of the bone by an optical probe was simulated using the Monte-Carlo (MC) method, to study if the changes in fat content along the probe path would still enable distinction between the bone types. Finally, the simulation findings were validated via an experimental insertion of an optical screw probe into the vertebra aided by x-ray image guidance. The DR spectra indicate that the amount of fat, blood, and photon scattering is significantly higher in cancellous bone than in cortical bone ($p < 0.01$), which allows distinction between the bone types. The MC simulations showed a change in fat content more than 1 mm before the optical probe came in contact with the cortical bone. The experimental insertion of the optical screw probe gave similar results. This study shows that spectral tissue sensing, based on DR spectroscopy at the instrument tip, is a promising technology to identify the transition zone from cancellous to cortical vertebral bone.

Swamy A., Burström G., Spliethoff J.W., Babic D., Reich C., Groen J., Edström E., Elmi-Terander A., Racadio J.M., Dankelman J. and Hendriks B.H.W. Diffuse reflectance spectroscopy, a potential optical sensing technology for the detection of cortical breaches during spinal screw placement. Journal of biomedical optics, 24(1), 2019.

2.1. INTRODUCTION

Spinal fusion surgeries have been increasing all over the world due to a rise in aging population and recent advances in surgical techniques and anesthesia [2–4]. In these surgeries, screws are commonly placed through the bony pedicles into the vertebral bodies of the spinal vertebra. These serve as anchoring points for rigid constructs in order to fuse parts of the spine to regain and maintain spinal stability. Spinal instability might be caused by congenital, degenerative, or traumatic conditions.[5] The inaccurate placement of such screws in the spine can cause severe vascular and neurological injuries in patients [6–8]. The increase in aging population and pressure on healthcare systems has led to a trend toward minimally invasive spine (MIS) procedures. The benefits of these procedures are, among others, shorter hospital stays and faster recovery times. MIS aims to minimize the disruption of soft tissue, induce muscle splitting rather than stripping and to reduce blood loss. Surgery is performed through several small incisions, which emphasizes the need for techniques to guide the surgeon in order to compensate for the limited exposure of the surgical site. Moreover, the close proximity of vital neural and vascular structures and the variability in anatomy within and between patients contribute to the difficulty in accurate placement of spinal screws.

There are several techniques practiced by surgeons to accurately and safely place spinal screws. Techniques used in clinical practice for spinal screw placement include the free-hand technique and the image-guided technique. The image-guided technique involves the preplanning and intraoperative guidance of screws with the help of either 2-D fluoroscopy images or a 3-D navigation planning system [9–11]. In the conventional free-hand technique described by Kim et al.[12], the surgeons need to perform several additional steps before the final insertion of each of the screws into the vertebrae. These additional steps are usually performed to prepare a pilot hole in vertebral bone and to ensure a safe trajectory for the screw. The surgeons usually use anatomical landmarks, tactile feedback, and experience-based judgment, in order to plan the spinal screw path. The 2-D x-ray images are also commonly acquired intraoperatively to confirm safe trajectory of the screws [10]. Given that several spinal screws are usually placed per patient, these additional screw trajectory verification steps can contribute significantly to surgery time and radiation exposure, especially for the surgeon. Reoperation rates due to mislocated instrumentation are also a major concern for patients as well as the hospitals [8, 13, 14]. Some of the other screw guidance techniques have been described extensively by Manbachi et al. [9].

The complex nature of the procedure coupled with a heavy reliance on the surgeon's experience contributes to the high variability in accuracy rates reported in literature. Accuracy rates of screw placement are reported to be as low as 27.6 % and as high as 100 % based on a meta-analysis by Kosmopoulos and Schizas [15]. A more recent meta-analysis paper published by Mason et al.[16] found the accuracy rates to lie in the range of 50 % to 92 %. Therefore, there is a need for a reliable yet cost effective solution for increasing accuracy and safety in the placement of spinal screws during spinal fusion surgery.

Spectral tissue sensing by diffuse reflectance spectroscopy(DRS) may offer the possibility for tissue discrimination during surgery and thereby provide an early warning of an impending breach of the cortical bone boundary. Such a technique might help op-

timize the screw trajectory verification workflow thereby contributing to less radiation, shorter surgery time, and fewer revision surgeries. Thus, further contributing towards increased safety and surgeon confidence during spinal screw placement procedures. In this optical spectroscopy-based technique, tissue is probed by sending white light from a broadband light source through an optical fiber. After the light has interacted with the tissue, a similar optical fiber is used to collect the diffusely reflected light from the tissue. The light is then analyzed further to identify spectral changes. These spectral changes originate from the highly specific nature of the absorption and scattering characteristics of individual tissue types [17] Therefore, by analyzing the differences in reflected spectrum of light, different tissue types can be distinguished. DR spectroscopy has already been shown to be able to estimate the concentration of blood, fat, and other optical properties in various clinical applications, such as tumor and nerve detection [18–23].

Although DRS has been extensively studied for applications in oncology, its usefulness in accurate guidance of spinal screws has received little attention in the scientific community. The group of Li et al.[24–26] has recently investigated the possibility of monitoring the reduced scattering coefficients extracted after sending near-infrared light into the vertebral bone for tissue boundary detection. Their approach involves the use of a wavelength window of 200 to 1100 nm. A single parameter, namely a reduced scattering coefficient, was used to detect cortical breaches.

In our study, we use a broader wavelength window (400 to 1600 nm) and a spectrum analysis algorithm. This enables the quantification of various optical properties, such as blood content, fat content, water content, and photon scattering in various tissue types, each of them contributing to the possibility of breach detection. Therefore, the goal of this study is to investigate fundamental differences between the two tissue types namely cancellous and cortical vertebral bone. In the context of a clinical screw placement, we explore the possibility of cortical bone detection using DR spectroscopy. To this end, we extract optical properties from the DR spectra acquired from the two bone types making up the vertebra, in order to analyze the differences between them. We investigate the variability of optical property distribution across cancellous bone by spatially mapping the vertebral body using a stencil system. We attempt to measure the distribution of thickness of cortical bone surrounding the cancellous bone and spinal canal at various regions within the vertebra.

We also perform three-layered Monte-Carlo (MC) simulations in order to visualize and analyze the spectral changes that might occur as the modeled optical probe within cancellous bone, approaches a cortical bone boundary and subsequently other surrounding tissues. The MC model was used as it is the gold standard method to model light transport in tissues [27]. Finally, the results of the simulation are validated by a cadaver experiment involving the image-guided insertion of an in-house developed optical screw probe into a human vertebra.

2.2. METHODS

2.2.1. SPINAL TISSUES

Two cadaver experiments were conducted at the Radboud University Medical Center Nijmegen, The Netherlands, and Cincinnati Children's medical hospital, Ohio, United

States, respectively. All ethical guidelines for human cadaver studies were followed. The donors allowed their bodies and body parts to be used for research and educational purposes. One female (63 years; 90 kg; 180 cm) (cadaver1) and one male (78 years; 50 kg; 186 cm) (cadaver2) were used for the first cadaver experiment. One female (76 years; 63.5 kg; 145 cm) (cadaver3) was used for the second cadaver experiment. No embalming process was used, in order to preserve the optical properties of the cadaver specimens.

2.2.2. EXPERIMENTAL SETUP

The experimental set up for DR spectra acquisition consists of a tungsten halogen broadband light source (360 to 2500 nm) with two optical spectrometers, as shown in the schematic diagram of Fig. 2.1(a). The two spectrometers collectively cover the visible, near-infrared, and shortwave infrared wavelength range; the first spectrometer resolves light in the visible and near-infrared wavelength range of 400 to 1100 nm (Andor Technology, DU420ABRDD), and the second resolves light in the shortwave infrared wavelength range of 900 to 1700 nm (Andor Technology, DU492A-1.7). LabVIEW software (National Instruments, Austin, Texas) developed in-house was used to control the spectrometers and acquire the data. The DR spectroscopy system used in this study has been extensively described previously, together with the calibration method [28–30].

In the first cadaver experiment, a bare optical probe was used to obtain DR spectra, whereas in the second cadaver experiment [Fig. 2.1(b)], an optical screw probe was used, as shown in Fig. 2.1(c).

In both the cadaver experiments, the bare optical probe and optical screw probe had the same internal construction. Both optical probes consisted of two optical fibers with core diameter of 200 μm. One of the fibers was used to transport the light from the source to the tissue, and the other fiber was used to transport the light from the tissue to both spectrometers. The distance between the collecting fiber and the delivering fiber was set at 1.22 mm, as shown in Fig. 2.1(a). In earlier work, we found that a good trade-off between signal-to-noise ratio and probing depth can be achieved by choosing a fiber-to-fiber distance around 1.2 mm. The diameter of the optical screw probe and manufacturing constraints, in order to house the fibers in the screw, also influenced the fiber distance selection.

2.2.3. PRECLINICAL CADAVER EXPERIMENT 1:CROSS-SECTION EXPERIMENT

In the first cadaver experiment, resection of two cervical vertebrae, four thoracic vertebrae, and one lumbar vertebra were carried out collectively from cadaver1 and cadaver2 and sliced in the axial direction using a bone saw to visualize the view, as shown in Fig. 2(a). This axial view provided visual confirmation of cancellous and cortical bone. This allowed DR spectra acquisition of bone types at various locations. The axial crosssection of the vertebrae also helped the determination of cortical bone thickness. A senior medical doctor performed all surgical procedures.

DETERMINATION OF OPTICAL PROPERTIES OF VERTEBRAL BONE

Subsequently, the bony surface of a total of seven vertebrae was probed from cervical, thoracic, and lumbar regions. DR spectra were acquired from both cadavers (cadaver1 and cadaver2) using a bare optical probe, as shown in Fig. 2.1(b). In order to extract

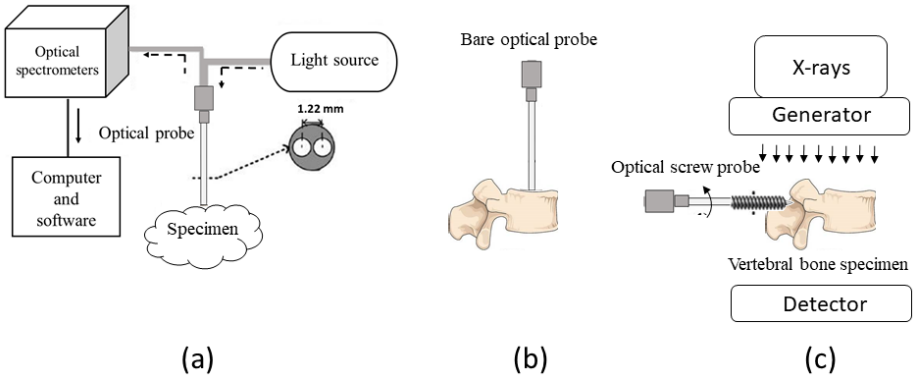

Figure 2.1: (a) Schematic of the general experimental setup used to perform DR spectra measurements.(b) Bare optical probe used for cross-section experiment. (c) Optical screw probe used for image-guided insertion.

the optical properties of vertebral bone, which consists of cancellous and cortical bone, the two bone tissue types were first identified visually under the supervision of a trained medical doctor. DR spectra were acquired across 147 random locations from cancellous bone and across 119 locations from cortical bone. Each location was probed five times. Adequate fiber-tissue coupling was achieved by applying gentle pressure. No coupling fluid was used.

DETERMINATION OF DISTRIBUTION OF OPTICAL PROPERTIES BASED ON VERTEBRAL BODY REGION

Figure 2.2(a) shows the vertebral body region, which consists of cancellous bone. In order to measure how the optical properties spatially vary across the entire region, DR spectra were acquired at various locations within the vertebral body. In order to perform the experiment in a systematic way, a transparent acrylic glass stencil was placed on top of the axial slice of a vertebra, as shown in Fig. 2.2(b). The stencil was a 120 × 120 × 10 mm plate with 289 patterned holes of diameter 1.9 mm spaced 5 mm apart from each other. DR spectra were acquired by inserting the bare optical probe into the stencil holes and ensuring that the probe is perpendicular to the tissue surface. DR spectra were acquired from all the stencil holes, which roughly cover the vertebral body region of the vertebra. The vertebral body was then divided into an inner and outer region, as shown in Fig. 2.2(b). The yellow dots indicate the locations, where DR spectra were extracted for analysis. The inner red region consisted of all the measurements within the inner ring and the outer blue region consisted of all the measurements within the outer annulus ring.

From the two cadavers, out of the seven vertebrae resected, DR spectra were acquired from three vertebrae belonging to cervical, thoracic, and lumbar regions. Spectra from a total of 80 unique locations were obtained, divided equally between the inner and outer vertebral body regions for further analysis.

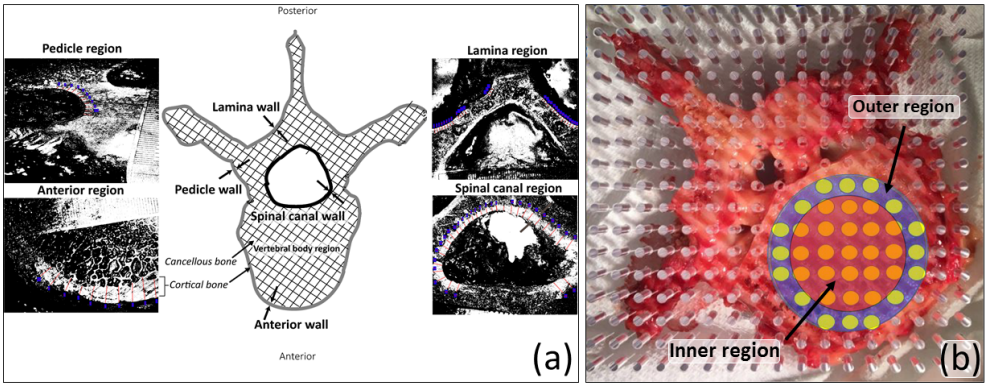

Figure 2.2: (a) Axial view of vertebra with grey scale images indicating cortical bone walls at various regions and (b) glass stencil with holes placed on top of a vertebra for spatial optical mapping.

CORTICAL THICKNESS MEASUREMENTS USING A MICROSCOPE

First, a portable microscope camera (5 megapixel, DigiMicro Profi, dnt®) was used for acquisition of magnified (6×) images of the sliced vertebrae. Images were then processed via image processing software (ImageJ) [31]. The red–green–blue images were converted into grayscale, and a suitable thresholding window (based on trial-and-error) was applied in order to better visualize the cortical bone boundary, as shown in Fig. 2.2(a). Four regions were identified during the measurement of the cortical boundary: spinal canal region, anterior wall region, pedicle wall region, and the lamina wall region. The spinal canal region is the region that houses the spinal cord. The anterior wall region surrounds the cancellous bone in the vertebral body. The pedicle wall region refers to mainly the pedicle wall separating the bony pedicle from the surrounding tissues. Measurements of cortical thickness surrounding the lamina region were also performed. This region makes up the bony structure surrounding the spinal cord posteriorly. During image acquisition, a reference scale of known lengths was placed in the camera view in order to set a measurement standard before any measurements were performed. The distance between each cortical thickness measurement was kept approximately constant.

2.2.4. MONTE-CARLO SIMULATIONS

MC simulations were performed by adopting the model developed by Wang et al.[32] known as the MC model of light transport in multilayered tissues. This model was applied because of its ability to simulate photon propagation through multiple tissue layers. A three-layered model was thus developed consisting of cancellous, cortical, and surrounding tissue, simulating the order of tissue types encountered by a spinal screw tip during a typical clinical insertion. The surrounding tissue in the thoracolumbar region could be subcutaneous fat, muscle, or ligament. The wavelength-dependent absorption and scattering coefficients for all three tissues were used as input for the model. These were derived after fitting the pure tissue spectra using a modified version of the model[28] developed by Farrell et al.[33]. Based on our experiments, pure tissue spectra refer to the spectra that contain information only about one type of tissue. The tissue

type was confirmed using x-ray imaging by a trained medical doctor.

Before performing a three-layered optical probe simulation, the MC simulations were first validated by using a single layer model for each of the three tissue types. The optical properties retrieved from the three experimental pure spectra were used as input for the MC model. Three MC simulation spectra were then calculated for the respective tissue types and compared to the experimental pure spectra.

In order to simulate the optical probe penetrating through different layers of tissue, the thickness of the layer equal to dz was reduced in steps, as shown in Fig. 3(b). At several depths, DR spectrum was recorded and subsequently fitted to obtain simulated estimates of fat content. Five simulations per step were performed.

Wavelengths were simulated at a sample rate of 2 nm over the near-infrared range of 1000 to 1600 nm. The fiber distance was chosen to be equal to 0.122 cm. A refractive index of 1.44 and an anisotropy factor of 0.9 were chosen for all the three tissue types as input for the MC model.[34] Each simulation was performed with 1 million photons, which led to one reflectance data point per wavelength. Simulations were processed using a Linux cluster made available at Philips Research, Eindhoven.

The cylindrical grid system adopted to model the geometry of a tissue layer is shown in Fig. 2.3(a). The geometry is a function of total depth z, total radius r, and a total sweep angle equal to α. The geometry is subdivided into grid elements using distances dr, dα, and dz. In this study, the radius grid width dr and the angular sweep width dα were chosen to be equal to 0.002 cm and 3.6deg, respectively. A pencil beam of light enters the tissue layer at the center of the grid system C as denoted by the red arrow perpendicular to the top surface. The top layer with dz = 0 contains information about the amount of diffuse reflectance. Tissue layer depth is chosen as an integer multiple of dz so that information within each grid element only pertains to one tissue type.

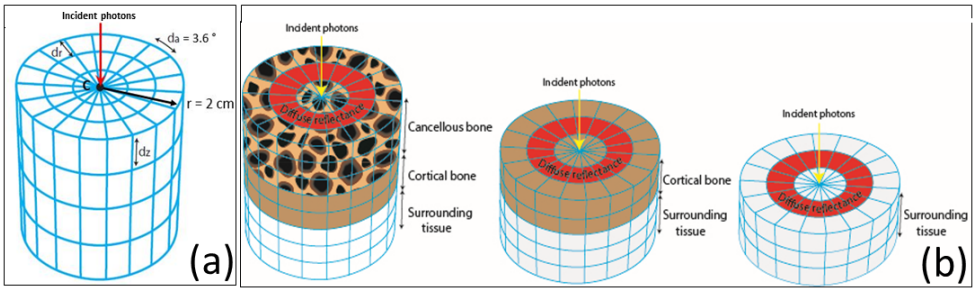

Figure 2.3: (a) Cylindrical grid system used to model a tissue layer in MC simulations. (b) Modeling insertion of optical probe by recording the reflectance spectra of top tissue layer (in red) followed by tissue layer removal in steps.

2.2.5. PRECLINICAL CADAVER EXPERIMENT 2:IMAGE-GUIDED INSERTION

A second cadaver experiment was performed to benchmark the MC simulation results. A custom-made optical screw probe (diameter: 55 mm) with integrated fiber-optics was used to perform an insertion in a vertebra of cadaver3. The bony vertebra was first exposed by stripping off the subcutaneous fat, muscles, and ligaments using scalpels. A

pilot hole was subsequently made in the vertebral bone using an awl in order to provide a gripping surface for the optical screw probe. The optical screw probe was then inserted turn by turn into the vertebral body, with DR spectra recorded at each turn [Fig. 2.1(c)]. X-ray images were also acquired in order to correlate the DR spectra to the optical screw probe tip position within the tissue. Five DR spectra were acquired per turn, and the corresponding fat content was averaged per turn.

2.2.6. DATA ANALYSIS

Data processing was performed by in-house developed software using MATLAB version 9.3 (MathWorks Inc.) and its statistics toolbox.

DETERMINATION OF TISSUE OPTICAL PROPERTIES

Tissue optical properties were extracted from the measured spectra by adopting a modified version of the model developed by Farrell et al.[33] The absorption coefficient $\mu_a(\lambda)$ and reduced scattering coefficients $\mu_{s'}(\lambda)$ can be extracted from the model expressed in cm^{-1}. From the known fiber distance between the emitting and collecting fibers as well as the wavelength dependent absorption coefficients, the amount of fat (%), water (%), and total hemoglobin in blood (%) present in the tissue was determined following a procedure, as previously described by our group [29, 30]. The scattering parameter (S800) was derived from the empirical model based on Rayleigh and Mie scattering described by

$$\mu_{s'}(\lambda) = S_{800}\left[F_{MR}\left(\frac{\lambda}{\lambda_0}\right)^{-b} + (1-F_{MR})\left(\frac{\lambda}{\lambda_0}\right)^{-4}\right],$$

where λ_0 is set to 800 nm, which corresponds to a wavelength normalization value, S800 is the reduced scattering amplitude at λ_0, b is the Mie scattering slope, the Mie-to-Rayleigh scattering fraction is denoted by F_{MR} [29].

STATISTICS

A Kolmogorov–Smirnov test was used to test the DR spectral data for normality. As the data were found not to be normally distributed, a nonparametric Wilcoxon rank-sum test was used to perform the necessary inferential statistics in order to analyze the differences between cancellous and cortical bone. The significance level was set to 0.01.

2.3. RESULTS

2.3.1. OPTICAL PROPERTIES DISTRIBUTION AMONG VERTEBRAL BONE TYPES

The amount of blood [Median (Mdn) = 4.2 %], fat (Mdn = 17.4 %),and light scattering (Mdn = 10.5 cm^{-1}) in cancellous bone is found to differ from amount of blood (Mdn = 2.2%), fat (Mdn = 3.2%), and light scattering (Mdn = 5.0 cm^{-1}) in cortical bone, as illustrated in Fig. 2.4. This result is found to be statistically significant ($p < 0.01$), as also indicated in Table 2.1. However, the amount of water found in cancellous bone (Mdn = 31.7%) did not significantly differ from the water content in cortical bone (Mdn = 53.1%), $p > 0.01$. Overall, all parameters except water concentration exhibit a drop from cancellous to cortical bone type.

2.3.2. OPTICAL PROPERTIES DISTRIBUTION AMONG VERTEBRAL BODY REGIONS

The inner and outer regions of the vertebral body do not seem to differ in terms of the optical properties, as shown via the non significant results of Table 2.2.

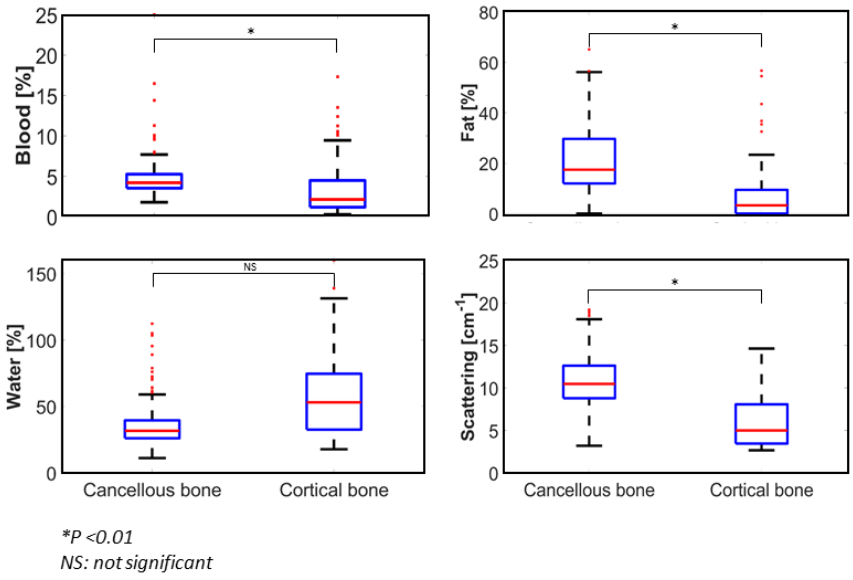

Figure 2.4: (a) Distribution of optical properties across cancellous and cortical vertebral bone types.

Table 2.1: Optical properties summary data across vertebral bone type.

	Vertebral bone type		
Optical properties	Cancellous bone (N = 147)	Cortical bone (N = 119)	
	Median	Median	P value
Blood [%]	4.2	2.1	$< 10^{-5}$
Fat [%]	17.4	3.2	$< 10^{-5}$
Water [%]	31.7	53.1	0.0115
Scattering $[cm^{-1}]$	10.5	5	$< 10^{-5}$

However, the high range indicates variability in the properties across the vertebral body, as illustrated via the box plots of Fig. 2.5.

2.3.3. CORTICAL WALL THICKNESS DISTRIBUTION ANALYSIS

Figure 2.6 describes the distribution of cortical thickness across different regions of the vertebra. The probability density curve indicates that a thickness range of 1 to 2 mm

Table 2.2: Optical properties summary data across vertebral body regions.

	Vertebral body regions		
Optical properties	Inner (N = 40)	Outer (N = 40)	
	Median	Median	P value
Blood [%]	4	2.8	0.04
Fat [%]	21	20	0.79
Water [%]	31.4	30.1	0.85
Scattering [cm^{-1}]	9.9	9.7	0.95

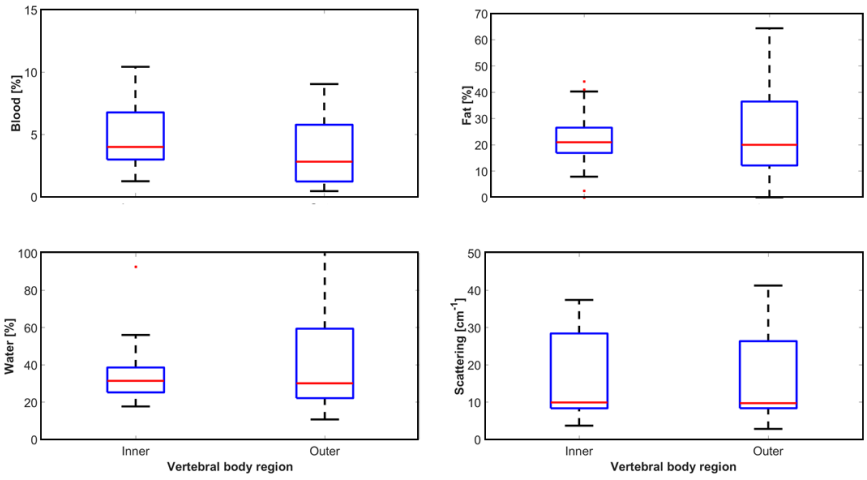

Figure 2.5: (a) Distribution of optical properties across vertebral body regions.

can be found for the cortical wall thickness surrounding the spinal canal. The median thickness in this region is found to be 1.5 mm, as shown in Table 2.3. The lamina wall, pedicle wall, and the anterior wall collectively have the highest probability distribution of cortical thickness in the range of 1 to 3 mm.

2.3.4. MONTE-CARLO MODEL VALIDATION

Figures 2.7(a)–2.7(c) show three typical spectra of the three tissue types probed. Qualitatively, from 1150 nm wavelength onward, the simulated spectra and measured spectra exhibit an overlap. Figures 2.7(d)–2.7(f) display the wavelength-dependent absorption and scattering coefficients of the three tissue types. The quantitative comparison between measured and simulated fat content (Table 2.4) shows that these values are similar for the three investigated tissue types.

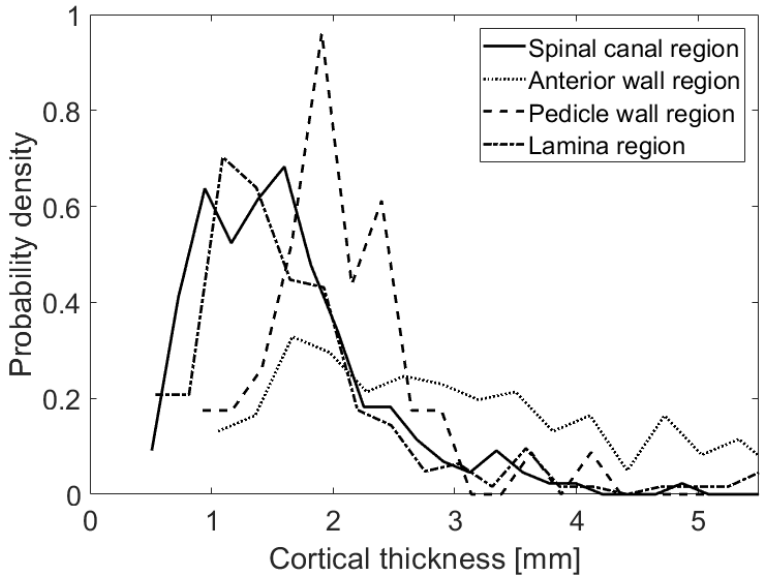

Figure 2.6: Distribution of cortical thickness across various vertebral regions.

Table 2.3: Cortical thickness central tendencies across various vertebral regions.

Vertebral region	Number of data points (N)	Median [mm]
Spinal Canal	201	1.5
Anterior	171	2.8
Pedicle	42	2
Lamina	213	1.5

2.3.5. COMPARISON OF MONTE-CARLO MODELED INSERTION WITH IMAGE-GUIDED EXPERIMENTAL INSERTION

In Fig. 2.8, the simulated changes in DR spectra [Fig. 2.8(a)] and corresponding fat content [Fig. 2.8(b)], as the modeled optical probe approaches the cortical boundary, are compared to an image-guided experimental insertion [Fig. 2.8(d)]. Note that during the modeled insertion, fat content is observed to decrease more than 1 mm before the optical probe comes in contact with the cortical bone boundary. The decrease in measured fat content [Fig. 2.8(d)] also begins more than 1 mm before reaching the cortical bone.

2.4. DISCUSSION

Accurate and safe placement of spinal screws remains a critical issue in spine surgery. In this study, we explored the potential of adopting a DR sensor at the tip of a spinal screw in order to detect cortical bone boundaries, thereby preventing screw misplacement. In the

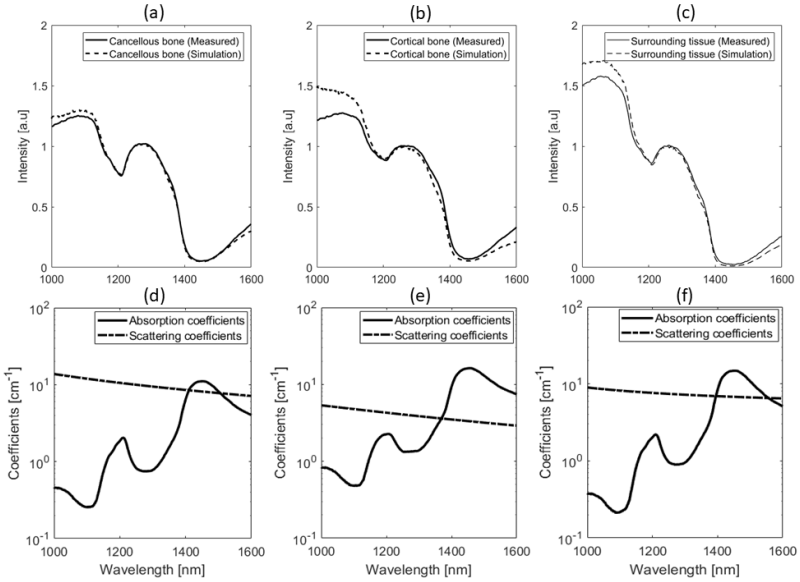

Figure 2.7: (a–c) Typical experimentally measured and MC simulated spectra of cancellous, cortical and surrounding tissue. (d–f) Wavelength-dependent absorption and scattering coefficients of the three tissue types.

Table 2.4: Quantitative comparison of measured and simulated spectra based on fat content.

Tissue type	Measured Fat [%]	Simulation Fat [%]
Cancellous bone	34	35
Cortical bone	0	0
Surrounding tissue	26	29

first cadaver experiment, vertebral bones were resected from the spine. DRS measurements were performed on the surface of the axial slice of these vertebrae to investigate the differences between cancellous and cortical bone. A range of cortical bone thickness was determined from thickness distributions. These were calculated for various regions within the vertebrae using images from a microscope. MC simulations were performed to simulate a modeled optical probe as it approaches a cortical bone boundary. Finally, a second cadaver experiment involving the turn by turn insertion of an optical screw probe with integrated fiber optics was carried out under image guidance, in order to validate the simulation findings.

Based on DR measurements of seven vertebrae across all spinal levels of two cadaver specimens, the blood content, fat content, and photon scattering were found to be higher in cancellous bone than in cortical bone. The higher amount of blood in the cancellous bone can potentially be attributed to the fact that cancellous bone houses red bone marrow, which is an important site for red blood cell formation [35]. However,

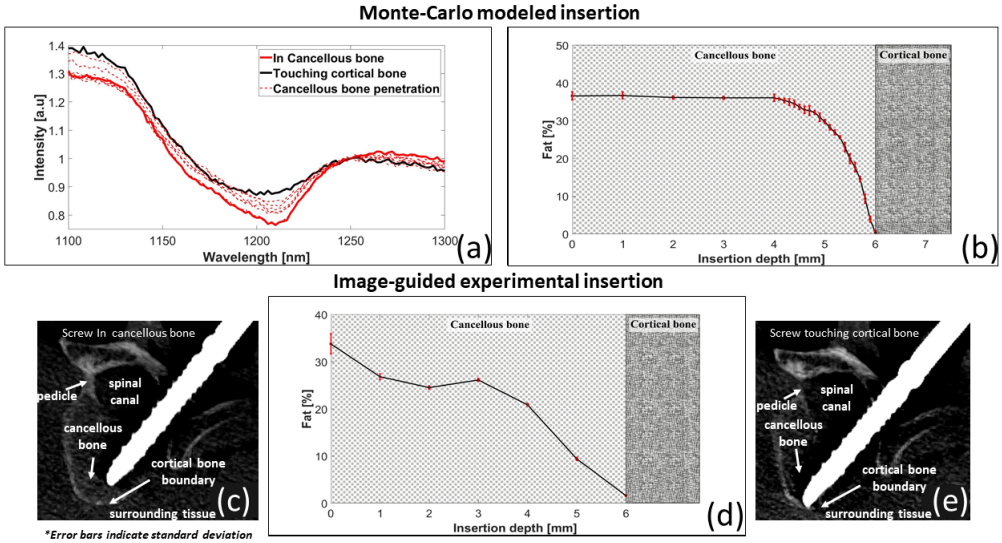

Figure 2.8: Comparison between simulated and measured probe insertion. (a) Simulated changes in DR spectra during the transition of the modeled optical probe from cancellous bone to cortical bone.(b) Corresponding drop in simulated fat content. (c) X-ray image showing optical screw probe in cancellous bone. (d) Drop in measured fat content as the optical screw probe approaches cortical bone. (e) X-ray image showing the tip of optical screw probe in contact with cortical bone.

this finding must be interpreted with caution as this study was performed in an *ex vivo* setting. Blood content and blood oxygen saturation are known to be different between *ex vivo* and *in vivo* settings. This is because the lack of blood circulation and uptake of oxygen from the air is bound to effect the local blood oxygenation concentration. The local blood content will also be influenced by the settling of blood (livor mortis) in the *ex vivo* setting [36]. The effect of blood derived from DR spectra in an *in vivo* setting needs to be investigated, before any solid conclusions can be drawn.

The higher fat content found in cancellous bone is also an intuitive finding as it is well known that cancellous bone houses triglyceride (fat) storage sites within its cavities [35] The higher photon scattering can be linked to this diverse mix of organic materials found within the same tissue type of cancellous bone. These mixtures of materials have different refractive indices, which could thereby increase the number of photon scattering events. As such in an *in vivo* setting, the tissues would be ideally at 37°C. The *ex vivo* human cadaver tissue used in this study was refrigerated at around 2°C to 4°C immediately after death and then allowed to rest at room temperature for several hours during the experiment. However, based on literature, lipids are known to be relatively less sensitive to temperature changes. Nachabé et al.[28] found no changes in the absorption values of lipids upon increasing the temperature of a sample tissue from 30°C to 45°C. Therefore, a large influence on fat values derived from bone due to the *ex vivo* nature of the tissues probed is less likely.

Several researchers have attempted to quantify fat or fat fraction in vertebral bones

for characterizations of cancerous tumors and as a diagnosis parameter for various diseases, such as osteoporosis, diabetes, HIV, and obesity[37–40]. Nachabé et al.[41] quantified fat fraction in liver specimens of mice using near-infrared spectroscopy, which is a specific type of DRS, and magnetic resonance spectroscopy. In this study, the fat fraction derived from cancellous bone via DRS was found to be 35.4 %, which falls within the wide range of proton density fat fraction (15% to 60%) found in published MRI literature [42, 43]. The effect of vertebral level, age, gender, and diseases on the fat content or fat fraction within vertebral bones shall be part of future investigations.

We showed that although cancellous bone is heterogeneous in nature, its optical properties spread across the vertebral body are very similar, as indicated by the non-significant results of Table 2.2.

In this study, we confirmed pervious findings of cortical thickness found in literature that are based on CT-imaging [44, 45]. However, Ritzel et al.[46] measured the cortical bone thickness using a bone staining approach and found the cortical thickness range to be lower than the range found in this study. The specimen preparation, staining, and subsequent evaluation of cortical thickness measurements by a semiautomatic image processing software could have all cumulatively caused the discrepancy in thickness measurements.

In this study, an attempt was made to substantially reduce the subjectivity in discerning the boundary between cortical and cancellous bone with the help of image analysis techniques, but it could not fully be eliminated. A reliable estimate of the cortical thickness in vertebral bone is mainly required to ascertain the optimal fiber distance of the optical probe and the effect of the thickness range on spectral changes. Ritzel et al.[46] found a significant loss of cortical thickness in the lower thoracic and lumbar spine in patients with osteoporosis. Effect of various bone related diseases on the thickness of cortical boundary needs to be further investigated.

We found a strong correlation between simulated and experimentally measured DR spectra (see Fig. 2.7). The initial deviation of the spectra between 1000 and 1100 nm can be attributed to the discrepancies in the wavelength-dependent scattering coefficients derived from the Farrell model [33], which is used as input for the MC model. The fact that the fat content found in the two spectra showed close agreement (Table 2.4), further strengthens this claim.

A three-layered MC model was developed and an insertion of an optical probe penetrating through cancellous bone and touching cortical bone was simulated. This simulated insertion was then compared to an image-guided experimental insertion (see Fig. 2.8) of an in-house developed optical screw probe.

During the modeled insertion, the fat content [Fig. 2.8(b)] was observed to drop more than 1 mm before the cortical bone boundary. The image-guided experimental insertion also showed a drop in fat more than 1 mm before cortical contact. However, the decrease in measured fat content was found to be more gradual [Fig. 2.8(d)]. In both types of insertions, the drop in fat content or the fat transition was seen before the modeled optical probe or optical screw probe reached the cortical boundary, thereby indicating the potential of breach detection. Although widely used, the MC model used in this study has limitations, which stem from the assumptions inherent in the model development. The model assumes each tissue layer to be homogenous in nature, which

implies that optical properties are uniformly distributed throughout each tissue layer. Cancellous bone consists of organic compounds, such as blood and fat, within its inorganic porous structure. Therefore, treating cancellous bone as a homogenous tissue is not fully true, which might influence the fat transition or the breach transition profile as the optical screw penetrates from cancellous to cortical bone. The higher variation in the fat content within cancellous bone, observed in the experimental insertion [Fig. 2.8(d)] as compared to the simulation [Fig. 2.8(b)] insertion, seems to support this observation. To overcome this limitation and model the heterogeneities of cancellous bone, one possible solution could be to randomly burry well-defined geometric shapes containing blood and fat optical properties within cancellous bone. Early work by Smithies and Butler,[47] Lucassen et al.[48], and Wang et al.[49] and more recent work by Zhu [50] could be a good starting point for such a model development. Margallo-Balbás and French [51] propose another interesting approach by modeling the complex trabecular bone structure using the geometry recovered from microCT data. All of these different approaches to model the bone tissue types as close to reality as possible could enhance the understanding of breach transition profiles. Assumptions made in the Farrell model used to calculate fat content from spectra might also influence the model validity [28].

It must be noted that these breach transition profiles are a function of several factors including fiber-to-fiber distance of the probe, incident light geometry, optical properties of the tissue layers, thickness of the cortical boundary, and probe angulation with respect to the cortical boundary. The influence and interaction of these parameters on the breach transition profile needs to be explored further.

Successful clinical adoption of DRS as a guidance system holds several different kinds of challenges. Real-time guidance of instrument or screw provided by DRS would have to be integrated seamlessly into the existing clinical workflow. In order to achieve this, several outcome measures, such as surgery time, radiation exposure, sensitivity, and specificity of breaches detection, would have to be tested in a clinical setting. We hypothesize that surgery time to either shorten or remain constant due to the added feedback at the tip of the instrument. This could potentially boost the surgeon's confidence for safe screw placement. This could also lead to fewer safety measures, such as repeated tactile probing events and image acquisitions during surgery, thereby contributing toward reduction in infection rates and revision surgeries [13, 14]. However, the additional set-up time for the DRS system to run optimally needs to be considered as well. Investigating the value of DRS in the clinical environment shall be part of future studies.

2.5. CONCLUSION

This study shows that spectral tissue sensing, based on DRS at the needle tip, is a promising technique to detect cortical boundary perforations or breaches during spinal screw placement. In this *ex vivo* study, fat content, blood content, and photon scattering were found to be statistically different in cancellous bone as compared to cortical bone. Fat content was found to be significantly higher in cancellous bone compared to cortical bone. This finding was consistent with a drop in fat content observed before a simulated probe reached the cortical bone. An image-guided experimental insertion gave similar results, thus pointing to the potential of DRS as a sensing tool at the instrument tip in aiding the detection of cortical boundary breaches.

REFERENCES

[1] A. Swamy, G. Burström, J. W. Spliethoff, D. Babic, C. Reich, J. Groen, E. Edström, A. E. Terander, J. M. Racadio, J. Dankelman, *et al.*, "Diffuse reflectance spectroscopy, a potential optical sensing technology for the detection of cortical breaches during spinal screw placement," *Journal of biomedical optics*, vol. 24, no. 1, p. 017002, 2019.

[2] K. Kobayashi, K. Ando, Y. Nishida, N. Ishiguro, and S. Imagama, "Epidemiological trends in spine surgery over 10 years in a multicenter database," *European Spine Journal*, vol. 27, no. 8, pp. 1698–1703, 2018.

[3] C. P. Thirukumaran, B. Raudenbush, Y. Li, R. Molinari, P. Rubery, and A. Mesfin, "National trends in the surgical management of adult lumbar isthmic spondylolisthesis: 1998 to 2011," *Spine*, vol. 41, no. 6, pp. 490–501, 2016.

[4] P. A. Cortesi, R. Assietti, F. Cuzzocrea, D. Prestamburgo, M. Pluderi, P. Cozzolino, P. Tito, R. Vanelli, D. Cecconi, S. Borsa, *et al.*, "Epidemiologic and economic burden attributable to first spinal fusion surgery," *Spine*, vol. 42, no. 18, pp. 1398–1404, 2017.

[5] R. W. Gaines Jr, "The use of pedicle-screw internal fixation for the operative treatment of spinal disorders," *JBJS*, vol. 82, no. 10, p. 1458, 2000.

[6] L. Balabaud, S. Pitel, I. Caux, C. Dova, B. Richard, P. Antonietti, and C. Mazel, "Lumbar spine surgery in patients 80 years of age or older: morbidity and mortality," *European Journal of Orthopaedic Surgery & Traumatology*, vol. 25, no. 1, pp. 205–212, 2015.

[7] J. Ma, S. Fan, and F. Zhao, "Intraoperative malposition of pedicle probe or screws: a potential cause of the acceleration of degeneration in superior adjacent intervertebral disc," *Medical hypotheses*, vol. 77, no. 6, pp. 1102–1104, 2011.

[8] N. E. Epstein, "A review of medicolegal malpractice suits involving cervical spine: what can we learn or change?," *Clinical Spine Surgery*, vol. 24, no. 1, pp. 15–19, 2011.

[9] A. Manbachi, R. S. Cobbold, and H. J. Ginsberg, "Guided pedicle screw insertion: techniques and training," *The Spine Journal*, vol. 14, no. 1, pp. 165–179, 2014.

[10] Y. Hojo, M. Ito, K. Suda, I. Oda, H. Yoshimoto, and K. Abumi, "A multicenter study on accuracy and complications of freehand placement of cervical pedicle screws under lateral fluoroscopy in different pathological conditions: Ct-based evaluation of more than 1,000 screws," *European Spine Journal*, vol. 23, no. 10, pp. 2166–2174, 2014.

[11] A. Elmi-Terander, H. Skulason, M. Söderman, J. Racadio, R. Homan, D. Babic, N. van der Vaart, and R. Nachabe, "Surgical navigation technology based on augmented reality and integrated 3d intraoperative imaging: a spine cadaveric feasibility and accuracy study," *Spine*, vol. 41, no. 21, p. E1303, 2016.

[12] Y. J. Kim, L. G. Lenke, K. H. Bridwell, Y. S. Cho, and K. D. Riew, "Free hand pedicle screw placement in the thoracic spine: is it safe?," *Spine*, vol. 29, no. 3, pp. 333–342, 2004.

[13] B. I. Martin, S. K. Mirza, B. A. Comstock, D. T. Gray, W. Kreuter, and R. A. Deyo, "Reoperation rates following lumbar spine surgery and the influence of spinal fusion procedures," *Spine*, vol. 32, no. 3, pp. 382–387, 2007.

[14] J. S. Smith, C. I. Shaffrey, C. A. Sansur, S. H. Berven, K.-M. G. Fu, P. A. Broadstone, T. J. Choma, M. J. Goytan, H. H. Noordeen, D. R. Knapp Jr, *et al.*, "Rates of infection after spine surgery based on 108,419 procedures: a report from the scoliosis research society morbidity and mortality committee," *Spine*, vol. 36, no. 7, pp. 556–563, 2011.

[15] V. Kosmopoulos and C. Schizas, "Pedicle screw placement accuracy: a meta-analysis," *Spine*, vol. 32, no. 3, pp. E111–E120, 2007.

[16] A. Mason, R. Paulsen, J. M. Babuska, S. Rajpal, S. Burneikiene, E. L. Nelson, and A. T. Villavicencio, "The accuracy of pedicle screw placement using intraoperative image guidance systems: A systematic review," *Journal of Neurosurgery: Spine*, vol. 20, no. 2, pp. 196–203, 2014.

[17] D. Evers, B. Hendriks, G. Lucassen, and T. Ruers, "Optical spectroscopy: current advances and future applications in cancer diagnostics and therapy," *Future oncology*, vol. 8, no. 3, pp. 307–320, 2012.

[18] D. Evers, R. Nachabe, D. Hompes, F. Van Coevorden, G. Lucassen, B. Hendriks, M.-L. van Velthuysen, J. Wesseling, and T. Ruers, "Optical sensing for tumor detection in the liver," *European Journal of Surgical Oncology (EJSO)*, vol. 39, no. 1, pp. 68–75, 2013.

[19] J. W. Spliethoff, E. Tanis, D. J. Evers, B. H. Hendriks, W. Prevoo, and T. J. Ruers, "Monitoring of tumor radio frequency ablation using derivative spectroscopy," *Journal of biomedical optics*, vol. 19, no. 9, p. 097004, 2014.

[20] J. W. Spliethoff, D. J. Evers, H. M. Klomp, J. W. van Sandick, M. W. Wouters, R. Nachabe, G. W. Lucassen, B. H. Hendriks, J. Wesseling, and T. J. Ruers, "Improved identification of peripheral lung tumors by using diffuse reflectance and fluorescence spectroscopy," *Lung cancer*, vol. 80, no. 2, pp. 165–171, 2013.

[21] L. De Boer, B. Molenkamp, T. Bydlon, B. Hendriks, J. Wesseling, H. Sterenborg, and T. J. Ruers, "Fat/water ratios measured with diffuse reflectance spectroscopy to detect breast tumor boundaries," *Breast cancer research and treatment*, vol. 152, no. 3, pp. 509–518, 2015.

[22] B. H. Hendriks, A. J. Balthasar, G. W. Lucassen, M. van der Voort, M. Mueller, V. V. Pully, T. M. Bydlon, C. Reich, A. T. van Keersop, J. Kortsmit, *et al.*, "Nerve detection with optical spectroscopy for regional anesthesia procedures," *Journal of translational medicine*, vol. 13, no. 1, p. 380, 2015.

[23] J. P. Rathmell, A. E. Desjardins, M. van der Voort, B. H. Hendriks, R. Nachabe, S. Roggeveen, D. Babic, M. Söderman, M. Brynolf, and B. Holmström, "Identification of the epidural space with optical spectroscopyanin vivo swine study," *Anesthesiology: The Journal of the American Society of Anesthesiologists*, vol. 113, no. 6, pp. 1406–1418, 2010.

[24] W. Li, Y. Liu, and Z. Qian, "Determination of detection depth of optical probe in pedicle screw measurement device," *Biomedical engineering online*, vol. 13, no. 1, p. 148, 2014.

[25] Y. Liu, Y. Wang, Z. Qian, J. Zhao, X. Cao, and W. Li, "Monitoring the reduced scattering coefficient of bone tissues on the trajectory of pedicle screw placement using near-infrared spectroscopy," *Journal of biomedical optics*, vol. 19, no. 11, p. 117002, 2014.

[26] W. Li, Y. Liu, H. Sun, Y. Pan, and Z. Qian, "Monitoring reduced scattering coefficient in pedicle screw insertion trajectory using near-infrared spectroscopy," *Medical & biological engineering & computing*, vol. 54, no. 10, pp. 1533–1539, 2016.

[27] C. Zhu and Q. Liu, "Review of monte carlo modeling of light transport in tissues," *Journal of biomedical optics*, vol. 18, no. 5, p. 050902, 2013.

[28] R. Nachabe, B. H. Hendriks, A. E. Desjardins, M. van der Voort, M. B. van der Mark, and H. J. Sterenborg, "Estimation of lipid and water concentrations in scattering media with diffuse optical spectroscopy from 900 to 1600 nm," *Journal of biomedical optics*, vol. 15, no. 3, p. 037015, 2010.

[29] R. Nachabé, B. H. Hendriks, M. van der Voort, A. E. Desjardins, and H. J. Sterenborg, "Estimation of biological chromophores using diffuse optical spectroscopy: benefit of extending the uv-vis wavelength range to include 1000 to 1600 nm," *Biomedical optics express*, vol. 1, no. 5, pp. 1432–1442, 2010.

[30] T. M. Bydlon, R. Nachabé, N. Ramanujam, H. J. Sterenborg, and B. H. Hendriks, "Chromophore based analyses of steady-state diffuse reflectance spectroscopy: current status and perspectives for clinical adoption," *Journal of biophotonics*, vol. 8, no. 1-2, pp. 9–24, 2015.

[31] C. T. Rueden, J. Schindelin, M. C. Hiner, B. E. DeZonia, A. E. Walter, E. T. Arena, and K. W. Eliceiri, "Imagej2: Imagej for the next generation of scientific image data," *BMC bioinformatics*, vol. 18, no. 1, p. 529, 2017.

[32] L. Wang, S. L. Jacques, and L. Zheng, "Mcml—monte carlo modeling of light transport in multi-layered tissues," *Computer methods and programs in biomedicine*, vol. 47, no. 2, pp. 131–146, 1995.

[33] T. J. Farrell, M. S. Patterson, and B. Wilson, "A diffusion theory model of spatially resolved, steady-state diffuse reflectance for the noninvasive determination of tissue optical properties in vivo," *Medical physics*, vol. 19, no. 4, pp. 879–888, 1992.

[34] T. Vo-Dinh, *Biomedical photonics handbook: biomedical diagnostics*. CRC press, 2014.

[35] E. N. Marieb and K. Hoehn, *Human anatomy & physiology*. Pearson education, 2007.

[36] M. Buchan and G. Anderson, "Time since death: a review of the current status of methods used in the later postmortem interval," *Canadian Society of Forensic Science Journal*, vol. 34, no. 1, pp. 1–22, 2001.

[37] A. Régis-Arnaud, B. Guiu1, P.-M. Walker, D. Krausé, F. Ricolfi, and D. B. Salem, "Bone marrow fat quantification of osteoporotic vertebral compression fractures: comparison of multi-voxel proton mr spectroscopy and chemical-shift gradient-echo mr imaging," *Acta radiologica*, vol. 52, no. 9, pp. 1032–1036, 2011.

[38] T. Baum, S. P. Yap, D. C. Karampinos, L. Nardo, D. Kuo, A. J. Burghardt, U. B. Masharani, A. V. Schwartz, X. Li, and T. M. Link, "Does vertebral bone marrow fat content correlate with abdominal adipose tissue, lumbar spine bone mineral density, and blood biomarkers in women with type 2 diabetes mellitus?," *Journal of Magnetic Resonance Imaging*, vol. 35, no. 1, pp. 117–124, 2012.

[39] R. V. Mulkern, J. Huang, S. Vajapeyam, A. B. Packard, K. Oshio, and S. Grinspoon, "Fat fractions and spectral t2 values in vertebral bone marrow in hiv-and non-hiv-infected men: a 1h spectroscopic imaging study," *Magnetic Resonance in Medicine: An Official Journal of the International Society for Magnetic Resonance in Medicine*, vol. 52, no. 3, pp. 552–558, 2004.

[40] M. A. Bredella, M. Torriani, R. H. Ghomi, B. J. Thomas, D. J. Brick, A. V. Gerweck, C. J. Rosen, A. Klibanski, and K. K. Miller, "Vertebral bone marrow fat is positively associated with visceral fat and inversely associated with igf-1 in obese women," *Obesity*, vol. 19, no. 1, pp. 49–53, 2011.

[41] R. Nachabé, J. W. van der Hoorn, R. van de Molengraaf, R. Lamerichs, J. Pikkemaat, C. F. Sio, B. H. Hendriks, and H. J. Sterenborg, "Validation of interventional fiber optic spectroscopy with mr spectroscopy, mas-nmr spectroscopy, high-performance thin-layer chromatography, and histopathology for accurate hepatic fat quantification," *Investigative radiology*, vol. 47, no. 4, pp. 209–216, 2012.

[42] S. Ruschke, A. Pokorney, T. Baum, H. Eggers, J. H. Miller, H. H. Hu, and D. C. Karampinos, "Measurement of vertebral bone marrow proton density fat fraction in children using quantitative water–fat mri," *Magnetic Resonance Materials in Physics, Biology and Medicine*, vol. 30, no. 5, pp. 449–460, 2017.

[43] J.-P. Kühn, D. Hernando, P. J. Meffert, S. Reeder, N. Hosten, R. Laqua, A. Steveling, S. Ender, H. Schröder, and D.-T. Pillich, "Proton-density fat fraction and simultaneous r2* estimation as an mri tool for assessment of osteoporosis," *European radiology*, vol. 23, no. 12, pp. 3432–3439, 2013.

[44] M. Yusof, L. Ming, and M. Abdullah, "Computed tomographic measurement of cervical pedicles for transpedicular fixation in a malay population," *Journal of Orthopaedic Surgery*, vol. 15, no. 2, pp. 187–190, 2007.

[45] P. Chanplakorn, C. Kraiwattanapong, K. Aroonjarattham, P. Leelapattana, G. Keorochana, S. Jaovisidha, and W. Wajanavisit, "Morphometric evaluation of subaxial cervical spine using multi-detector computerized tomography (md-ct) scan: the consideration for cervical pedicle screws fixation," *BMC musculoskeletal disorders*, vol. 15, no. 1, p. 125, 2014.

[46] H. Ritzel, M. Amling, M. Pösl, M. Hahn, and G. Delling, "The thickness of human vertebral cortical bone and its changes in aging and osteoporosis: A histomorphometric analysis of the complete spinal column from thirty-seven autopsy specimens," *Journal of Bone and Mineral Research*, vol. 12, no. 1, pp. 89–95, 1997.

[47] D. J. Smithies and P. H. Butler, "Modelling the distribution of laser light in port-wine stains with the monte carlo method," *Physics in Medicine & Biology*, vol. 40, no. 5, p. 701, 1995.

[48] G. W. Lucassen, W. Verkruysse, M. Keijzer, and M. J. van Gemert, "Light distributions in a port wine stain model containing multiple cylindrical and curved blood vessels," *Lasers in Surgery and Medicine: The Official Journal of the American Society for Laser Medicine and Surgery*, vol. 18, no. 4, pp. 345–357, 1996.

[49] L. V. Wang, R. E. Nordquist, and W. R. Chen, "Optimal beam size for light delivery to absorption-enhanced tumors buried in biological tissues and effect of multiple-beam delivery: a monte carlo study," *Applied optics*, vol. 36, no. 31, pp. 8286–8291, 1997.

[50] C. Zhu and Q. Liu, "Hybrid method for fast monte carlo simulation of diffuse reflectance from a multilayered tissue model with tumor-like heterogeneities," *Journal of biomedical optics*, vol. 17, no. 1, p. 010501, 2012.

[51] E. Margallo-Balbás and P. J. French, "Shape based monte carlo code for light transport in complex heterogeneous tissues," *Optics express*, vol. 15, no. 21, pp. 14086–14098, 2007.

3

VALIDATION OF DIFFUSE REFLECTANCE SPECTROSCOPY WITH MAGNETIC RESONANCE IMAGING FOR ACCURATE VERTEBRAL BONE FAT FRACTION QUANTIFICATION

Safe and accurate placement of pedicle screws remains a critical step in open and minimally invasive spine surgery. The diffuse reflectance spectroscopy (DRS) technique may offer the possibility of intra-operative guidance for pedicle screw placement. Currently, Magnetic Resonance Imaging (MRI) is one of the most accurate techniques used to measure fat concentration in tissues. Therefore, the purpose of this study is to compare the accuracy of fat content measured invasively in vertebrae using DRS and validate it against the Proton density fat fraction (PDFF) derived via MRI. Chemical shift-encoding-based water-fat imaging of the spine was first performed on six cadavers. PDFF images were computed and manually segmented. 23 insertions using a custom-made screw probe with integrated optical fibers were then performed under cone beam computer tomography (CBCT). DR spectra were recorded at several positions along the trajectory as the optical screw probe was inserted turn by turn into the vertebral body. Fat fractions determined via DRS and MRI techniques were compared by spatially correlating the optical screw probe position within the vertebrae on CBCT images with respect to the PDFF images. The fat fraction determined by DRS was found to have a high correlation with those determined by MRI, with a Pearson coefficient of 0.950 (P< 0.001) as compared with PDFF measurements calculated from the MRI technique.

Swamy A., Burström G., Spliethoff J.W., Babic D., Ruschke S., Racadio J.M., Edström E., Elmi-Terander A., Dankelman J. and Hendriks B.H.W. Validation of diffuse reflectance spectroscopy with magnetic resonance imaging for accurate vertebral bone fat fraction quantification. Biomedical optics express., 10(8), 2019.

3.1. INTRODUCTION

Spinal fusion surgeries are on the rise all over the world due to aging populations and a trend towards accepting elderly patients with increasingly complex medical histories [2, 3]. During spinal fusion surgery, pedicle screws are commonly placed into the vertebrae to serve as anchoring points for rigid constructs, in order to fuse parts of the spine [4]. Inaccurate placement of pedicle screws could potentially lead to severe vascular and neurological injuries in patients [5–7]. Adding to the complexity of the procedure, minimally invasive surgeries (MIS) are rapidly increasing and might involve more than half of all spinal procedures by 2020 [8]. MIS procedures, significantly reduce blood loss, shorten hospital stay and decrease surgical site infections [9–13]. MIS is performed through a series of small incisions, and requires guidance techniques to compensate for the limited visibility of important anatomical landmarks. There are several guidance techniques for accurate and safe pedicle screw placement. These include navigation systems and other non-imaging based techniques[14]. Pedicle screws could be placed by free-hand technique or fluoroscopy guided techniques, where the surgeon relies on experience, tactile feedback, and identifying anatomical landmarks. However, the accuracy rates of pedicle screw placement as reported in the literature are as low as 27.6 % and as high as 100 % based on a meta-analysis by Kosmopoulous et al. [15]. A more recent meta-analysis study found an accuracy range of 50- 92 % [16]. These inaccuracies translates into screw revisions being needed in 6.0 % of operated patients, according to a recent systematic review by Staartjes et al.[17]. Therefore, there is a need for more reliable and cost-effective solutions for increasing the accuracy and safety in the placement of spinal screw implants during spinal fusion surgery.

Diffuse reflectance spectroscopy (DRS) may offer the possibility of intra-operative guidance of surgical instruments or implants by determining fat and water content in vertebral bone in real-time along the screw path. The quantification of fat content relative to water content from DR spectra or Diffuse Reflectance-based Fat Fraction (DRFF) has been studied extensively by previous researchers [18–21]. Previously, the DRS technique has been used for fat fraction quantification in tissue types such as liver and breast for early diagnosis of nonalcoholic fatty liver disease and tumor detection [21–23]. The use of a custom-made screw probe with integrated fiber-optics to perform image-guided insertions in an *ex vivo* (human) setting has previously been described [24]. The optical screw probe was inserted into the vertebrae and with each turn, the local fat content of the bone at the probe tip was measured in real-time. It was found that fat content was a good discriminator for cancellous and cortical bone. Moreover, the probe could be used to predict the transition between the two bone types and thereby potentially be used to prevent pedicle screws from breaching the cortical border [24].

A logical next step is to get a better understanding of the variation of DRFF within vertebrae of patients who undergo spinal fusion surgery, as this is pivotal in the development of a robust optical guidance technique for pedicle screw placement procedures.

Currently, Magnetic Resonance Spectroscopy (MRS) and Magnetic Resonance Imaging (MRI) are the most common techniques used to non-invasively measure fat concentration in vertebral bone tissues [25–36]. The quantitative assessment of fat fraction in vertebral bone has multiple clinical applications, including the characterization of bone health for evaluating conditions such as osteoporosis [28, 33, 34, 37] diagnosis

of metabolic disorders such as obesity and diabetes [32, 38]; and cancer [39, 40]. Proton density fat fraction (PDFF) is the de facto standardized MR-based biomarker for the determination of tissue fat concentration measured via MRI, and is considered to accurately reflect the concentration of fat in tissues [25, 41]. Extensive clinical literature on PDFF measured non-invasively in vertebrae across patient cohorts of spinal fusion surgery, might help in providing crucial insights into the variation in DRFF measured along the optical screw path by the DRS technique. However, in order to do so, the DRFF would have to be benchmarked against the PDFF.

Therefore, the purpose of this study is to compare the accuracy of fat fraction measured invasively in vertebrae by the DRS technique (DRFF) and benchmark it to the PDFF parameter measured non-invasively via MRI.

3.2. METHODS

3.2.1. SPINAL TISSUES

A cadaver-based experiment was conducted at the Cincinnati Children's Hospital Medical Center, Ohio, United States. The donors allowed their bodies and body parts to be used for research and educational purposes. All ethical guidelines for human cadaver studies were followed. The characteristics of the studied cadavers (5 female, 1 male) are depicted in Table 3.1. No embalming process was used, neither were any of the cadavers frozen, in order to preserve the optical properties of the cadaver specimens.

Table 3.1: Cadaver information.

Cadaver #	Gender	Age (years)	Weight (kg)
1	Female	92	82
2	Female	82	77
3	Male	78	82
4	Female	53	77
5	Female	79	68
6	Female	83	77

3.2.2. MEASUREMENT PROTOCOL

MAGNETIC RESONANCE IMAGING

The entire spine of the cadavers was scanned on a 1.5 Tesla (T) whole-body scanner (Ingenia, Philips Healthcare, Best, Netherlands) while placed in the prone position on the table coil array. To obtain whole spine coverage, the MR exam consisted of three sagittal 3D spoiled gradient echo sequences placed on the cervical, thoracic and lumbar spine, respectively. The temperature of the cadavers was maintained close to room temperature prior to scanning.

A three-dimensional (3D) six-echo spoiled gradient-echo sequence was used for chemical shift-encoding-based water-fat separation. The typical imaging parameters used in this study were: 45-60 sagittal slices with a slice thickness of 3 mm; AP and FH field of view = 220-310 and 240-350 mm; in-plane resolution = (0.45-0.67) × (0.45-0.67) mm; flip angle = 5 degrees; TR = 9.9-15.87 ms; TE1 = 1.41-1.43 ms; $\triangle TE$ = 1.2 ms; total scan time per cadaver was approximately 5-10 minutes.

DIFFUSE REFLECTANCE SPECTROSCOPY

The DRS system consists of a tungsten halogen broadband light source (360 – 2500 nm) and optical spectrometers as shown in the schematic diagram of Fig. 3.1. The spectrometers collectively cover the visible, near-infrared and shortwave infrared wavelength range; the first spectrometer resolves light in the visible (Ocean Optics Maya2000Pro), while the second resolves light in the infrared wavelength range (Ocean Optics NirQuest), together resolving the light between 400 to 1600 nm. An in-house developed LabVIEW software (National Instruments, Austin, Texas) was used to control the spectrometers and acquire the data. The DRS system used in this study has been thoroughly described previously, along with the calibration procedure [19, 20, 42].

The custom-made optical screw probe (diameter: 5.5 mm) used to obtain DR spectra is illustrated in Fig. 3.1. The optical screw probe consisted of two optical fibers with core diameter of 200 μm. One of the fibers was used to transport the light from the source to the tissue, while the second fiber was used to transport the diffusely reflected light from the tissue to both spectrometers. The center-to-center distance between the collecting fiber and the delivering fiber was set at 1.22 mm as shown in Fig. 3.1. In previous work, a good trade-off was found between signal-to-noise ratio and probing depth based on a fiber-to-fiber distance of around 1.2 mm. The fiber distance was also chosen based on the largest penetration depth achievable, which was bounded by the optical screw probe diameter and manufacturing tolerances, in order to house the fibers in the screw.

After the MR exam, the cadavers were transferred to an operating table and placed in prone position. The spine was exposed using a midline approach. A total of 23 insertions were performed in six cadavers across levels ranging from cervical (C2) to lumbar (L5) using the optical screw probe. DR spectra were recorded at several positions along the trajectory, as the optical screw probe was inserted turn-by-turn into the vertebral body (Fig. 3.1). Five to ten DR spectra were acquired per turn. Subsequently, cone beam computer tomography (CBCT) images (AlluraClarity FD20; Philips Healthcare, Best, the Netherlands) were acquired at regular intervals based on the approximate probe positions within vertebral body. CBCT's were also acquired whenever a change in DRS readings were encountered to increase the likelihood of capturing all relevant positions within the vertebral body. The number of CBCT images acquired per insertion were 5-10.

3.2.3. DETERMINATION OF FAT FRACTION IN VERTEBRAL BONES

PROTON DENSITY FAT FRACTION

The scanner image reconstruction was utilized to obtain fat and water images using a DICOM image viewer software (Philips DICOM viewer R3.0-SP04, Philips Healthcare, Best, The Netherlands). The water—fat separation was based on a complex seven-peak

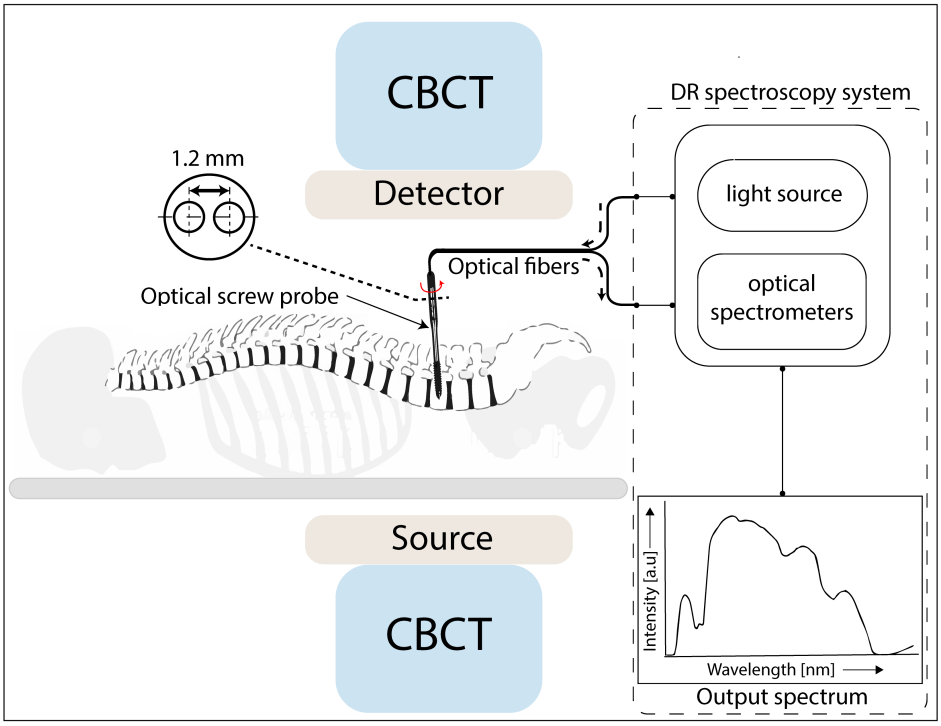

Figure 3.1: Schematic of the experimental setup. Turn-by-turn insertion of the optical screw probe with DR output spectra recording performed by the DRS system under intraoperative cone beam computer tomography (CBCT) acquisitions.

water—fat spectral model. Based on the fat (F) and water images (W), PDFF was thus calculated as:

$$PDFF[\%] = \frac{F}{F+W} \times 100.$$

In order to validate the PDFF images for accurate fat fraction quantification, a phantom of known fat fraction values ranging from 0 to 100 % (Calimetrix Fat fraction Phantom (Model 100), Sl no. F0008100) was scanned three times using the scatter settings mentioned above. The averaged PDFF measurements from multiple phantom scans were then compared to known fat fraction values of the phantom.

DIFFUSE REFLECTANCE FAT FRACTION

A modified version of the model developed by Farrell et al. [43] was used to extract tissue optical properties from the measured spectra. The absorption coefficient $\mu_a(\lambda)$ and reduced scattering coefficients $\mu_{s'}(\lambda)$ were extracted from the model expressed in cm^{-1}. From the known wavelength-dependent absorption coefficients and fiber distance between the emitting and collecting fibers, the amount of fat [%] and water [%] present in

the tissue probed locally were determined following a procedure as previously described by the group [17, 41]. DRFF was calculated as follows:

$$DRFF[\%] = \frac{Fat}{Fat + Water} \times 100.$$

3.2.4. FAT FRACTION CORRELATION SCHEME BETWEEN PDFF AND DRFF DETERMINATION

VERTEBRAL BODY REGION CORRELATION

In order to compare the DRFF and PDFF, the spatial location of the optical screw probe within the vertebral body was correlated with respect to CBCT images and PDFF images. First, a suitable image slice showing the location of the optical screw probe within the vertebral body was selected by a trained physician by toggling through the sagittal, axial and coronal slices of the CBCT data sets. A CBCT image showing the optical screw probe in a sagittal slice of one such insertion is shown in Fig. 3.1a. By identifying and matching anatomical landmarks and features in the CBCT image, the corresponding PDFF image was then selected. Manual determination of the vertebral bone marrow fat fraction was performed by placing circular regions of interests (ROIs) in the PDFF image as shown in Fig. 2b. The radius of the circular ROI was set between 2.7- 3.0 pixels. The ROI radius was calculated based on the approximate linear distance travelled by the optical screw probe due to 1-2 consecutive turns from the position found in the CBCT image. Thus, spatially correlating the PDFF pixels with DRFF probing volume. The average PDFF, standard deviation (SD), standard error (SE) from all pixels lying within the circular ROI were extracted and compared to DRS measurements.

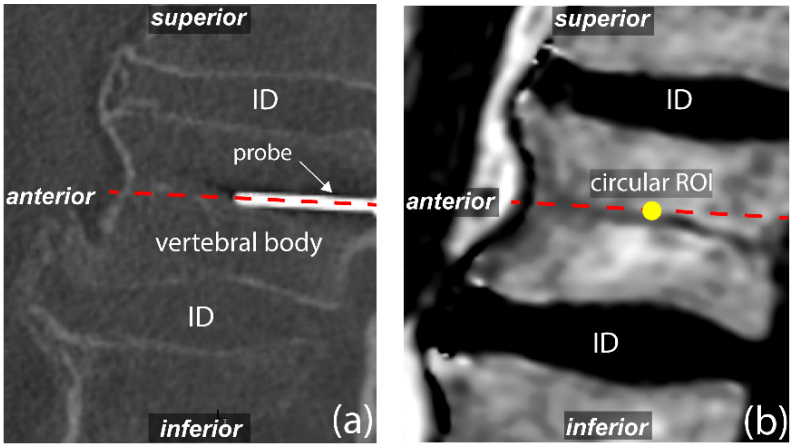

Figure 3.2: (a) Sagittal slice showing optical screw probe within vertebral body. (b) MR image depicting circular ROI placement for PDFF extraction. Thick dashed line illustrates trajectory of optical screw probe. *ID = Intervertebral disc.

3.2.5. STATISTICAL ANALYSIS

The data obtained from each technique was tested using the Jarque-Bera test for normality [44] and was found to come from a normal distribution. Thus, the estimated fat fractions are calculated as mean ± SD and SE.

A one-sample t-test was applied to evaluate whether fat fraction obtained via DRS is significantly different from fat fraction obtained via MRI. Pearson correlation coefficient was used to assess the linearity in the estimated fat fraction determined by DRS as compared to PDFF values determined by MRI. Pairwise linear regression fits were also performed to assess the relation of fat fraction estimation between DRS and MRI. SE values were taken as weighing factor in the linear regression fits based on the maximum likelihood estimation statistical technique [45]. For each regression coefficient, a 95% confidence interval was also calculated.

3.3. RESULTS

3.3.1. PHANTOM FAT FRACTION MEASUREMENTS

PDFF values calculated via MRI were found to be statistically similar to the known fat fraction values of the reference phantom (P = 0.187). MRI for PDFF quantification showed a very high correlation with Pearson coefficient above 0.990 (P<0.001), as compared to known reference phantom fat fraction measurements as depicted in Fig. 3.3a.

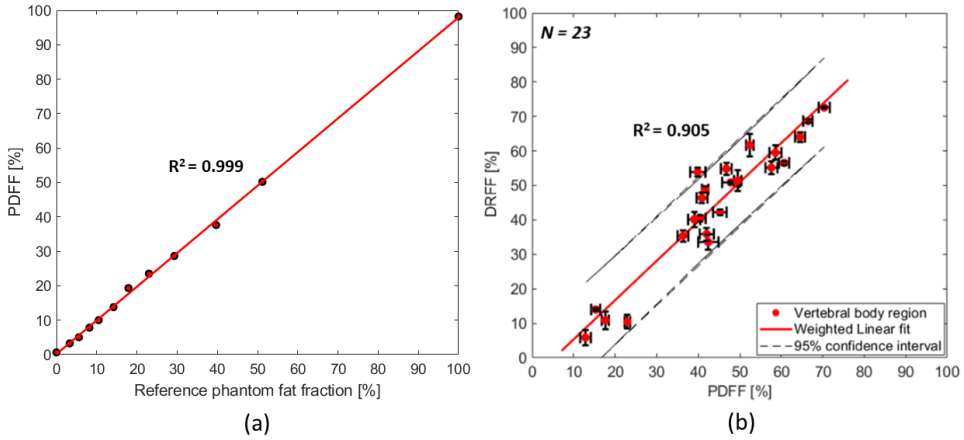

Figure 3.3: (a) Correlation plot depicting PDFF determined via MRI as compared to known phantom fat fraction measurements.(b) Correlation plot depicting mean and standard error of fat fraction determined by DRS versus MRI Imaging. Correlation of fat fraction between two techniques in vertebral body region of the vertebrae. Error bars indicate SE.

3.3.2. CADAVER FAT FRACTION MEASUREMENTS

Figure 3.3b. shows the correlation of PDFF versus DRFF. The DRFF values were found to be statistically similar to the PDFF values (P = 0.969). DRFF was found to have high correlation with Pearson coefficient of 0.950 (P< 0.001) as compared to PDFF measurements. Additionally, based on the linear regression coefficient (R^2 = 0.905), the results of

the two techniques were highly correlated. Figure 3.4b(a)-(f) illustrate the spatial variation of vertebral fat fraction along the spines of six cadavers studied according to the MRI measurements. PDFF averaged over cervical, thoracic and lumbar regions of the spine for all cadavers is given in Table 2.

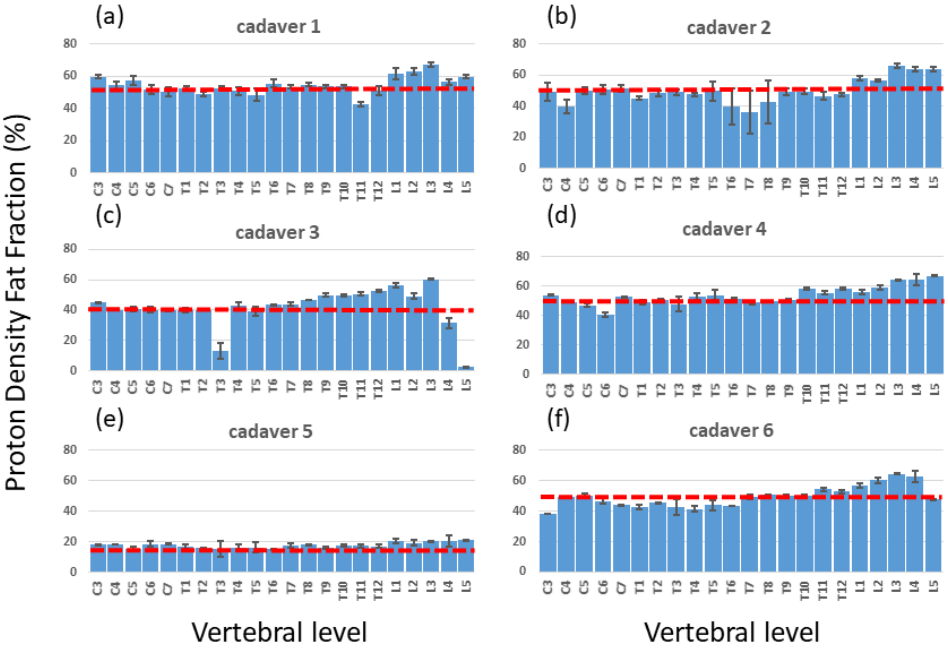

Figure 3.4: (a) Anatomical variation of vertebral body PDFF across whole spines of six cadavers. The dotted line represents the mean fat fraction across cervical to lumbar vertebral levels.

3.4. DISCUSSION

In the present study, we evaluated the measurements of fat fraction, determined by the DRS sensing technique during insertion of a custom-made optical screw probe into the vertebrae of six human cadavers. These measurements were compared with *ex vivo* MRI measurements, which is the clinically standardized technique for non-invasive fat fraction measurements in biological tissues [41].

Fat fraction quantification within vertebral body regions of the spine using the DRS technique, showed to be in good agreement with values obtained by MRI technique. The error bars arising from the fat fraction measurement via the MRI technique are a consequence of variation of fat fraction within the chosen region of interest on the PDFF images. The source of variation indicated by the error bars in Fig. 3.3b can be attributed to inherent heterogeneities within vertebrae especially due to random distribution of triglyceride (fat) storage sites within the trabecular structure of cancellous bone [46]. The source of variation in DRFF can also be linked to the inherent heterogeneities of vertebral bone samples since, each DRS mean and SE value is based on two to three

Table 3.2: Mean ± SD of vertebral body region PDFF averaged over cervical, thoracic and lumbar vertebral levels according to MRI measurements.

Levels	Cadaver 1	Cadaver 2	Cadaver 3	Cadaver 4	Cadaver 5	Cadaver 6
C3-C7	54.7 ± 3.9%	48.2 ± 4.9%	41.2 ± 2.2%	48.7 ± 5.3%	17.7 ± 1.4%	45.6 ± 4.8%
T1-T6	51.4 ± 2.7%	46.5 ± 3.7%	36.6 ± 11.6%	51.0 ± 2.3%	15.9 ± 0.6%	43.4 ± 1.3%
T7-T12	51.5 ± 4.6%	45.3 ± 5.1%	48.8 ± 3.1%	53.4 ± 4.3%	17.2 ± 0.7%	51.3 ± 1.9%
L1-L5	61.4 ± 3.9%	61.7± 4.2%	39.9 ± 23.6%	62.1 ± 4.4%	20.2 ± 0.6%	58.4 ± 6.7%
All levels	54.5 ± 5.4%	50.0 ± 7.8%	41.7 ± 12.8%	53.6 ± 6.3%	17.6 ± 1.8%	49.5 ± 6.9%

unique measurement positions of the probe tip within the bone. Uncertainties also arise from the assumptions made by the Farrell model used to quantify fat fraction from the DRS signal [19].

It is worth noting that there is a fundamental difference between how fat fraction is determined via the MRI and DRS technique. The MR signal and assumed signal model reflects a tissue property referred to as proton density. It aims for the proton density of only triglycerides and water, respectively. Whereas, the DR signal model reflects the tissue property based on the interactions of photons within the finite volume of tissue probed locally. Although PDFF is capturing a fundamentally different property as compared to DRFF, the measured properties should highly correlate with each other as they attempt to measure similar tissue properties.

The PDFF distribution within the vertebral body across L1-L5 lumbar levels of the spine was found in the range of 40 – 62% across all cadavers with an exception of cadaver 5 (Fig. 3.4a-f). These cadavers had a mean age of 78 years (Table 3.1). Cadavers studied in the *ex vivo* setting in this study belonged to the older adults patient cohort. This patient cohort is the most common cohort for spinal surgery, suffering from back pain due to a wide variety of indications including degenerative disorders such as degenerative disc disease, spinal stenosis, spondylolysis, spondylolisthesis [47] and vertebral fractures [48].

Kuhn et al. [49] measured the PDFF of 51 men and women (mean age = 69.7 ± 9 years) from four levels (L1-L4) and found the average PDFF to be equal to 57.7 ± 14.4% in all patients. Patients whose vertebral bodies were osteoporotic had a significantly higher PDFF (mean PDFF = 62.4 ± 11%) compared to patients with healthy vertebrae (mean PDFF = 56.3 ± 14.8%). A similar study conducted by the group of Yeung et al. [50] found the same ball park of PDFF between healthy and osteoporotic patients. Schwartz et al. [51] measured bone marrow fat in an Icelandic population, from four vertebral levels (L1-L4) of 257 men and women (mean age = 79 ± 3.1 years), using the MRS technique. They found the mean fat fraction to be equal to 53.5% ± 8.1% in men and 55.0% ± 8.4%

in women.

The PDFF measured non-invasively in these older patient cohorts' indicate differences in fat content in vertebrae due to gender and diseases such as osteoporosis. However, the range of PDFF measured in these patients in an *in vivo* setting were found to lie within the range of 40-62% of PDFF measured in the *ex vivo* human setting in this study.

Cadaver5 was found to have lower PDFF compared to the rest of the cadavers studied. The patient was found to suffer from malignant neoplasm of the esophagus, which might have been the cause of the low PDFF found across all spinal levels. Patients with active malignancy would have a higher chance of perioperative complications [52] and would be less likely to be considered for spinal fusion surgery. Still, in cases of malignances, the DRS technique needs to be further investigated before its use in a clinical setting.

Cadaver3 was found to have low fat fraction within the vertebral body of T3, L4 and L5 (Fig. 3.4c) using the method described in this study. It should be noted, however, that these vertebrae showed a clear pathology and altered anatomy based on water and fat MRI images. Thus, the measurements were most likely not representative of vertebral body tissue at all. Possible reasons for this could be an underlying malignancy or posterior vertebral scalloping, an effect of a multitude of different conditions including dural ectasia and intraspinal tumors deforming the vertebra [53].

Another patient cohort who undergoes spinal fusion surgery are adolescents suffering from spinal deformities. Adolescent Idiopathic Scoliosis (AIS) is a structural threedimensional deformity of the spine that affects children during puberty [54]. In cases of severe deformity, surgical intervention is needed and typically involves instrumentation at multiple vertebral levels in both the thoracic and lumbar spine. None of the cadavers in this study belonged to this patient cohort. However, Ruschke et al. [56] measured the PDFF of 93 otherwise healthy children whose ages ranged between 9 and 18 years. They found the variation of PDFF in this patient cohort to be between 19% (at C3) and 40% (at L5) with a mean PDFF of 33.8%.

Therefore, based on *in vivo* human PDFF measurements across these MR studies, variation of fat fraction due to age, gender, vertebral levels and diseases exists [30, 55, 56]. Moreover, variations of fat fraction across the two patient cohorts', older adults and adolescents also exists.

Exploring the performance of DRS closer to the cortical bone than was measured in this study would be of interest for verifying it in the context of detecting the cortical border. However, such measurements introduce significant measurement inaccuracies when trying to correlate the position of probe in the CBCT (hence, the DRFF) to the precise location of cortical bone boundary ahead of probe in the PDFF image. Therefore, for the purpose of this study, we focused on correlating fat fraction values in areas where spatial correlation was less sensitive to errors. In future studies, it will therefore be of interest to further investigate the fat correlation close to or at the cortical border.

Our study had some limitations. Identification of the appropriate PDFF sagittal slice based on position of the optical screw probe within the bone from CBCT images was performed manually. An automated algorithm to fuse PDFF images with CBCT images in order to precisely match the probe position within the PDFF map might be a superior approach. Fat fraction maps were segmented manually. An automatic segmentation al-

gorithm might be preferable. However, the method of fat fraction quantification via MRI was reproduced based on studies by previous researchers [30, 55]. The assumed water-fat model for the calculation of PDFF does not correct for temperature shifts and may also be prone to potential model mismatches. However, the expected bias is expected to be low as the validation of PDFF measurements were performed using a calibration phantom.

Previously, Meritt et al. [57] used a combination of frequency-domain and steady-state optical spectroscopy system to compare the fat fraction with MRI on emulsion phantoms. They used a wavelength window of 650-1000 nm range and found a high correlation between the two techniques as well. Nachabe et al. [21] used an even wider wavelength window of 450-1800 nm for benchmarking the spectroscopy technique with MRS in liver of mice and found a high Pearson's correlation coefficient of 0.993. However, to the best of our knowledge this is the first study to validate the invasive DRS technique against the MRI technique in order to use fat fraction as a sensing parameter for instrument breach detection during spinal fusion surgery.

In our study, the distribution of fat fraction in the vertebral body across all vertebral levels was found to be in the range of 41.7-54.5% (Table 3.2) in the older adult cohort. However, for the DRS technique to measure fat fraction along the screw path, the technique would have to accommodate for the variation in fat fraction within the vertebral body region due to age, gender, vertebral levels and comorbidities. These factors could be used as classification categories during the development of the breach detection algorithm. For instance, the apparent large differences in fat fraction ranges between older patient cohort and the young adolescent cohort should be taken into account by possibly adapting the fat fraction thresholding window manually or by incorporating artificially intelligent data-driven statistical techniques into the sensing algorithm. Moreover, in a previous study [24] we showed that apart from fat fraction, blood content and photon scattering might also be useful parameters for breach detection; however, further studies are required to strengthen this claim.

Successful adoption of the DRS technique into the surgical theatre depends on its clinical usefulness in relation to other currently used methods for improving accuracy. These methods include 3D navigation and robotics [58–61]. They have both been shown to improve accuracy and to decrease revision surgery rates compared to the free-hand technique. However, even though these technologies improve the accuracy there is still a remaining share of misplaced screws [17, 62, 63]. DRS would provide an additional, and different, approach to reducing the rate of misplaced screws. Where navigation and robotics improve spatial orientation, DRS would provide a warning that there was a tissue change. This means DRS implementation in surgical instruments could be an adjunct to other technologies to further increase accuracy. Where costs are of great importance, DRS could also prove to be a more cost-effective solution, compared to the large investments needed for navigation and robotics, as a standalone technical aid. Investigating the value of the DRS technique as a breach detection tool in the clinical environment will be part of future studies.

3.5. CONCLUSION

This study investigated the potential of DRS for fat fraction quantification in vertebrae. The technique was validated against a highly accurate non-invasive technique for fat fraction quantification namely MRI. Thus, we hypothesize that optical fibers integrated into a surgical instrument can accurately measure fat content within vertebrae and might therefore be used as a promising breach detection tool during pedicle screw placement procedures.

REFERENCES

[1] A. Swamy, G. Burström, J. W. Spliethoff, D. Babic, S. Ruschke, J. M. Racadio, E. Edström, A. Elmi-Terander, J. Dankelman, and B. H. Hendriks, "Validation of diffuse reflectance spectroscopy with magnetic resonance imaging for accurate vertebral bone fat fraction quantification," *Biomedical optics express*, vol. 10, no. 8, pp. 4316–4328, 2019.

[2] S. T. Kha, H. Ilyas, J. E. Tanenbaum, E. C. Benzel, M. P. Steinmetz, and T. E. Mroz, "Trends in lumbar fusion surgery among octogenarians: A nationwide inpatient sample study from 2004 to 2013," *Global spine journal*, vol. 8, no. 6, pp. 593–599, 2018.

[3] K. Kobayashi, K. Ando, Y. Nishida, N. Ishiguro, and S. Imagama, "Epidemiological trends in spine surgery over 10 years in a multicenter database," *European Spine Journal*, vol. 27, no. 8, pp. 1698–1703, 2018.

[4] R. W. Gaines Jr, "The use of pedicle-screw internal fixation for the operative treatment of spinal disorders," *JBJS*, vol. 82, no. 10, p. 1458, 2000.

[5] L. Balabaud, S. Pitel, I. Caux, C. Dova, B. Richard, P. Antonietti, and C. Mazel, "Lumbar spine surgery in patients 80 years of age or older: morbidity and mortality," *European Journal of Orthopaedic Surgery & Traumatology*, vol. 25, no. 1, pp. 205–212, 2015.

[6] J. Ma, S. Fan, and F. Zhao, "Intraoperative malposition of pedicle probe or screws: a potential cause of the acceleration of degeneration in superior adjacent intervertebral disc," *Medical hypotheses*, vol. 77, no. 6, pp. 1102–1104, 2011.

[7] N. E. Epstein, "A review of medicolegal malpractice suits involving cervical spine: what can we learn or change?," *Clinical Spine Surgery*, vol. 24, no. 1, pp. 15–19, 2011.

[8] F. M. Phillips, I. Cheng, Y. R. Rampersaud, B. A. Akbarnia, L. Pimenta, W. B. Rodgers, J. S. Uribe, N. Khanna, W. D. Smith, J. A. Youssef, *et al.*, "Breaking through the "glass ceiling" of minimally invasive spine surgery," 2016.

[9] M. Vazan, J. Gempt, B. Meyer, N. Buchmann, and Y.-M. Ryang, "Minimally invasive transforaminal lumbar interbody fusion versus open transforaminal lumbar interbody fusion: a technical description and review of the literature," *Acta neurochirurgica*, vol. 159, no. 6, pp. 1137–1146, 2017.

[10] C. L. Goldstein, K. Macwan, K. Sundararajan, and Y. R. Rampersaud, "Perioperative outcomes and adverse events of minimally invasive versus open posterior lumbar fusion: meta-analysis and systematic review," *Journal of Neurosurgery: Spine*, vol. 24, no. 3, pp. 416–427, 2016.

[11] V. M. Lu, P. Kerezoudis, H. E. Gilder, B. A. McCutcheon, K. Phan, and M. Bydon, "Minimally invasive surgery versus open surgery spinal fusion for spondylolisthesis: a systematic review and meta-analysis," *Spine*, vol. 42, no. 3, pp. E177–E185, 2017.

[12] M.-H. Wu, N. K. Dubey, Y.-Y. Li, C.-Y. Lee, C.-C. Cheng, C.-S. Shi, and T.-J. Huang, "Comparison of minimally invasive spine surgery using intraoperative computed tomography integrated navigation, fluoroscopy, and conventional open surgery for lumbar spondylolisthesis: a prospective registry-based cohort study," *The Spine Journal*, vol. 17, no. 8, pp. 1082–1090, 2017.

[13] J. H. Oppenheimer, I. DeCastro, and D. E. McDonnell, "Minimally invasive spine technology and minimally invasive spine surgery: a historical review," *Neurosurgical focus*, vol. 27, no. 3, p. E9, 2009.

[14] A. Manbachi, R. S. Cobbold, and H. J. Ginsberg, "Guided pedicle screw insertion: techniques and training," *The Spine Journal*, vol. 14, no. 1, pp. 165–179, 2014.

[15] V. Kosmopoulos and C. Schizas, "Pedicle screw placement accuracy: a meta-analysis," *Spine*, vol. 32, no. 3, pp. E111–E120, 2007.

[16] A. Mason, R. Paulsen, J. M. Babuska, S. Rajpal, S. Burneikiene, E. L. Nelson, and A. T. Villavicencio, "The accuracy of pedicle screw placement using intraoperative image guidance systems: A systematic review," *Journal of Neurosurgery: Spine*, vol. 20, no. 2, pp. 196–203, 2014.

[17] V. E. Staartjes, A. M. Klukowska, and M. L. Schröder, "Pedicle screw revision in robot-guided, navigated, and freehand thoracolumbar instrumentation: a systematic review and meta-analysis," *World neurosurgery*, vol. 116, pp. 433–443, 2018.

[18] T. M. Bydlon, R. Nachabé, N. Ramanujam, H. J. Sterenborg, and B. H. Hendriks, "Chromophore based analyses of steady-state diffuse reflectance spectroscopy: current status and perspectives for clinical adoption," *Journal of biophotonics*, vol. 8, no. 1-2, pp. 9–24, 2015.

[19] R. Nachabe, B. H. Hendriks, A. E. Desjardins, M. van der Voort, M. B. van der Mark, and H. J. Sterenborg, "Estimation of lipid and water concentrations in scattering media with diffuse optical spectroscopy from 900 to 1600 nm," *Journal of biomedical optics*, vol. 15, no. 3, p. 037015, 2010.

[20] R. Van Veen, H. J. Sterenborg, A. Pifferi, A. Torricelli, E. Chikoidze, and R. Cubeddu, "Determination of visible near-ir absorption coefficients of mammalian fat using time-and spatially resolved diffuse reflectance and transmission spectroscopy," *Journal of biomedical optics*, vol. 10, no. 5, p. 054004, 2005.

[21] R. Nachabé, J. W. van der Hoorn, R. van de Molengraaf, R. Lamerichs, J. Pikkemaat, C. F. Sio, B. H. Hendriks, and H. J. Sterenborg, "Validation of interventional fiber optic spectroscopy with mr spectroscopy, mas-nmr spectroscopy, high-performance thin-layer chromatography, and histopathology for accurate hepatic fat quantification," *Investigative radiology*, vol. 47, no. 4, pp. 209–216, 2012.

[22] B. J. Tromberg, N. Shah, R. Lanning, A. Cerussi, J. Espinoza, T. Pham, L. Svaasand, and J. Butler, "Non-invasive in vivo characterization of breast tumors using photon migration spectroscopy," *Neoplasia (New York, NY)*, vol. 2, no. 1-2, p. 26, 2000.

[23] L. Spinelli, A. Torricelli, A. Pifferi, P. Taroni, G. M. Danesini, and R. Cubeddu, "Bulk optical properties and tissue components in the female breast from multiwavelength time-resolved optical mammography," *Journal of biomedical optics*, vol. 9, no. 6, pp. 1137–1143, 2004.

[24] A. Swamy, G. Burström, J. W. Spliethoff, D. Babic, C. Reich, J. Groen, E. Edström, A. E. Terander, J. M. Racadio, J. Dankelman, *et al.*, "Diffuse reflectance spectroscopy, a potential optical sensing technology for the detection of cortical breaches during spinal screw placement," *Journal of biomedical optics*, vol. 24, no. 1, p. 017002, 2019.

[25] D. C. Karampinos, S. Ruschke, M. Dieckmeyer, M. Diefenbach, D. Franz, A. S. Gersing, R. Krug, and T. Baum, "Quantitative mri and spectroscopy of bone marrow," *Journal of Magnetic Resonance Imaging*, vol. 47, no. 2, pp. 332–353, 2018.

[26] E. De Bisschop, R. Luypaert, O. Louis, and M. Osteaux, "Fat fraction of lumbar bone marrow using in vivo proton nuclear magnetic resonance spectroscopy," *Bone*, vol. 14, no. 2, pp. 133–136, 1993.

[27] B. Guiu, R. Loffroy, J.-M. Petit, S. Aho, D. B. Salem, D. Masson, P. Hillon, J.-P. Cercueil, and D. Krause, "Mapping of liver fat with triple-echo gradient echo imaging: validation against 3.0-t proton mr spectroscopy," *European radiology*, vol. 19, no. 7, pp. 1786–1793, 2009.

[28] I. J. MacEwan, N. E. Glembotski, D. D'Lima, W. Bae, K. Masuda, H. H. Rashidi, L. K. Mell, and M. Bydder, "Proton density water fraction as a biomarker of bone marrow cellularity: validation in ex vivo spine specimens," *Magnetic resonance imaging*, vol. 32, no. 9, pp. 1097–1101, 2014.

[29] W.-T. Chen and T. T.-F. Shih, "Correlation between the bone marrow blood perfusion and lipid water content on the lumbar spine in female subjects," *Journal of Magnetic Resonance Imaging: An Official Journal of the International Society for Magnetic Resonance in Medicine*, vol. 24, no. 1, pp. 176–181, 2006.

[30] T. Baum, S. P. Yap, M. Dieckmeyer, S. Ruschke, H. Eggers, H. Kooijman, E. J. Rummeny, J. S. Bauer, and D. C. Karampinos, "Assessment of whole spine vertebral bone marrow fat using chemical shift-encoding based water-fat mri," *Journal of Magnetic Resonance Imaging*, vol. 42, no. 4, pp. 1018–1023, 2015.

[31] A. Régis-Arnaud, B. Guiu1, P.-M. Walker, D. Krausé, F. Ricolfi, and D. B. Salem, "Bone marrow fat quantification of osteoporotic vertebral compression fractures: comparison of multi-voxel proton mr spectroscopy and chemical-shift gradient-echo mr imaging," *Acta radiologica*, vol. 52, no. 9, pp. 1032–1036, 2011.

[32] M. A. Bredella, M. Torriani, R. H. Ghomi, B. J. Thomas, D. J. Brick, A. V. Gerweck, C. J. Rosen, A. Klibanski, and K. K. Miller, "Vertebral bone marrow fat is positively associated with visceral fat and inversely associated with igf-1 in obese women," *Obesity*, vol. 19, no. 1, pp. 49–53, 2011.

[33] X. Li, D. Kuo, A. L. Schafer, A. Porzig, T. M. Link, D. Black, and A. V. Schwartz, "Quantification of vertebral bone marrow fat content using 3 tesla mr spectroscopy: reproducibility, vertebral variation, and applications in osteoporosis," *Journal of Magnetic Resonance Imaging*, vol. 33, no. 4, pp. 974–979, 2011.

[34] M. Dieckmeyer, S. Ruschke, C. Cordes, S. P. Yap, H. Kooijman, H. Hauner, E. J. Rummeny, J. S. Bauer, T. Baum, and D. C. Karampinos, "The need for t2 correction on mrs-based vertebral bone marrow fat quantification: implications for bone marrow fat fraction age dependence," *NMR in Biomedicine*, vol. 28, no. 4, pp. 432–439, 2015.

[35] E. Roldan-Valadez, C. Piña-Jimenez, R. Favila, and C. Rios, "Gender and age groups interactions in the quantification of bone marrow fat content in lumbar spine using 3t mr spectroscopy: a multivariate analysis of covariance (mancova)," *European journal of radiology*, vol. 82, no. 11, pp. e697–e702, 2013.

[36] G. Gokalp, F. S. Mutlu, Z. Yazici, and N. Yildirim, "Evaluation of vertebral bone marrow fat content by chemical-shift mri in osteoporosis," *Skeletal radiology*, vol. 40, no. 5, pp. 577–585, 2011.

[37] J. M. Patsch, X. Li, T. Baum, S. P. Yap, D. C. Karampinos, A. V. Schwartz, and T. M. Link, "Bone marrow fat composition as a novel imaging biomarker in postmenopausal women with prevalent fragility fractures," *Journal of bone and mineral research*, vol. 28, no. 8, pp. 1721–1728, 2013.

[38] T. Baum, S. P. Yap, D. C. Karampinos, L. Nardo, D. Kuo, A. J. Burghardt, U. B. Masharani, A. V. Schwartz, X. Li, and T. M. Link, "Does vertebral bone marrow fat content correlate with abdominal adipose tissue, lumbar spine bone mineral density, and blood biomarkers in women with type 2 diabetes mellitus?," *Journal of Magnetic Resonance Imaging*, vol. 35, no. 1, pp. 117–124, 2012.

[39] Y. P. Kim, S. Kannengiesser, M.-Y. Paek, S. Kim, T.-S. Chung, Y. H. Yoo, C.-S. Yoon, H.-T. Song, Y. H. Lee, and J.-S. Suh, "Differentiation between focal malignant marrow-replacing lesions and benign red marrow deposition of the spine with t2*-corrected fat-signal fraction map using a three-echo volume interpolated breath-hold gradient echo dixon sequence," *Korean journal of radiology*, vol. 15, no. 6, pp. 781–791, 2014.

[40] C. Schraml, M. Schmid, S. Gatidis, H. Schmidt, C. la Fougère, K. Nikolaou, and N. F. Schwenzer, "Multiparametric analysis of bone marrow in cancer patients using simultaneous pet/mr imaging: Correlation of fat fraction, diffusivity, metabolic activity, and anthropometric data," *Journal of Magnetic Resonance Imaging*, vol. 42, no. 4, pp. 1048–1056, 2015.

[41] S. B. Reeder, H. H. Hu, and C. B. Sirlin, "Proton density fat-fraction: a standardized mr-based biomarker of tissue fat concentration," *Journal of magnetic resonance imaging*, vol. 36, no. 5, pp. 1011–1014, 2012.

[42] R. Nachabé, B. H. Hendriks, M. van der Voort, A. E. Desjardins, and H. J. Sterenborg, "Estimation of biological chromophores using diffuse optical spectroscopy: benefit of extending the uv-vis wavelength range to include 1000 to 1600 nm," *Biomedical optics express*, vol. 1, no. 5, pp. 1432–1442, 2010.

[43] T. J. Farrell, M. S. Patterson, and B. Wilson, "A diffusion theory model of spatially resolved, steady-state diffuse reflectance for the noninvasive determination of tissue optical properties in vivo," *Medical physics*, vol. 19, no. 4, pp. 879–888, 1992.

[44] C. M. Jarque and A. K. Bera, "A test for normality of observations and regression residuals," *International Statistical Review/Revue Internationale de Statistique*, pp. 163–172, 1987.

[45] D. York, N. M. Evensen, M. L. Martınez, and J. De Basabe Delgado, "Unified equations for the slope, intercept, and standard errors of the best straight line," *American Journal of Physics*, vol. 72, no. 3, pp. 367–375, 2004.

[46] E. N. Marieb and K. Hoehn, *Human anatomy & physiology*. Pearson education, 2007.

[47] R. A. Deyo, D. T. Gray, W. Kreuter, S. Mirza, and B. I. Martin, "United states trends in lumbar fusion surgery for degenerative conditions," *Spine*, vol. 30, no. 12, pp. 1441–1445, 2005.

[48] T. Toyone, T. Ozawa, K. Kamikawa, A. Watanabe, K. Matsuki, T. Yamashita, R. Shiboi, M. Takeuchi, Y. Wada, K. Inada, *et al.*, "Subsequent vertebral fractures following spinal fusion surgery for degenerative lumbar disease: a mean ten-year follow-up," *Spine*, vol. 35, no. 21, pp. 1915–1918, 2010.

[49] J.-P. Kühn, D. Hernando, P. J. Meffert, S. Reeder, N. Hosten, R. Laqua, A. Steveling, S. Ender, H. Schröder, and D.-T. Pillich, "Proton-density fat fraction and simultaneous r2* estimation as an mri tool for assessment of osteoporosis," *European radiology*, vol. 23, no. 12, pp. 3432–3439, 2013.

[50] D. K. Yeung, J. F. Griffith, G. E. Antonio, F. K. Lee, J. Woo, and P. C. Leung, "Osteoporosis is associated with increased marrow fat content and decreased marrow fat unsaturation: a proton mr spectroscopy study," *Journal of Magnetic Resonance Imaging: An Official Journal of the International Society for Magnetic Resonance in Medicine*, vol. 22, no. 2, pp. 279–285, 2005.

[51] A. V. Schwartz, S. Sigurdsson, T. F. Hue, T. F. Lang, T. B. Harris, C. J. Rosen, E. Vittinghoff, K. Siggeirsdottir, G. Sigurdsson, D. Oskarsdottir, *et al.*, "Vertebral bone marrow fat associated with lower trabecular bmd and prevalent vertebral fracture in older adults," *The Journal of Clinical Endocrinology & Metabolism*, vol. 98, no. 6, pp. 2294–2300, 2013.

[52] K. d. C. B. Ribeiro and L. P. Kowalski, "Apache ii, possum, and asa scores and the risk of perioperative complications in patients with oral or oropharyngeal cancer," *Archives of Otolaryngology–Head & Neck Surgery*, vol. 129, no. 7, pp. 739–745, 2003.

[53] S. L. Wakely, "The posterior vertebral scalloping sign," *Radiology*, vol. 239, no. 2, pp. 607–609, 2006.

[54] E. R. Westrick and W. T. Ward, "Adolescent idiopathic scoliosis: 5-year to 20-year evidence-based surgical results," *Journal of Pediatric Orthopaedics*, vol. 31, pp. S61–S68, 2011.

[55] S. Ruschke, A. Pokorney, T. Baum, H. Eggers, J. H. Miller, H. H. Hu, and D. C. Karampinos, "Measurement of vertebral bone marrow proton density fat fraction in children using quantitative water–fat mri," *Magnetic Resonance Materials in Physics, Biology and Medicine*, vol. 30, no. 5, pp. 449–460, 2017.

[56] T. Baum, A. Rohrmeier, J. Syväri, M. N. Diefenbach, D. Franz, M. Dieckmeyer, A. Scharr, H. Hauner, S. Ruschke, J. S. Kirschke, *et al.*, "anatomical variation of age-related changes in vertebral bone marrow composition using chemical shift encoding-based water–fat magnetic resonance imaging," *Frontiers in endocrinology*, vol. 9, p. 141, 2018.

[57] S. Merritt, G. Gulsen, G. Chiou, Y. Chu, C. Deng, A. E. Cerussi, A. J. Durkin, B. J. Tromberg, and O. Nalcioglu, "Comparison of water and lipid content measurements using diffuse optical spectroscopy and mri in emulsion phantoms," *Technology in cancer research & treatment*, vol. 2, no. 6, pp. 563–569, 2003.

[58] G. Burström, R. Nachabe, O. Persson, E. Edström, and A. E. Terander, "Augmented and virtual reality instrument tracking for minimally invasive spine surgery: a feasibility and accuracy study," *Spine*, vol. 44, no. 15, pp. 1097–1104, 2019.

[59] M. J. Tormenti, D. B. Kostov, P. A. Gardner, A. S. Kanter, R. M. Spiro, and D. O. Okonkwo, "Intraoperative computed tomography image–guided navigation for posterior thoracolumbar spinal instrumentation in spinal deformity surgery," *Neurosurgical focus*, vol. 28, no. 3, p. E11, 2010.

[60] A. Elmi-Terander, G. Burström, R. Nachabe, H. Skulason, K. Pedersen, M. Fagerlund, F. Ståhl, A. Charalampidis, M. Söderman, S. Holmin, *et al.*, "Pedicle screw placement using augmented reality surgical navigation with intraoperative 3d imaging: a first in-human prospective cohort study," *Spine*, vol. 44, no. 7, p. 517, 2019.

[61] D. P. Devito, L. Kaplan, R. Dietl, M. Pfeiffer, D. Horne, B. Silberstein, M. Hardenbrook, G. Kiriyanthan, Y. Barzilay, A. Bruskin, *et al.*, "Clinical acceptance and accuracy assessment of spinal implants guided with spineassist surgical robot: retrospective study," *Spine*, vol. 35, no. 24, pp. 2109–2115, 2010.

[62] J. P. Du, Y. Fan, Q. N. Wu, J. Zhang, D. J. Hao, *et al.*, "Accuracy of pedicle screw insertion among 3 image-guided navigation systems: systematic review and meta-analysis," *World neurosurgery*, vol. 109, pp. 24–30, 2018.

[63] A. Ghasem, A. Sharma, D. N. Greif, M. Alam, and M. Al Maaieh, "The arrival of robotics in spine surgery: a review of the literature," *Spine*, vol. 43, no. 23, pp. 1670–1677, 2018.

4

PROTON DENSITY FAT FRACTION DISTRIBUTION ANALYSIS FOR SPINAL SCREW PLACEMENT BREACH DETECTION: A MRI CADAVERIC STUDY

Proton Densiy Fat Fraction (PDFF) is known to accurately reflect concentration of fat in tissues. Diffuse Reflectance-based fat fraction (DRFF) measured via integrating optical fibers into a surgical instrument was found to correlate well with non-invasive PDFF measurements in the previous study. Studying the true variation of fat fraction across the spinal column becomes important to understand the generalizability of fat fraction as a breach detection parameter. To this end, regions of interests were defined within the MR midsagittal images. PDFF distributions across the spinal columns of six cadavers were studied. The PDFF distribution of the cortical bone boundary is found to be lower as compared to the PDFF of cancellous bone for the six cadavers. Moreover, a gradial drop in PDFF distributions is observed from cancellous bone towards cortical bone boundary which further points towards the possibility of using fat fraction as a breach detection parameter for instrument guidance during spinal screw placement procedures. However, the variability in PDFF distributions between cadavers exists and should be taken into account.

Swamy A., Losch M., Elmi-Terander A., Edström E., Dankelman J. and Hendriks B.H.W. Proton density fat fraction distribution analysis for spinal screw placement breach detection: A MRI cadaveric study (in preparation).

4.1. INTRODUCTION

In the previous chapter (Chapter 3) it was found that fat fraction determined via the DRS and MRI techniques showed good correlation. Moreover, the fat fraction range within the vertebral bodies were found to lie in a similar range compared to *in vivo* studies in literature.

Several research groups have used the MRI technique to non-invasively measure fat conentration in the vertebral body in order to evaluate various clinical conditions such as osteoporosis [1–4], diagnosis of metabolic disorders such as obesity and diabeties [5, 6] and cancer [7, 8]. However, studies focusing on the distribution of fat fraction close to the cortical border across the spinal column is lacking. Such information can provide important insights into the variation of fat fraction within vertebra as well as across different spinal levels. Moreover, determination of the true variation of fat fraction across the spinal column can be useful in the development of a robust breach detection algorithm for instrument guidance during spinal screw placement procedures.

To this end, several zones close to the cortical bone boundary were defined and the PDFF distributions within these zones were studied across the spinal column.

4.2. METHODS

The characteristics of the studied cadavers (5 female, 1 male) are depicted in Table 4.1. All ethical guidelines for human cadaver studies were followed. No embalming process was used, neither were any of the cadavers frozen, in order to preserve the optical properties of the cadaver specimens.

Table 4.1: Cadaver information.

Cadaver #	Gender	Age (years)	Weight (kg)
1	Female	92	82
2	Female	82	77
3	Male	78	82
4	Female	53	77
5	Female	79	68
6	Female	83	77

4.2.1. MEASUREMENT PROTOCOL

MAGNETIC RESONANCE IMAGING

The entire spine of the cadavers was scanned on a 1.5 Tesla (T) whole-body scanner (Ingenia, Philips Healthcare, Best, Netherlands) while placed in the prone position on the table coil array. To obtain whole spine coverage, the MR exam consisted of three sagittal 3D spoiled gradient echo sequences placed on the cervical, thoracic and lumbar spine,

respectively. The temperature of the cadavers was maintained close to room temperature prior to scanning.

A three-dimensional (3D) six-echo spoiled gradient-echo sequence was used for chemical shift-encoding-based water-fat separation. The typical imaging parameters used in this study were: 45-60 sagittal slices with a slice thickness of 3 mm; AP and FH field of view = 220-310 and 240-350 mm; in-plane resolution = (0.45-0.67) × (0.45-0.67) mm; flip angle = 5 degrees; TR = 9.9-15.87 ms; TE1 = 1.41-1.43 ms; $\triangle TE$ = 1.2 ms; total scan time per cadaver was approximately 5-10 minutes.

4.2.2. DETERMINATION OF PROTON DENSITY FAT FRACTION

The scanner image reconstruction was utilized to obtain fat and water images using a DICOM image viewer software (Philips DICOM viewer R3.0-SP04, Philips Healthcare, Best, The Netherlands). The water—fat separation was based on a complex seven-peak water—fat spectral model. Based on the fat (F) and water images (W), Proton Density Fat Fraction (PDFF) was thus calculated as:

$$PDFF[\%] = \frac{F}{F+W} \times 100.$$

The visual representation of the fat fraction image is shown in Figure 4.1.

Figure 4.1: Sagittal cross-sectional MR PDFF image.

ROI selection: Semi-automated determination of the PDFF was performed by placing regions of interests (ROIs) on the PDFF map on the central slice per vertebral level from C3 to L5 using imageJ software [9].

Anatomical ROI of cortical bone boundaries surrounding the anterior, inferior and superior walls were semi-automatically detected based on the gray scale values on the MRI image as shown in Figure 4.2a. Three pre-cortical zones (PCZ's) were then defined as PCZ1, PCZ2 and PCZ3 by automatically growing an ROI with 1 mm increment from the detected cortical bone boundary as shown in Figure 4.2b . The cancellous bone zone was defined based on the entire region beyond 3mm as shown via the shaded region in figure 4.2b.

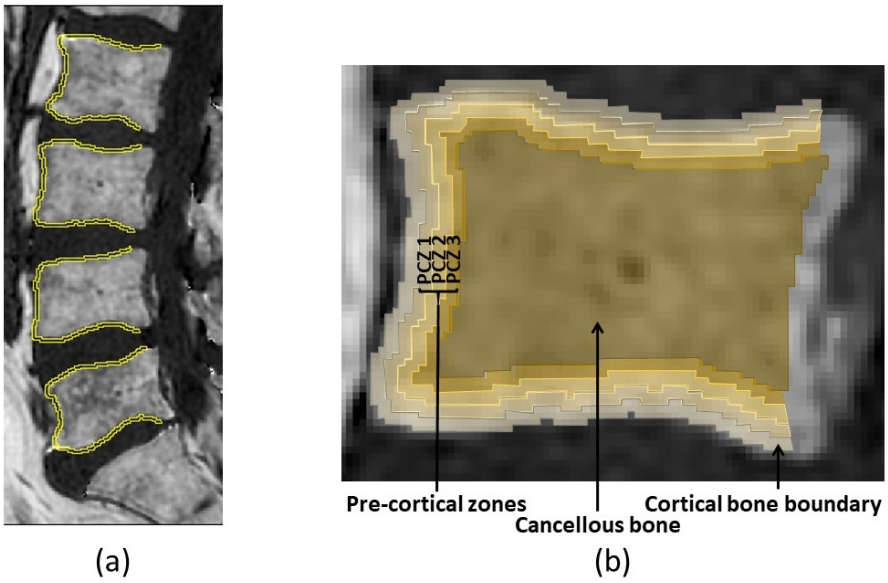

Figure 4.2: ROI selection process within MR PDFF image.(a) Sagittal cross-sectional MR image of lumbar spine and ROI selection of anterior, inferior and superior cortical bone boundary. (b) Anatomical ROI's including pre-cortical bone and cancellous bone defined.

4.2.3. IMAGING DATA ANALYSIS

Fat fraction distributions were calculated for each of the different shaded zones shown in figure 4.2b by calculating PDFF per pixel using MATLAB [10]. Anatomical regions of interest were defined as pre- cortical zone (PCZ), which was defined as the distance within 3 mm from the cortical bone, based on previous experience from Chapter 2. Pre-cortical zones were further subdivided based on distance from cortical border as (PCZ1) [0-1]mm, PCZ2 [1-2]mm, PCZ3 [2-3]mm.

4.2.4. STATISTICAL ANALYSIS

The data obtained from each technique was tested using the Kolmogorov-Smirnov test [11] for normality and was found to not come from a normal distribution. Thus, the estimated fat fractions are calculated as medians and the variation was represented as interquartile ranges, minimum and maximum values.

4.3. RESULTS

The PDFF distribution across cervical to lumbar vertebral levels for the six cadavers is shown in Figure 4.3a-f. The PDFF distribution of the cortical bone boundary is lower as compared to the PDFF of cancellous bone for all six cadavers.

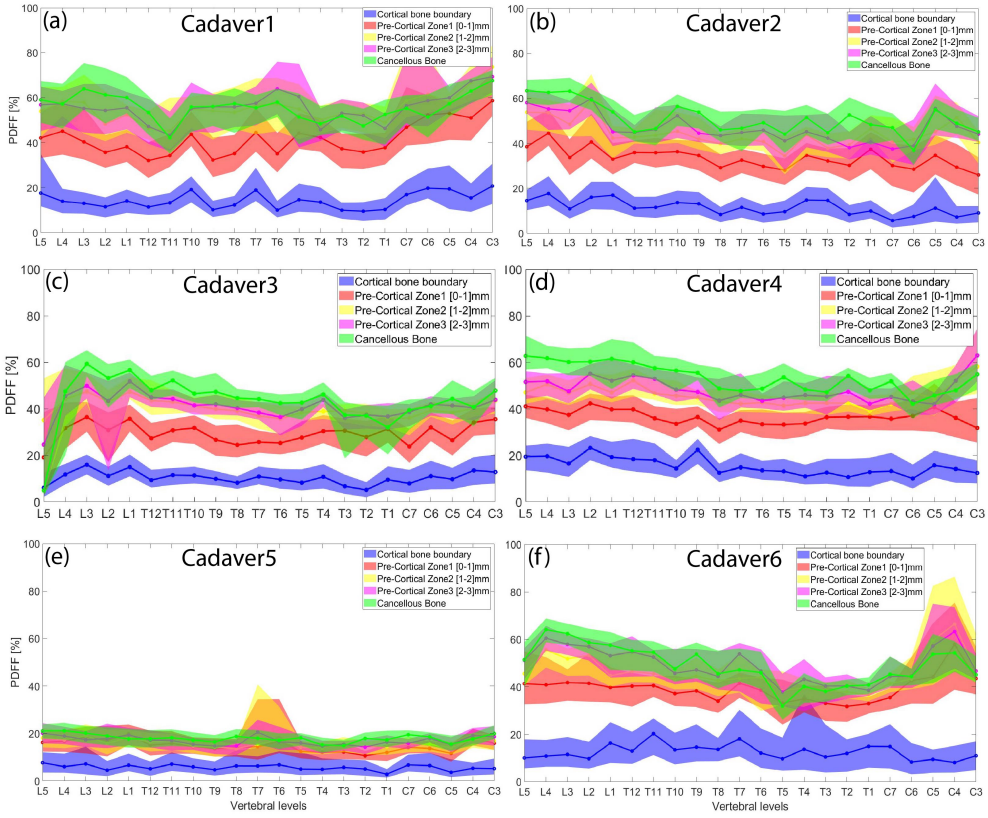

Figure 4.3: Proton Density Fat Fraction distribution across six cadavers. Each datapoint represents the median. The variation is represented via the interquartile range.

The aggregate PDFF distributions of the intravertebral zones across cervical to thoracic levels among the six cadavers are shown in Figure 4.4. A gradual drop in fat fraction is observed from cancellous bone to pre cortical zones and cortical bone boundary respectively.

4.3.1. DISCUSSSIONS

PDFF is the standardized MR-based biomarker for deterimination of tissue fat concentration and is considered to accurately reflect the concentration of fat in tissues [12]. Studying the true variation of fat fraction in the spinal column can be useful in developing insights into DRS determined fat fraction for breach detection during spinal screw

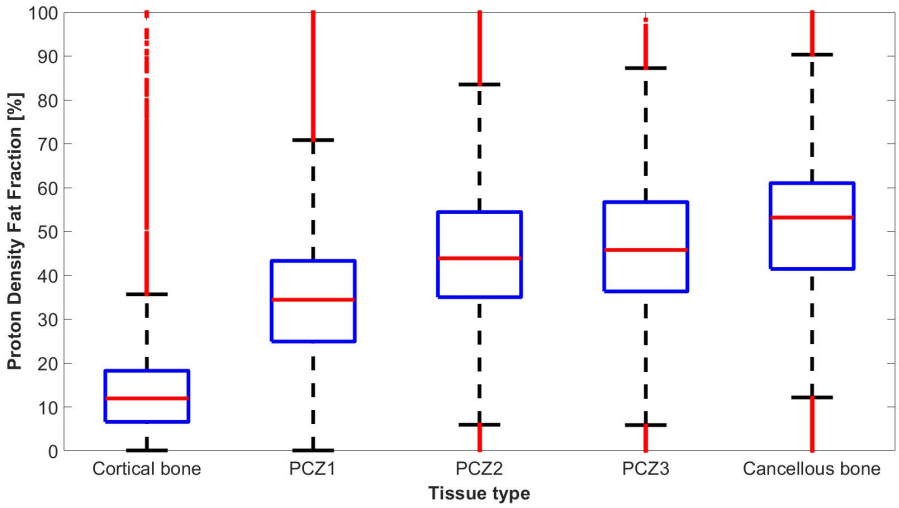

Figure 4.4: Aggregate Proton Density Fat Fraction distributions of the six cadavers based on intravertebral zones.

placement procedures.

For the six cadavers studied, PDFF distribution of cortical bone boundary was found to be lower than the cancellous bone zone (Figure.4.3). This trend appears to be consistent across the spinal column from lumar to cervical regions based on a qualitative comparison. However, variation of PDFF does exist as shown via the spread using interquartile range.

The various intravertebral zones created were found to have a effect on the PDFF distribution as illustrated via the box plots in Figure 4.4. Moreover, a downward median trend of PDFF was observed from cancellous bone towards cortical bone boundary zone. Such a global trend confirms the drop in Diffuse Reflectance-based Fat Fraction (DRFF) observed during an image-guided experimental insertion of an optical screw probe in 2.8.

However, the large spread does indicate a significant variation within each intervertebral zone. Sources of variation arises from aggregating the distributions from the six cadavers across all spinal levels. Moreover, it is known that cancellous bone is biologically heterogenous in nature [13]. The relatively low PDFF distributions observed in Cadaver5 is also a contributor towards such a spread. Cadaver5 was known to have suffered from malignant neoplasm of the esophagus making such a patient an unlikely candidate for spinal fusion surgery [3]. The cortical bone boundary ROI was semi-automatically grown based on the assumption of a cortical thickness of 1 mm. Figure 2.6 illustrates the cortical bone thickness variation between 1-3mm. This is also a source of the spread in the regions as observed in Figure 4.3a-f. However, even with this assumption, cortical bone boundary was found to show a lower PDFF trend compared to other zones.

This study has a few limitations. Selection of cortical bone boundary was done semi-

automatically by manually detecting the low gray scale values on the MRI image. Although the process was kept consistent for the entire dataset, it is prone to bias. Using CT images as ground truth for cortical bone boundary detection is recommended as part of future studies. Another possible approach to mitigate the bias might be to increase magnetic field strength from 1.5T to 3T for better fat and water seperation and thereby creating better image contrast between cortical and cancellous zones for bone boundary detection [14].

The semi-automatic ROI selection of the cortical bone boundary was performed by combining the anterior, superior and lateral cortical boundary walls. To gain a deeper insights into the PDFF distributions across each of the three cortical boundary walls, separate ROI selection per cortical boundary wall is recommended.

Unusually low PDFF was found between the narrow of range of 48-52% across all the six cadavers studied. This can be attributed as an artifact. It might be related to a potential model mismatch or the way the online water-fat separation was performed. Temperature dependence of the water signal during scanning of the specimen might also have contributed towards the artifact.

Lastly, the mid-sagittal slices were used for each of the six cadavers to produce PDFF distributions across the spinal column based on the intravertebral zones. The PDFF variation across other sagittal slices and 3D planes needs to be further investigated.

4.4. CONCLUSIONS

PDFF distributions across the spinal columns shows a consistently lower PDFF within the cortical bone boundary region as compared to the cancellous bone region. Moreover, a drop in PDFF was observed from cancellous bone towards the cortical bone boundary. These findings confirm the differences in the true fat fraction distributions within vertebral bones. Thus exhibiting potential to be used for the development of a robust breach detection algorithm. However, the variation within the intravertebral zones cannot be ignored.

REFERENCES

[1] I. J. MacEwan, N. E. Glembotski, D. D'Lima, W. Bae, K. Masuda, H. H. Rashidi, L. K. Mell, and M. Bydder, "Proton density water fraction as a biomarker of bone marrow cellularity: validation in ex vivo spine specimens," *Magnetic resonance imaging*, vol. 32, no. 9, pp. 1097–1101, 2014.

[2] X. Li, D. Kuo, A. L. Schafer, A. Porzig, T. M. Link, D. Black, and A. V. Schwartz, "Quantification of vertebral bone marrow fat content using 3 tesla mr spectroscopy: reproducibility, vertebral variation, and applications in osteoporosis," *Journal of Magnetic Resonance Imaging*, vol. 33, no. 4, pp. 974–979, 2011.

[3] M. Dieckmeyer, S. Ruschke, C. Cordes, S. P. Yap, H. Kooijman, H. Hauner, E. J. Rummeny, J. S. Bauer, T. Baum, and D. C. Karampinos, "The need for t2 correction on mrs-based vertebral bone marrow fat quantification: implications for bone marrow fat fraction age dependence," *NMR in Biomedicine*, vol. 28, no. 4, pp. 432–439, 2015.

[4] J. M. Patsch, X. Li, T. Baum, S. P. Yap, D. C. Karampinos, A. V. Schwartz, and T. M. Link, "Bone marrow fat composition as a novel imaging biomarker in postmenopausal women with prevalent fragility fractures," *Journal of bone and mineral research*, vol. 28, no. 8, pp. 1721–1728, 2013.

[5] M. A. Bredella, M. Torriani, R. H. Ghomi, B. J. Thomas, D. J. Brick, A. V. Gerweck, C. J. Rosen, A. Klibanski, and K. K. Miller, "Vertebral bone marrow fat is positively associated with visceral fat and inversely associated with igf-1 in obese women," *Obesity*, vol. 19, no. 1, pp. 49–53, 2011.

[6] T. Baum, S. P. Yap, D. C. Karampinos, L. Nardo, D. Kuo, A. J. Burghardt, U. B. Masharani, A. V. Schwartz, X. Li, and T. M. Link, "Does vertebral bone marrow fat content correlate with abdominal adipose tissue, lumbar spine bone mineral density, and blood biomarkers in women with type 2 diabetes mellitus?," *Journal of Magnetic Resonance Imaging*, vol. 35, no. 1, pp. 117–124, 2012.

[7] Y. P. Kim, S. Kannengiesser, M.-Y. Paek, S. Kim, T.-S. Chung, Y. H. Yoo, C.-S. Yoon, H.-T. Song, Y. H. Lee, and J.-S. Suh, "Differentiation between focal malignant marrow-replacing lesions and benign red marrow deposition of the spine with t2*-corrected fat-signal fraction map using a three-echo volume interpolated breath-hold gradient echo dixon sequence," *Korean journal of radiology*, vol. 15, no. 6, pp. 781–791, 2014.

[8] C. Schraml, M. Schmid, S. Gatidis, H. Schmidt, C. la Fougère, K. Nikolaou, and N. F. Schwenzer, "Multiparametric analysis of bone marrow in cancer patients using simultaneous pet/mr imaging: Correlation of fat fraction, diffusivity, metabolic activity, and anthropometric data," *Journal of Magnetic Resonance Imaging*, vol. 42, no. 4, pp. 1048–1056, 2015.

[9] C. A. Schneider, W. S. Rasband, and K. W. Eliceiri, "Nih image to imagej: 25 years of image analysis," *Nature methods*, vol. 9, no. 7, pp. 671–675, 2012.

[10] MATLAB, *version 9.5.0944444 (R2018b)*. Natick, Massachusetts: The MathWorks Inc., 2018.

[11] P. Armitage, T. Colton, *et al.*, *Encyclopedia of biostatistics*. J. Wiley, 1998.

[12] S. B. Reeder, H. H. Hu, and C. B. Sirlin, "Proton density fat-fraction: a standardized mr-based biomarker of tissue fat concentration," *Journal of magnetic resonance imaging*, vol. 36, no. 5, pp. 1011–1014, 2012.

[13] E. N. Marieb and K. Hoehn, *Human anatomy & physiology*. Pearson education, 2007.

[14] B. J. Soher, B. M. Dale, and E. M. Merkle, "A review of mr physics: 3t versus 1.5 t," *Magnetic resonance imaging clinics of North America*, vol. 15, no. 3, pp. 277–290, 2007.

5

DIFFUSE REFLECTANCE SPECTROSCOPY ACCURATELY IDENTIFIES THE PRE-CORTICAL ZONE FOR BREACH DETECTION DURING SPINAL FIXATION SURGERY

Pedicle screw placement accuracy during spinal fixation surgery varies greatly and severe misplacement has been reported in 1-6.5% of screws. Diffuse reflectance spectroscopy (DRS) has previously been shown to reliably discriminate between tissues in the human body. We postulate that it could be used to discriminate between cancellous and cortical bone. Therefore, the purpose of this study is to provide proof-of-concept for DRS as a warning system to detect impending pedicle screw breach. DRS was incorporated at the tip of an integrated pedicle screw and screw driver used for tissue probing during pedicle screw insertions on six cadavers. Measurements were collected in the wavelength range of 400-1600 nm and each insertion was planned to result in a breach. Measurements were labelled as cancellous, cortical or representing a pre-cortical zone (PCZ) in between, based on information from cone beam computed tomographies at corresponding positions. In addition, DRS data was recorded after breach. Four typical pedicle breach types were performed, and a total of 45 pedicle breaches were recorded. For each breach direction, the technology was able to detect the transition of the screw tip from the cancellous bone to the PCZ (P<0.001), to cortical bone (P<0.001), and to a subsequent breach (P<0.001). Impending breach could reliably be detected within 3 mm from the cortical border. We conclude that DRS reliably identifies the area of transition from cancellous to cortical bone in typical breach scenarios and can warn the surgeon of impending pedicle breach, thereby resulting in safer spinal fixation surgeries.

Burström G., Swamy A., Spliethoff J.W., Reich C., Babic D., Hendriks B.H.W., Skulason H., Persson O., Elmi-Terander A. and Edström E. Diffuse reflectance spectroscopy accurately identifies the pre-cortical zone to avoid impending pedicle screw breach in spinal fixation surgery. Biomedical optics express., 10(11), 2019.

5.1. INTRODUCTION

Spinal fusion is the standard treatment for a variety of spine-related diseases. With more than 450.000 surgeries annually, it accounts for the highest share of aggregate hospital costs for stays with OR procedures in the US [2]. The procedure is routinely performed using a free-hand technique with or without fluoroscopic guidance. A crucial step involves placing screws in the pedicles of vertebrae to provide fixation points to fuse neighboring vertebrae. The accuracy of pedicle screw placement in published studies varies greatly. Recent reviews and meta-analyses indicate breaches >4 mm in 1-6,5% of pedicle screws placed using the free-hand technique [3–5]. Misplaced screws may result in complications ranging from inadequate fixation to serious vascular and neurological injury. In turn, this may result in repeat surgery, new complications and extended hospital stay [6].

Improved surgical accuracy could increase patient safety and reduce complications. Several technological aids have been investigated in order to detect an impending pedicle breach. Electrical conductivity has been used in order to allow detection of the cortical bone at the edge of vertebrae [7, 8]. It has the drawback that it does not allow for feedback regarding in what direction the cortical bone is detected. Optical technologies have the potential to allow for a directed optical measurement to be performed. Raman spectroscopy, typically based on laser illumination of tissues, has been used to asses bone quality both invasively and transcutaneously [9, 10]. However, Raman spectroscopy has yet to be applied surgically, possibly due to acquisition times being one to two orders of magnitude higher than those typically used in other optical methods [11, 12].

Diffuse reflectance (DR) spectroscopy is a spectral sensing technique that has been investigated and adapted to discriminate between cancellous and cortical bone through Monte Carlo simulations, but not yet statistically validated in tissues nor in a surgical setting [13]. Using this optical spectroscopy-based technique, tissue is illuminated by sending white light from a broad-spectrum light source through an optical fiber. After hitting the tissue, the light is reflected, scattered, or absorbed. The net effect is a diffuse reflectance pattern, which is collected through a second optical fiber and analyzed for spectral changes [14]. These changes originate from highly specific reflection, scattering, and absorption and scattering characteristics of individual tissue types [15]. Thus, by analyzing the reflected light, different tissue types can be distinguished [16]. It has previously been demonstrated that the estimated fraction of blood, lipids, and collagen as well as specific optical properties such as scattering parameters can be used to discriminate between tissues during breast, liver, esophagus, maxillofacial, and colon surgery as well as needle insertions during lumbar punctures [17–22]. In spinal fixation surgery, DR spectroscopy technology at the tip of a surgical instrument could provide real time feedback to the surgeon regarding the tissue type that the instrument passes through. We postulate that such a smart instrument could warn the surgeon before breaching through the cortical bone, to reduce the number and severity of complications.

In this study, we examine the utility of DR spectroscopy in a surgical setting, while performing pedicle screw placements in human cadavers. The study was designed to illustrate typical pedicle screw breaches and the corresponding DR spectroscopy data to provide a basis for future research, elucidating if the technology can be used to detect clinically relevant breaches in the lateral, medial, inferior and anterior direction.

The area where cancellous bone shifts into cortical bone is given special interest, as its recognition could be used to warn the surgeon of impending breach. We define this area as the pre-cortical zone (PCZ). Based on the findings of this study, the technology could be used to design a "smart" and clinically valuable surgical instrument.

5.2. METHODS

5.2.1. SURGICAL SETUP

Surgeries were performed on six human cadavers, 5 females and 1 males with an age range of 53-92 years. The study was conducted in compliance with ethical guidelines for human cadaver studies. All cadavers were donated for scientific research. Informed consent had been signed before death by the donors or after death by relatives, according to local guidelines.

The cadavers were placed in the prone position on an operating table and midline incisions were made along the thoracic and lumbar spine. Soft tissue was dissected with standard surgical technique to gain access to the posterior aspects of the spine, including spinous processes, lamina, facet joints and transverse processes. Pedicle screw paths were planned using an augmented reality surgical navigation (ARSN) system, as previously described in the literature [23]. Accordingly, a cone beam computed tomography (CBCT) acquisition was performed and used for automatic spine segmentation and creation of a 3D-model of the spine [24]. Based on this 3D-model, using the system's surgical navigation software, pedicle screws were purposefully planned to result in either lateral, inferior, anterior, or medial breach. Subsequently, an integrated pedicle screw and screwdriver equipped with optical fibers at the tip was used to place pedicle screws according to the planned trajectories. DR spectra were recorded systematically throughout the procedure and matching navigation data was recorded for every DR-spectra measurement to provide positional data. CBCT acquisitions were performed at key positions close to, or at, tissue borders to verify exact position of the device. Tissue labelling was later performed based on anatomical position according to the CBCT imaging by a trained physician blinded to the DR-spectral readings.

5.2.2. DIFFUSE REFLECTANCE SPECTROSCOPY SYSTEM

DR spectroscopy measurements were performed using a semi-portable spectroscopic system. The general principles of DR spectroscopy, calibration procedure and instrumentation have been previously described [24]. Tissue was probed using an integrated pedicle screw and screwdriver equipped with two optical fibers at the tip of the screw. The fiber-to-fiber distance between the optical fibers was 1.22 mm (Fig. 5.1). This inter-fiber distance was chosen based on previous studies and is based on a trade-off between wanting to maximize the separation for good DR readings while keeping a mechanical strength needed for bone sampling [13, 25]. The tool consists of an inner stylet containing the optical fibers, leading up to the tip of the screw, that allows for turning the tool without twisting the optical fibers. An in-depth description of the tool setup has been published previously [13]. One fiber was connected to a broad-spectrum halogen light source (Avantes AvaLight-Hal-S) to transmit light into the tissue, while the other was used to receive reflected light. To resolve light between 400 and 1600 nm, the receiving

fiber was connected to two spectrometers resolving light in the visible (Maya2000 Pro, Ocean Optics) and near-infrared regions (NirQuest 512, Ocean Optics). The acquisition time of each measurement was set to 50-150 ms. An in-house developed LabVIEW software (National Instruments, USA) was used to control the spectrometers and acquire the spectral data.

Figure 5.1: A depiction of the integrated pedicle screw and screwdriver used in the study, equipped with two optical fibers at the tip of the screw with a fiber distance of 1.22 mm.

5.2.3. DIFFUSE REFLECTANCE SPECTRAL DATA ANALYSIS

Spectral analysis was performed with custom developed software using Matlab (MathWorks Inc., Natick, MA). DR spectra acquired from the pedicle screw insertions were analyzed in the wavelength range of 400 to 1600 nm. A fitting algorithm was used in which the measured spectra could be translated into meaningful physiological or chemical parameters, as has been described previously [19, 26, 27]. To do this, a light propagation computational model was first used to generate spectra based on chromophore volume fractions and light-scattering [19, 27, 28]. The fraction of each parameter within the tissues was then estimated by fitting chromophore spectra generated by the computational model to the spectra collected from tissues. The fitting algorithm worked by iteratively minimizing the difference between spectra generated by the computational model and the spectrum acquired from the tissue. The computational model included chromophore simulations of hemoglobin, beta-carotene, methemoglobin, lipids, water, and collagen [17, 27]. It also included light-scattering simulations including Mie-to-Rayleigh scattering fraction, Mie scattering slope, and scattering amplitude at a wavelength of 800nm, as has been described previously [26]. As output for the lipid content, a normalized ratio was used; lipid content divided by the sum of total lipid and water content. For collagen volume fraction, a non-normalized reading denoted by arbitrary units (a.u.) was used, as previously described [29]. In our study, the use of hemoglobin and methemoglobin were considered of less value since all insertions were done on cadav-

ers. Thus, these tissue constituents were part of the fitting algorithm to provide a reliable output but were not included in the final data analysis.

5.2.4. IMAGING DATA ANALYSIS

Each pedicle insertion and breach were classified as either an anterior, inferior, medial or lateral pedicle breach. All labelling of tissue type based on anatomical positions was done using CBCT verification scans and carried out by an experienced physician in a blinded fashion, i.e. without knowledge of the corresponding DR-spectral readings. Anatomical regions of interest were defined as cancellous bone, cortical bone, a pre-cortical zone (PCZ), i.e. the zone of transition between the cancellous and cortical bone, and extravertebral tissue, i.e. breach. Based on previous experience, the PCZ was defined as the distance within 3 mm from the cortical bone [13]. Breach was defined as the first 3 mm after breaking through the cortical bone.

5.2.5. SUPPORT VECTOR MACHINE

To investigate the performance of the technology in detecting impending breach using multiple tissue constituents, support vector machine (SVM) classification [30] was used. Before training the SVMs, all features were scaled to a mean of 0 and a standard deviation of 1. For training the SVMs, RStudio (RStudio Team. RStudio: Integrated Development for R. RStudio, Inc., Boston) and the e1071 package (Probability Theory Group, 2019), based on LIBSVM [31], was used with a radial kernel and standard parameters (cost: 1, and gamma: 1/no. of data dimensions). First, a 1:2 ratio split was used to train a model on 66% of the data. The remaining 33% was used as validation data to calculate accuracy, sensitivity and specificity for the model based on the confusion matrix of the validation data. Second, a leave-one-specimen-out cross-validation approach was used where the classification models were trained on all but one cadaver, and the validation was performed on the remaining cadaver. Validation was only performed on cadavers with >5 tissue readings in both cancellous and cortical bone, to ensure enough validation data. This approach was repeated until all included cadavers had been left out once, with the confusion matrices being added up. This was to show how the classification algorithms work on truly independent data.

5.2.6. STATISTICAL ANALYSIS

A P-value less than 0.01 was considered significant. Data was normally distributed except DRS readings for collagen in the PCZ and all breached data, both with bimodal distributions on a group level. Given that most tissues on a group level, as well as specific insertion data, were normally distributed, DR spectroscopy readings were reported as means (standard deviations). For analyzing “DRS profiles of typical breaches”, DRS data from single insertions were categorized according to tissue type and a Mann-Whitney-Wilcoxon test was used to evaluate differences between tissues. For analyzing “aggregated data for detecting the cortical border”, DRS data from all insertions were grouped according to tissue type and a Mann-Whitney-Wilcoxon test was used to evaluate differences. Statistical analysis was performed using RStudio (RStudio Team. RStudio: Integrated Development for R. RStudio, Inc., Boston).

5.3. RESULTS

5.3.1. DRS PROFILES OF TYPICAL BREACHES

The four types of breach studied are presented below. In Figs. 5.2 to 5.5 they are illustrated in axial and sagittal CBCT images with corresponding DRS analysis results presented in conjunction.

An illustration of an inferior breach is presented in Fig. 5.2. The initial position of the screw tip in the cancellous bone at the superficial entry into the pedicle saw a high lipid fraction (69.11± 0.47 %) and medium collagen fraction (0.60 ± 0.01 a.u.). The transition of the screw tip from cancellous bone to the PCZ saw a drop in lipid fraction and an increase in collagen fraction (9.71±3.21 % and 1.41±0.02 a.u., respectively).

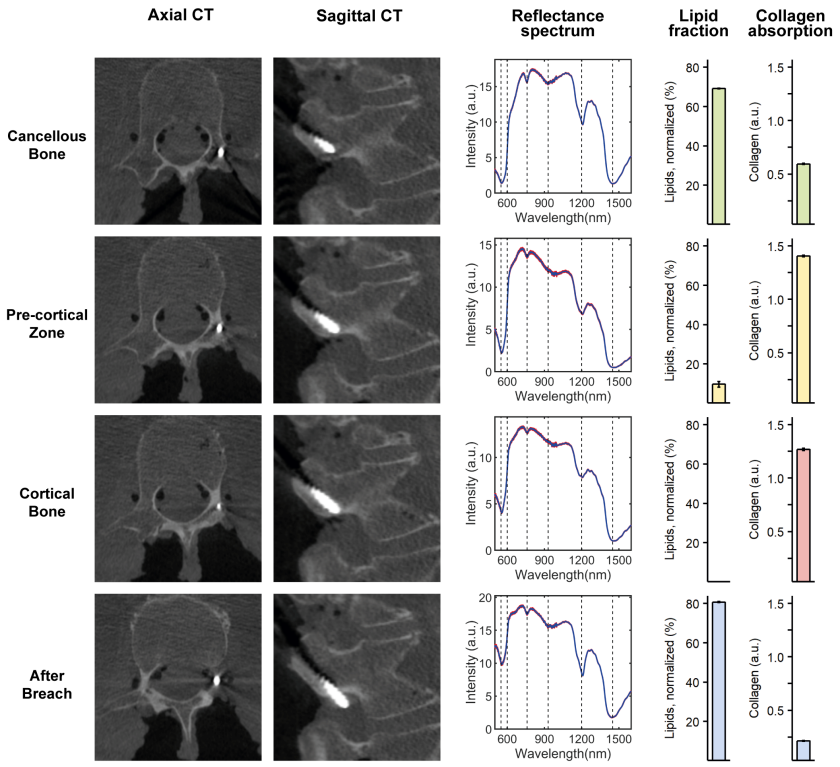

Figure 5.2: DR spectroscopy readings and associated imaging of an inferior pedicle screw breach. The first and second column shows axial and sagittal computed tomographies of each position, respectively. The third column shows acquired spectra at each position in red and the fitted spectrum in blue. The fourth and fifth column shows the measured lipid and collagen fractions, respectively.

When progressed into the cortical bone a further decline in lipid fraction (<0.01±0.00 %) and continued high collagen fraction (1.27±0.05 a.u.) was observed. Finally, when the screw tip was breached outside the vertebra a sharp increase in lipid fraction (80.71±0.52 %) and a steep drop in collagen fraction (0.21±0.01 a.u.) occurred. CBCT imaging confirmed a likely position in the spinal nerve root canal, in accordance with the very high

lipid content.

As seen in Fig. 5.3, a typical lateral breach was associated with cancellous bone readings similar to those of the inferior breach insertion. However, due to the shallow depth of the screw into the bone, it could not hold and support the weight of the probe. Thus, performing a CBCT to document probe position was not possible in cancellous bone in any of the lateral breach cases. Instead, navigational data is presented. The transition of the screw tip from cancellous bone to the pre-cortical transition zone (PCZ) was associated with a steep drop in the lipid fraction (64.32±8.78 to 47.33±0.28 %) and an increase in collagen fraction(0.57±0.01 to 1.10±0.01 a.u.) and as the tip advanced into cortical bone a gradual decline in lipid fraction (to 4.15±2.65 %) and continued high collagen fraction (1.19±0.01 a.u.) was seen. As the screw protruded outside of the vertebra, a sharp increase in lipid fraction (to 53.67±2.14 %) and a drop in collagen fraction (to 0.77±0.03 a.u.) was seen, in accordance with reading more lipid-rich tissues just outside the bone.

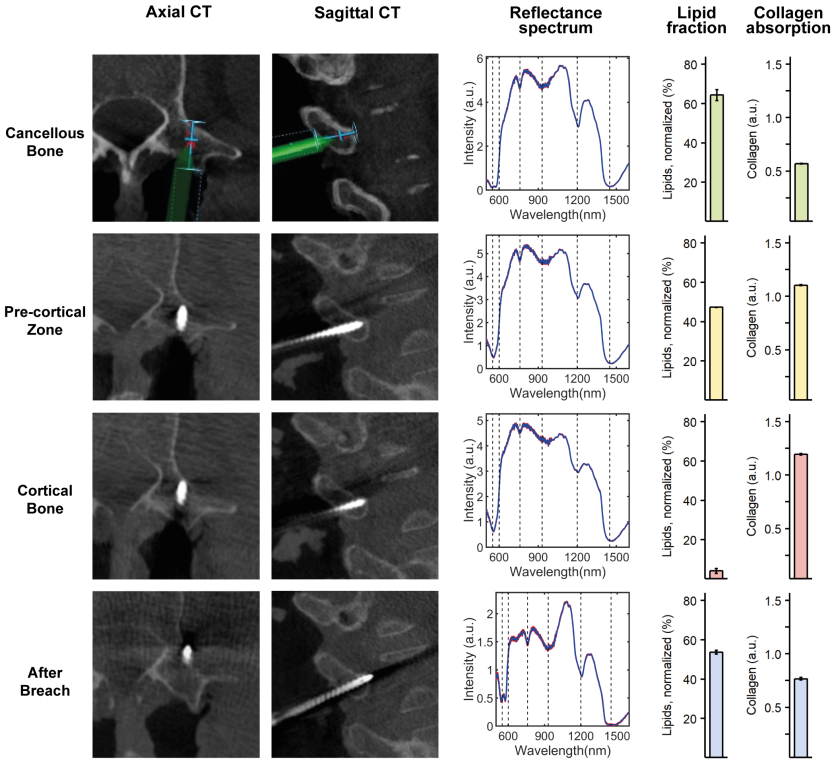

Figure 5.3: DR spectroscopy readings and associated imaging of a lateral pedicle screw breach. The first and second column shows axial and sagittal computed tomographies (CT) of each position, respectively. For cancellous bone, imaging from the navigation software is shown, since pedicle screw depth was not enough to allow for a CT. The screw is represented in green and the planned trajectory in blue. The third column shows acquired spectra at each position in red and the fitted spectrum in blue. The fourth and fifth column shows the measured lipid and collagen fractions, respectively.

A medial breach is presented in Fig. 5.4. In accordance with previous insertions, cancellous bone had a high lipid fraction (48.28±1.95 %) and relatively low collagen fraction (0.68±0.02 a.u.). As the screw tip was slowly progressed into the PCZ and subsequently the cortical bone, a decline in lipid fraction (14.13±1.83 to 2.78±6.03 %) and corresponding increase in collagen fraction (1.02±0.01 to 1.16±0.15 a.u.) was seen. When breaching medially, consecutive readings in the spinal canal was met with low lipid values (4.35±1.28 %) and low collagen values (0.13±0.01 a.u.).

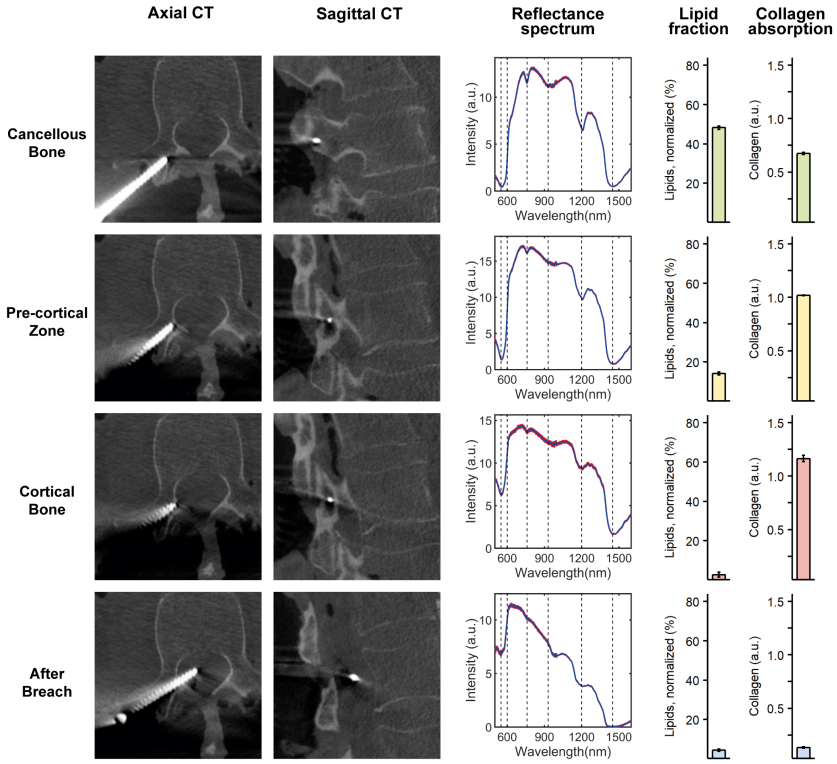

Figure 5.4: DR spectroscopy readings and associated imaging of a medial pedicle screw breach. The first and second column shows axial and sagittal computed tomographies of each position, respectively. The third column shows acquired spectra at each position in red and the fitted spectrum in blue. The fourth and fifth column shows the measured lipid and collagen fractions, respectively.

An illustration of a typical anterior breach is presented in Fig. 5.5. The transition of the screw tip from cancellous bone in the vertebral body to the pre-cortical transition zone (PCZ) was associated with a steep drop in the lipid fraction (from 50.19±0.59 to 21.74±0.73 %) and an increase in collagen fraction (from 0.37±0.01 to 0.77±0.01 a.u.). As the screw tip was slowly progressed into the cortical bone a further gradual decline in lipid fraction (to <0.01±0.00 %) and corresponding increase in collagen fraction (to 0.95±0.01 a.u.) was noticed. Finally, the transition from cortical bone to a clear breach of the screw tip outside of the vertebra was met with an increase in lipid fraction (to

46.22±0.85 %) while the collagen fraction continued to stay high (1.04±0.01 a.u.). CBCT imaging confirmed a likely position in the aortic wall, in accordance with the high presence of collagen.

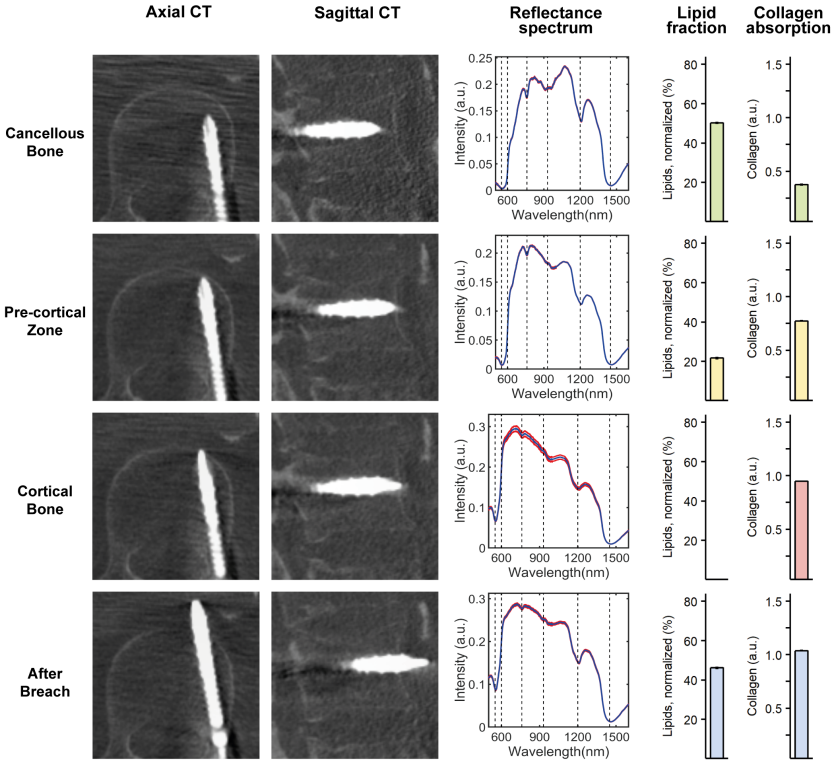

Figure 5.5: DR spectroscopy readings and associated imaging of an anterior pedicle screw breach. The first and second column shows axial and sagittal computed tomographies of each position, respectively. The third column shows acquired spectra at each position in red and the fitted spectrum in blue. The fourth and fifth column shows the measured lipid and collagen fractions, respectively.

5.3.2. AGGREGATED DATA FOR DETECTING THE CORTICAL BORDER

A total of 45 pedicle screw breaches were performed in thoracic (21) and lumbar (24) vertebrae of the six cadavers. The complete dataset included 1615 DR spectroscopy measurements with verified tissue positions. The mean lipid fraction was 49.19±16.28 %, 25.06±14.76 %, 0.42±2.12 %, and 42.79±32.28 % for cancellous bone, PCZ, cortical bone, and after breach, respectively (Fig. 5.6A). There were statistically significant changes in mean lipid fraction between all consecutive tissues ($P < 0.001$ for all). For collagen, there were statistically significant changes as well between all consecutive tissues ($P < 0.001$ for all), with mean collagen readings of 0.60±0.26 a.u., 0.84±0.25 a.u., 1.03±0.19 a.u., and 0.60±0.37 a.u. for cancellous bone, PCZ, cortical bone, and after breach, respectively (Fig. 5.6B).

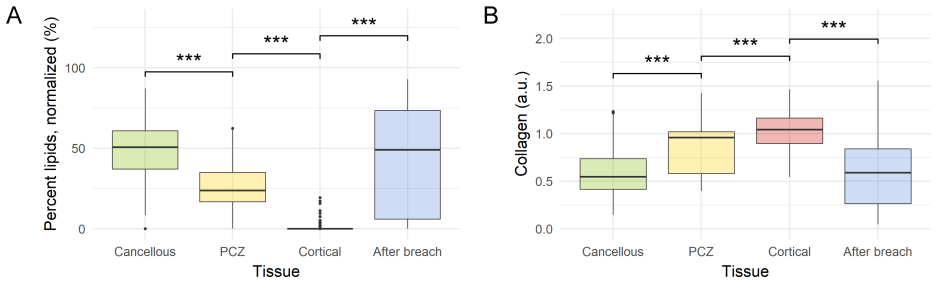

Figure 5.6: Mean lipid fraction (A) and collagen volume fraction (B) for each tissue type during 45 pedicle screw breaches of varying types (anterior, lateral, medial, and inferior). Each step-wise change is associated with a statistically significant change as indicated by asterisks (*** = P < .001) Abbreviations: PCZ = Pre-cortical zone

The PCZ was found to correlate to a binomial distribution of lipid fraction readings indicating a step-wise decrease in lipid content as the probe moved closer to the cortical bone (Fig. 5.7A). However, the spread of collagen readings in the PCZ indicated a dichotomous behavior (Fig. 5.7B) with binomially distributed peaks well correlated to either cancellous or cortical bone.

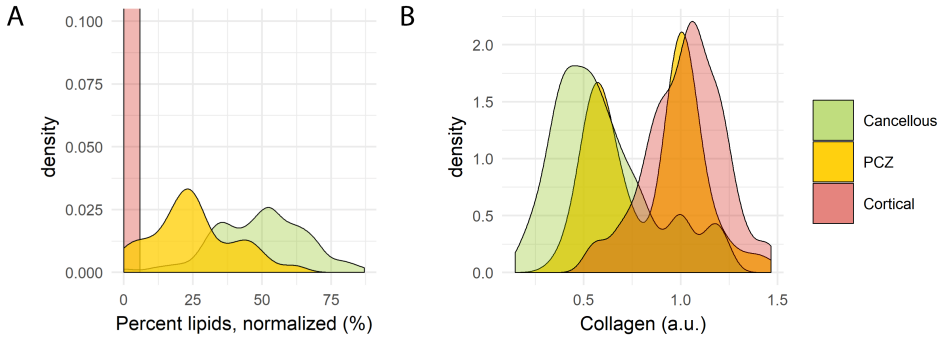

Figure 5.7: Density plots of lipid fraction (A) and collagen volume fraction (B) for all 45 pedicle screw breaches for cancellous bone, cortical bone, and the pre-cortical zone. In (A), the lipid content of the pre-cortical zone follows a binomial distribution in between the two bone types whereas in (B) collagen exhibits a dichotomous behavior in the pre-cortical zone. Abbreviations: PCZ = Pre-cortical zone

5.3.3. TISSUE CLASSIFICATION USING SUPPORT VECTOR MACHINES

By training the model on 66% of the data and validating on the remaining 33 %, the model achieved a sensitivity of 98.1 %, specificity of 98.9 %, and an accuracy of 98.7% when using only fat fraction and collagen content as input. For the LOO method, 4 cadavers met the criteria for acting as a validation set, meaning 4 cross-over validations were performed. The LOO method resulted in a mean sensitivity of 98.3% [94.3-100 %], a mean specificity of 97.7% [91.0-100 %], and a mean accuracy of 97.6[93.0 %-100 %] when using fat fraction and collagen as input to the model. When basing the LOO-models on fat fraction, collagen, and scattering parameters (Mie scattering slope and Mie-to-

Rayleigh fraction) the mean sensitivity was 99.4% [97.8-100 %], the mean specificity was 97.6% [90.2-100 %], and the mean accuracy was 97.9% [92.5-100 %].

5.4. DISCUSSION

In this study, we examined the use of DR spectroscopy for cortical breach detection in spinal fixation surgery. The method accurately and reproducibly detected impending breach defined as entry into the pre-cortical zone (PCZ) and subsequently the cortical bone, for various types of breaches. The most robust spectral change was seen in measurements of lipid fraction. In each type of pedicle breach, a sharp drop in DR spectroscopy levels representing lipid fraction was seen with the transition from fatty cancellous bone to the PCZ and cortical bone with a very low lipid fraction (Fig. 5.2–5.5). On an aggregate level, lipid fraction also showed a narrow spread of the data for each tissue type. The limited overlap of lipid fraction readings between cancellous and cortical bone meant that the tissue type could, in many cases, be reliably determined from analysis of lipid fraction only. The use of lipid fraction is also supported by a strong correlation between lipid fraction levels according to DRS and MRI, meaning that the generalizability of lipid values is facilitated when extending the technology to different patient groups [32]. However, the inclusion of collagen and scattering parameters would increase reliability for safe clinical use.

Previously, the same technology was investigated using Monte-Carlo simulations and tested during a single vertebral insertion [13]. It was found that water did not significantly contribute to discriminatory power. Blood (hemoglobin) did contribute, but in a cadaveric setting makes little sense to study when the use-case would be in the living. Meanwhile, collagen content was not studied. In this manuscript our purpose was to validate the technology in a cadaveric setting and in actual surgical use-cases with statistical rigor. As part of this, we also added collagen as a discriminatory factor because of the well-known difference in collagen content between cancellous and cortical bone [33].

When applying SVMs to distinguish between cancellous and cortical bone, a sensitivity of 98-99% and a specificity of 98-99% was achieved. Although this indicates that clinically relevant reliability is possible, it should be further validated in larger study. The same approach can be applied to separate cancellous bone from the PCZ, but would require a significantly larger dataset to test reliably on. Still, having a high accuracy for distinguishing cancellous and cortical bone ensures that breaches are very rarely missed while giving few false alarms.

5.4.1. POSSIBLE FUTURE COMPONENTS OF TISSUE LABELLING ALGORITHMS

While collagen and scattering parameters were significantly different between tissue types, the spread of data was large enough that one-parameter readings would not be sufficient for determining the tissue type. However, by using the parameters selectively in conjunction to the lipid fraction the overall reliability could be increased, as was done with the SVMs. A practical example of this is demonstrated in Fig. 5.3, where a comparatively high lipid content was present in all tissue types when compared to other insertions. If relying only on lipid fraction, and in absence of knowing the previous cancellous

readings, both the PCZ and cortical reading could have been misinterpreted as cancellous bone due to the high lipid content. However, from the aggregated data (Fig. 5.6) we found that while a low collagen fraction has a low sensitivity and specificity for tissue identification, high values are almost exclusively encountered in the PCZ and cortical bone. Thus, the high collagen fraction seen in the case of Fig. 5.3 would clearly indicate that the tissue belongs to either the PCZ or cortical bone. In a similar fashion, scattering parameters could be structured for increasing the discriminatory power of DR spectroscopy for tissue labelling in future studies. This has previously been demonstrated by Liu et al, using only scattering parameters to detect the cortical border in a lab setup [34]. They reached a similar conclusion, that more parameters would be needed to increase the reliability in detecting the cortical border. Thus, we suggest that these parameters be used in combination with lipid fraction to increase sensitivity and specificity in future breach prevention algorithms.

An interesting finding was the dissimilar behavior of the lipid and collagen fractions in the PCZ. The lipid fraction was seen to predictably decrease during the transition from cancellous bone, to the PCZ, and to cortical bone. On the other hand, the collagen fraction showed a clear bimodal distribution indicating a dichotomous behavior (Fig. 5.7B) where the distribution peaks correlated well with the distributions of the cancellous and cortical bone, respectively. This indicates that collagen might be used as a distinct indicator of impending breach while lipid content could provide a progressive scale indicating distance to the border. However, this hypothesis could not fully be proven in this study because of the small distances in question (0-3 mm) in relation to the distance between the optical fibers in the probe (1.22 mm), meaning that the uncertainty of fiber position (which could not be visualized on CBCT) was large enough not to enable investigation of a direct linear relationship between distance and DRS readings in the PCZ.

Another way of increasing the precision of the technology for determining tissue types is implementing a temporal component in the analysis. During an insertion, while continuously providing values on lipid fraction, collagen fraction, scattering etc., a considerable relative change in the right direction, e.g. a drop in lipid fraction when approaching the cortex, could be as valuable as the absolute DR spectroscopy values. This relative change-model could thus be beneficial in situations where an atypical bone constitution leads to unreliable absolute values, which could be the case in bone altering diseases such as osteoporosis or osteoarthritis. This is one of the natural next steps in future studies in the research area.

5.4.2. RISK OF MISCLASSIFICATION OF TISSUES

In our analysis of spectral data, we primarily relied on fitted parameters for determining tissue constituents, and specific physical parameters such as scattering. The data included both visible light and the near-infrared spectrum. This has the advantage of being less sensitive to aberrant readings at certain specified wavelengths, as was the case for early DR spectroscopy studies in human tissues [35, 36]. Conversely, there is still a risk of misclassification either due to aberrant tissue composition or due to an abundancy of chromophores making readings of other tissue constituents harder. This was one of the limitations of our study, as hemoglobin is one such chromophore and our experiments were done on cadavers where, although hemoglobin was present, perfusion

was absent. However, studies on other parts of the body using the same type of DR spectroscopy technology have shown good reliability for determining tissue types despite this fact [17, 37].

One way to reduce the likelihood of a tissue misclassification having a clinical impact, would be to introduce a warning system for 'bad fits' of the spectral curve. Aberrant spectral readings or light inferences would most likely lead to spectral curves that are not immediately recognizable by the fitting algorithms, therefore, such interference can be detected by above-normal discrepancies between the actual spectral curve and the fitted curve. Such a warning system was already part of the research software used in this study and provided an indication on when the spectral output and the resultant fitted curve contained deviations beyond a pre-determined threshold. In such a circumstance, the surgeon would receive an indication that the DR spectroscopy readings were of limited quality.

5.4.3. SIMILAR TECHNOLOGIES AND USES

Current widely used breach detection methods involves simple tactile feedback using pedicle feelers as well as neurophysiological monitoring involving electrical stimulation at the pedicle screws after placement to detect any direct contact with nerve roots [38]. These methods may help to identify pedicle breach but have not sufficed in reducing pedicle screw misplacements rates to acceptable levels [3].

There have been other forays into the field of surgical instruments aiming to warn surgeons of impending breach in spinal surgery. One of the alternative technologies relies on electrical conductivity at the tip of a probe used during surgery [7, 8]. This technology provides a validated warning system for impending pedicle breach in real-time, in a similar fashion to what this study investigates by applying DR spectroscopy to the tip of a probe. One of the draw-backs of relying on electrical conductivity, however, is that such technology does not provide feedback on the direction of the impending breach, including if the cortical border is simply close but in parallel to the instrument [7]. Instead, it is left to the surgeon to figure out what went wrong and how to correct it. This shortcoming could potentially be corrected using DR spectroscopy instead of electrical conductivity, as the light cone has a specific direction. By using one forward-looking light cone, as was done in this study, the system will give a warning only if the cortical border is in front of the instrument and at risk of breach. A DR spectroscopy probe with multiple light cones in different directions could even provide directional feedback to the surgeon, i.e. how to correct the screw path in order to avoid breach.

In summary, the addition of an optical sensing technology to the tip of a surgical instrument used in spine surgery for pedicle screw placement, can potentially improve surgical outcomes and reduce complication rates by preventing cortical breaches. This, in turn, may also prevent repeat surgeries and thereby lower overall medical costs related to spine surgery. This initial cadaveric study serves as a proof-of-concept that the technology reliably identifies differences between cancellous bone, cortical bone, and an in-between transition zone we call the pre-cortical zone.

5.5. CONCLUSIONS

DR spectroscopy technology reliably identifies the area of transition from cancellous to cortical bone in typical breach scenarios. DRS technology in the tip of a surgical instrument has the potential to help the surgeon avoid pedicle screw breach in spinal fixation surgery.

REFERENCES

[1] G. Burström, A. Swamy, J. W. Spliethoff, C. Reich, D. Babic, B. H. Hendriks, H. Skulason, O. Persson, A. E. Terander, and E. Edström, "Diffuse reflectance spectroscopy accurately identifies the pre-cortical zone to avoid impending pedicle screw breach in spinal fixation surgery," *Biomedical Optics Express*, vol. 10, no. 11, pp. 5905–5920, 2019.

[2] A. Weiss, A. Elixhauser, and R. Andrews, "Characteristics of operating room procedures in us hospitals, 2011: statistical brief# 170," 2006.

[3] V. Kosmopoulos and C. Schizas, "Pedicle screw placement accuracy: a meta-analysis," *Spine*, vol. 32, no. 3, pp. E111–E120, 2007.

[4] N.-F. Tian, Q.-S. Huang, P. Zhou, Y. Zhou, R.-K. Wu, Y. Lou, and H.-Z. Xu, "Pedicle screw insertion accuracy with different assisted methods: a systematic review and meta-analysis of comparative studies," *European Spine Journal*, vol. 20, no. 6, pp. 846–859, 2011.

[5] I. D. Gelalis, N. K. Paschos, E. E. Pakos, A. N. Politis, C. M. Arnaoutoglou, A. C. Karageorgos, A. Ploumis, and T. A. Xenakis, "Accuracy of pedicle screw placement: a systematic review of prospective in vivo studies comparing free hand, fluoroscopy guidance and navigation techniques," *European Spine Journal*, vol. 21, no. 2, pp. 247–255, 2012.

[6] P. A. Helm, R. Teichman, S. L. Hartmann, and D. Simon, "Spinal navigation and imaging: history, trends, and future," *IEEE transactions on medical imaging*, vol. 34, no. 8, pp. 1738–1746, 2015.

[7] P. T. Guillen, R. G. KnoPPeR, J. KRoGeR, N. D. Wycliffe, O. A. Danisa, and W. K. Cheng, "Independent assessment of a new pedicle probe and its ability to detect pedicle breach: a cadaveric study," *Journal of Neurosurgery: Spine*, vol. 21, no. 5, pp. 821–825, 2014.

[8] C. Bolger, M. O. Kelleher, L. McEvoy, M. Brayda-Bruno, A. Kaelin, J.-Y. Lazennec, J.-C. Le Huec, C. Logroscino, P. Mata, P. Moreta, *et al.*, "Electrical conductivity measurement: a new technique to detect iatrogenic initial pedicle perforation," *European Spine Journal*, vol. 16, no. 11, pp. 1919–1924, 2007.

[9] P. Matousek, E. R. Draper, A. E. Goodship, I. P. Clark, K. L. Ronayne, and A. W. Parker, "Noninvasive raman spectroscopy of human tissue in vivo," *Applied spectroscopy*, vol. 60, no. 7, pp. 758–763, 2006.

[10] M. D. Morris and G. S. Mandair, "Raman assessment of bone quality," *Clinical Orthopaedics and Related Research®*, vol. 469, no. 8, pp. 2160–2169, 2011.

[11] C. Krafft, D. Codrich, G. Pelizzo, and V. Sergo, "Raman and ftir microscopic imaging of colon tissue: a comparative study," *Journal of biophotonics*, vol. 1, no. 2, pp. 154–169, 2008.

[12] D. R. Rohleder, G. Kocherscheidt, K. Gerber, W. Kiefer, W. Köhler, J. Möcks, and W. H. Petrich, "Comparison of mid-infrared and raman spectroscopy in the quantitative analysis of serum," *Journal of biomedical optics*, vol. 10, no. 3, p. 031108, 2005.

[13] A. Swamy, G. Burström, J. W. Spliethoff, D. Babic, C. Reich, J. Groen, E. Edström, A. E. Terander, J. M. Racadio, J. Dankelman, *et al.*, "Diffuse reflectance spectroscopy, a potential optical sensing technology for the detection of cortical breaches during spinal screw placement," *Journal of biomedical optics*, vol. 24, no. 1, p. 017002, 2019.

[14] R. Van Veen, H. J. Sterenborg, A. Pifferi, A. Torricelli, E. Chikoidze, and R. Cubeddu, "Determination of visible near-ir absorption coefficients of mammalian fat using time-and spatially resolved diffuse reflectance and transmission spectroscopy," *Journal of biomedical optics*, vol. 10, no. 5, p. 054004, 2005.

[15] T. J. Farrell, M. S. Patterson, and B. Wilson, "A diffusion theory model of spatially resolved, steady-state diffuse reflectance for the noninvasive determination of tissue optical properties in vivo," *Medical physics*, vol. 19, no. 4, pp. 879–888, 1992.

[16] R. Doornbos, R. Lang, M. Aalders, F. Cross, and H. Sterenborg, "The determination of in vivo human tissue optical properties and absolute chromophore concentrations using spatially resolved steady-state diffuse reflectance spectroscopy," *Physics in Medicine & Biology*, vol. 44, no. 4, p. 967, 1999.

[17] J. P. Rathmell, A. E. Desjardins, M. van der Voort, B. H. Hendriks, R. Nachabe, S. Roggeveen, D. Babic, M. Söderman, M. Brynolf, and B. Holmström, "Identification of the epidural space with optical spectroscopyanin vivo swine study," *Anesthesiology: The Journal of the American Society of Anesthesiologists*, vol. 113, no. 6, pp. 1406–1418, 2010.

[18] Z. I. Volynskaya, A. S. Haka, K. L. Bechtel, M. Fitzmaurice, R. Shenk, N. Wang, J. Nazemi, R. R. Dasari, and M. S. Feld, "Diagnosing breast cancer using diffuse reflectance spectroscopy and intrinsic fluorescence spectroscopy," *Journal of biomedical optics*, vol. 13, no. 2, p. 024012, 2008.

[19] G. Zonios, L. T. Perelman, V. Backman, R. Manoharan, M. Fitzmaurice, J. Van Dam, and M. S. Feld, "Diffuse reflectance spectroscopy of human adenomatous colon polyps in vivo," *Applied optics*, vol. 38, no. 31, pp. 6628–6637, 1999.

[20] F. Stelzle, A. Zam, W. Adler, K. Tangermann-Gerk, A. Douplik, E. Nkenke, and M. Schmidt, "Optical nerve detection by diffuse reflectance spectroscopy for feedback controlled oral and maxillofacial laser surgery," *Journal of translational medicine*, vol. 9, no. 1, p. 20, 2011.

[21] J. H. Nilsson, N. Reistad, H. Brange, C.-F. Öberg, and C. Sturesson, "Diffuse reflectance spectroscopy for surface measurement of liver pathology," *European Surgical Research*, vol. 58, no. 1-2, pp. 40–50, 2017.

[22] M. G. Müller, T. A. Valdez, I. Georgakoudi, V. Backman, C. Fuentes, S. Kabani, N. Laver, Z. Wang, C. W. Boone, R. R. Dasari, *et al.*, "Spectroscopic detection and

evaluation of morphologic and biochemical changes in early human oral carcinoma," *Cancer: Interdisciplinary International Journal of the American Cancer Society*, vol. 97, no. 7, pp. 1681–1692, 2003.

[23] A. Elmi-Terander, G. Burström, R. Nachabe, H. Skulason, K. Pedersen, M. Fagerlund, F. Ståhl, A. Charalampidis, M. Söderman, S. Holmin, *et al.*, "Pedicle screw placement using augmented reality surgical navigation with intraoperative 3d imaging: a first in-human prospective cohort study," *Spine*, vol. 44, no. 7, p. 517, 2019.

[24] G. Burström, C. Buerger, J. Hoppenbrouwers, R. Nachabe, C. Lorenz, D. Babic, R. Homan, J. M. Racadio, M. Grass, O. Persson, *et al.*, "Machine learning for automated 3-dimensional segmentation of the spine and suggested placement of pedicle screws based on intraoperative cone-beam computer tomography," *Journal of Neurosurgery: Spine*, vol. 31, no. 1, pp. 147–154, 2019.

[25] W. Li, Y. Liu, and Z. Qian, "Determination of detection depth of optical probe in pedicle screw measurement device," *Biomedical engineering online*, vol. 13, no. 1, p. 148, 2014.

[26] B. H. Hendriks, A. J. Balthasar, G. W. Lucassen, M. van der Voort, M. Mueller, V. V. Pully, T. M. Bydlon, C. Reich, A. T. van Keersop, J. Kortsmit, *et al.*, "Nerve detection with optical spectroscopy for regional anesthesia procedures," *Journal of translational medicine*, vol. 13, no. 1, p. 380, 2015.

[27] L. L. De Boer, T. M. Bydlon, F. Van Duijnhoven, M.-J. T. V. Peeters, C. E. Loo, G. A. Winter-Warnars, J. Sanders, H. J. Sterenborg, B. H. Hendriks, and T. J. Ruers, "Towards the use of diffuse reflectance spectroscopy for real-time in vivo detection of breast cancer during surgery," *Journal of translational medicine*, vol. 16, no. 1, p. 367, 2018.

[28] R. Nachabe, B. H. Hendriks, A. E. Desjardins, M. van der Voort, M. B. van der Mark, and H. J. Sterenborg, "Estimation of lipid and water concentrations in scattering media with diffuse optical spectroscopy from 900 to 1600 nm," *Journal of biomedical optics*, vol. 15, no. 3, p. 037015, 2010.

[29] P. Taroni, D. Comelli, A. Pifferi, A. Torricelli, and R. Cubeddu, "Absorption of collagen: effects on the estimate of breast composition and related diagnostic implications," *Journal of Biomedical Optics*, vol. 12, no. 1, p. 014021, 2007.

[30] W. S. Noble, "What is a support vector machine?," *Nature biotechnology*, vol. 24, no. 12, pp. 1565–1567, 2006.

[31] C.-C. Chang and C.-J. Lin, "Libsvm: A library for support vector machines," *ACM transactions on intelligent systems and technology (TIST)*, vol. 2, no. 3, pp. 1–27, 2011.

[32] A. Swamy, G. Burström, J. W. Spliethoff, D. Babic, S. Ruschke, J. M. Racadio, E. Edström, A. Elmi-Terander, J. Dankelman, and B. H. Hendriks, "Validation of diffuse reflectance spectroscopy with magnetic resonance imaging for accurate vertebral

bone fat fraction quantification," *Biomedical optics express*, vol. 10, no. 8, pp. 4316–4328, 2019.

[33] W. R. Walsh, M. Walton, W. Bruce, Y. Yu, R. M. Gillies, and M. Svehla, "Cell structure and biology of bone and cartilage," in *Handbook of histology methods for bone and cartilage*, pp. 35–58, Springer, 2003.

[34] Y. Liu, Y. Wang, Z. Qian, J. Zhao, X. Cao, and W. Li, "Monitoring the reduced scattering coefficient of bone tissues on the trajectory of pedicle screw placement using near-infrared spectroscopy," *Journal of biomedical optics*, vol. 19, no. 11, p. 117002, 2014.

[35] S. A. Toms, W.-C. Lin, R. J. Weil, M. D. Johnson, E. D. Jansen, and A. Mahadevan-Jansen, "Intraoperative optical spectroscopy identifies infiltrating glioma margins with high sensitivity," *Operative Neurosurgery*, vol. 57, no. suppl_4, pp. ONS–382, 2005.

[36] R. Andrews, R. Mah, A. Aghevli, K. Freitas, A. Galvagni, M. Guerrero, R. Papsin, C. Reed, and D. Stassinopoulos, "Multimodality stereotactic brain tissue identification: the nasa smart probe project," *Stereotactic and functional neurosurgery*, vol. 73, no. 1-4, pp. 1–8, 1999.

[37] J. W. Spliethoff, W. Prevoo, M. A. Meier, J. de Jong, H. M. Klomp, D. J. Evers, H. J. Sterenborg, G. W. Lucassen, B. H. Hendriks, and T. J. Ruers, "Real-time in vivo tissue characterization with diffuse reflectance spectroscopy during transthoracic lung biopsy: a clinical feasibility study," *Clinical cancer research*, vol. 22, no. 2, pp. 357–365, 2016.

[38] S. L. Parker, M. J. McGirt, S. H. Farber, A. G. Amin, A.-M. Rick, I. Suk, A. Bydon, D. M. Sciubba, J.-P. Wolinsky, Z. L. Gokaslan, *et al.*, "Accuracy of free-hand pedicle screws in the thoracic and lumbar spine: analysis of 6816 consecutive screws," *Neurosurgery*, vol. 68, no. 1, pp. 170–178, 2011.

6

DIFFUSE REFLECTANCE SPECTROSCOPY FOR BREACH DETECTION: A FIRST *in vivo* INVESTIGATION IN A PORCINE MODEL

The study presents the first in vivo minimally invasive procedure using DRS sensing at the tip of a Jamshidi needle with an integrated optical K-wire. We investigate the effect of tissue perfusion and probe handling conditions on the reliability of fat fraction measurements for breach detection in vivo. A Jamshidi needle with an integrated fiber-optic K-wire was gradually inserted into the vertebrae under intraoperative image guidance. The fiber-optic K-wire consisted of two optical fibers with a fiber-to fiber distance of 1.024 mm. DRS spectra in the wavelength ranges of 450 to 1600 nm were acquired at several positions along the path inside the vertebrae. Probe handling conditions were varied by changing the amount of pressure exerted on the probe within the vertebrae. Continuous spectra were recorded as the probe was placed in the center of the vertebral body while the porcine specimen was sacrificed via a lethal injection. A typical insertion of the fiber-optic K-wire showed a drop in fat fraction during an anterior breach as the probe transitioned from cancellous to cortical bone. Fat fraction measurements were found to be similar irrespective of the amount of pressure exerted on the probe (p= 0.65). The 95% confidence interval of fat fraction determination was found in the narrow range of 1.5-3.6% under various probe handling conditions. The fat fraction measurements remained stable during 70 minutes of decreased blood flow after the animal was sacrificed. These findings indicate that changes in tissue perfusion and probe handling conditions have a relatively low measureable effect on the DRS signal quality and thereby on the determination of fat fraction as a breach detection signal.

Adapted from article: Swamy A., Spliethoff J.W., Burström G., Babic D., Reich C., Groen J., Edström E., Elmi-Terander A., Racadio J.M., Dankelman J. and Hendriks B.H.W. Diffuse Reflectance Spectroscopy for breach detection during pedicle screw placement: A first *in vivo* investigation in a porcine model. Biomedical Engineering OnLine, 19(1) 2020.

6.1. BACKGROUND

In spinal fusion surgery, pedicle screws are placed into the vertebrae and connected with rods to fuse parts of the spine in order to regain and maintain spinal stability [1]. Serious vascular and neurological injuries can occur due to inaccurate placement of pedicle screws [2–4]. Currently, there is a trend towards minimally invasive surgery (MIS) [5], owing to benefits such as reduced surgical trauma, decreased postoperative pain and shortened hospital stays [6]. However, MIS requires technical aids, since the small surgical wounds do not allow visualization of anatomical landmarks. Several guidance techniques including navigation systems and other non-imaging based techniques have been developed for safe and accurate pedicle screw placement [7]. However, accuracy rates of pedicle screw placement reported in the literature vary widely. Meta-analysis studies indicate that using the free-hand technique, breaches of greater than 4 mm occur in 1-6.5% of the placed pedicle screws [8–10]. Based on a recent systematic review by Staartjes et al. [11], these inaccuracies lead to screw revisions in 6.0 % of operated patients. Misplaced screws can also lead to new complications and extended hospital stays [12]. Therefore, using pedicle screw guidance solutions may further improve the safety of these procedures.

Currently, surgeons may use an electrical conductivity-based device to assist them in detecting impending breach [13, 14]. However, this device is known to be affected by variations in probe handling conditions during the maneuvering of the probe in perfused vertebrae [15]. Neurophysiological monitoring techniques, whereby a placed pedicle screw is electrically stimulated and distal motor responses are monitored, can also be used for breach detection but are employed only after the screws are placed and are known to have low sensitivity in identifying screw misplacement [16]. Thus, this technology cannot serve to predict or prevent a breach.

Real-time monitoring of tissue characteristics using diffuse reflectance spectroscopy (DRS) at the tip of an instrument, may offer a new possibility for intra-operative guidance. The technology can be used to determine physiological parameters such as fat and water content and fat fraction, within the tissues ahead of an instrument and has previously been investigated for detection of breaches during pedicle screw placement [17, 18]. Using a custom-built screw probe with integrated optical fibers to sample fat fraction within vertebrae, the technology could accurately predict the transition from cancellous to cortical bone with high sensitivity and specificity [18]. However, these studies were all performed *ex vivo* and the possible influence of blood at the tip of the probe could not be studied.

Thus, a natural next step is to gauge the reliability of the DRS technique in an *in vivo* setting. Spliethoff et al. [19] investigated the clinical use of DRS for lung biopsy guidance in an *in vivo* setting and found that the reliability of DRS measurements were not influenced by the presence of blood due to tissue perfusion. However, the findings from lung biopsy cannot be assumed to be transferrable to the case of breach detection in the spine. The tissue composition, and the effects of probe handling within the tissue, and the effects of perfusion within the vertebrae need to be fully understood to develop a novel and robust breach detection algorithm. Moreover, the effect of changes in probe handling or probe contact pressure on the *in vivo* DRS measurements need to be studied. Literature shows that the spectral response to probe contact pressure is complex,

and dependent upon several factors including probe contact area, wavelength window, tissue type and the probe operator involved. The majority of these studies focused on application of probe pressure on soft tissues such as human skin, liver and heart [20–24]. However, the effect of contact pressure on DRS based physiological measurements in vertebrae, has not been studied. Therefore, the purpose of this study was to investigate the reliability of fat fraction measurements as a breach detection method, in an *in vivo* model during different probe handling conditions and during normal as well as abnormal tissue perfusion conditions.

6.2. METHODS

6.2.1. PORCINE ANIMAL MODEL

An animal experiment was conducted at the Cincinnati Children's Hospital Medical Center, Ohio, United States. The study was approved by the Institutional Animal Care and Use Committee in compliance with the ethical guidelines for animal studies. For the experiment a 5 months and 18 days old pig weighing 78.4 Kg was used in an *in vivo* setting under general anesthesia. The animal was euthanized at the conclusion of the experiment. Additional data was collected during and after this phase.

6.2.2. EXPERIMENTAL DESIGN

The animal was positioned on the table in prone position on an operating table. Cone beam computed tomography (CBCT) images were acquired (AlluraClarity FD20; Philips Healthcare, Best, the Netherlands) and an augmented reality surgical navigation system (ARSN) was used to plan the trajectories of the insertions [25]. After an initial skin incision, a Jamshidi needle was navigated towards the pedicle with ARSN guidance as previously described [26, 27]. Once the entry point on the vertebrae was encountered, the Jamshidi needle was hammered, in a stepwise fashion to penetrate the pedicle and the vertebral body. The position of the Jamshidi needle along with the navigation path was verified by acquiring consecutive CBCT images. Once bone purchase of the Jamshidi needle within the vertebra was achieved, the inner stylet was removed and the fiber-optic K-wire was introduced, as show in in Fig. 6.1. A set containing three types of measurement conditions were performed for each position: (first) 10 DRS measurements were acquired while a low axial pressure was applied to the probe ($1.2 \pm 0.3 N/mm^2$); (second) 10 measurements were acquired while a high axial pressure was applied ($6.1 \pm 0.5 N/mm^2$); (third) the fiber-optic K-wire was retracted by 1-2 mm from its initial position and 10 measurements were performed. Low and high probe pressures were quantified in a prior study. The fiber-optic K-wire was then removed, the inner stylet reinserted, and the Jamshidi needle was then hammered to a new position along the intended trajectory. Additional CBCT's were acquired whenever a change in DRS readings was encountered to document positions along an insertion trajectory. A final analysis of the effect of blood flow and tissue perfusion, on DRS parameters, was performed once all other measurements were taken; the porcine specimen was sacrificed by a lethal injection while the fiber-optic K-wire was left to record continuously (70 min) in the center of a vertebral body.

6.2.3. DRS INSTRUMENT

The vertebrae were probed using a Jamshidi needle with a K-wire integrated with two optical fibers at the tip of the probe i.e. the fiber-optic K-wire (diameter = 1.35 mm). The fiber-to fiber distance was 1.042 mm (Fig. 6.1). The fiber distance was chosen based on experience from previous studies and is related to the largest light penetration depth achievable for high quality DRS measurements and to ensure mechanical durability needed for bone sampling [17]. One fiber was connected to a tungsten halogen broadband light source (Avantes AvaLight-Hal-S) to transmit the light into the tissue, while the second, receiving fiber, was connected to two optical spectrometers (via a fiber splitter) as shown in Fig. 6.1. The core diameter of the source and recording receiving fibers was 200 µm. The spectrometers resolved the light in the visible (Maya2000 Pro, Ocean Optics) and near-infrared wavelength regions (NirQuest 512, Ocean Optics), to produce a spectrum in the wavelength range of 450-1600 nm. An in-house developed LabVIEW software (National Instruments, Austin, Texas) was used to control the spectrometers and perform data acquisition. The general principles of the DRS system along with the calibration method has been described previously [28–30].

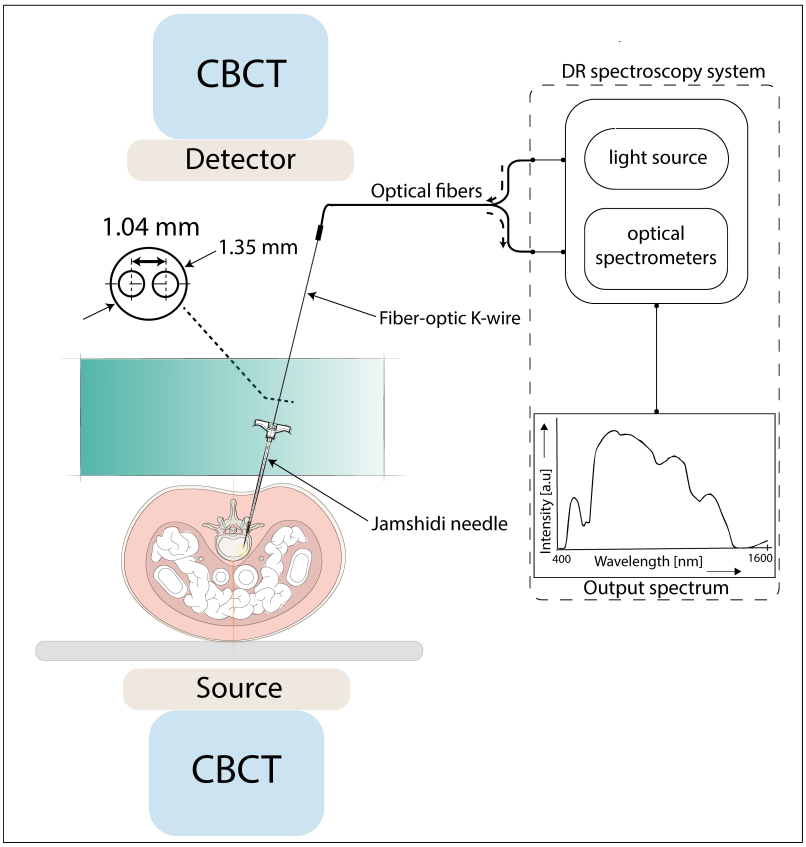

Figure 6.1: Schematic of the experimental setup.

6.2.4. DATA ANALYSIS

Six insertions were performed in six thoracic and lumbar vertebrae. A total of 270 spectra were recorded *in vivo* and analyzed further. Continuous DRS measurements were performed while the specimen was sacrificed, and a total of 2020 spectra were recorded for further analyses.

Tissue labelling of DRS measurements were performed by a trained physician, blinded to the DRS spectral readings, based on anatomical position of the probe on the CBCT verification scans. Anatomical regions of interest were defined as cancellous bone, cortical bone, pre-cortical zone (PCZ) and breach based on experience from a previous study [18]. PCZ was defined as the distance within 3 mm from cortical bone boundary. Breach was defined as the first 3 mm outside the vertebrae after the probe broke through the cortical bone [18].

6.2.5. DETERMINATION OF DRS BASED PHYSIOLOGICAL PARAMETERS

A previously described fitting model was used to translate the measured diffuse reflectance spectra into meaningful physiological parameters [29–31]. The model estimates the absorption $\mu_a(\lambda)$ and reduced scattering coefficient $\mu_{s'}(\lambda)$ expressed in cm^{-1}. From the a-priori knowledge of fiber distance and wavelength-dependent absorption coefficients, the amount of deoxygenated- hemoglobin (Hb) and oxygenated hemoglobin (HbO2), fat and water present in the probed tissue was determined using a previously described method [28]. The blood content is defined as the total concentration of hemoglobin which is the sum of concentrations of oxyhemoglobin and deoxyhemoglobin. It is expressed as a percentage of total concentration of hemoglobin in normal human blood (150 g/liter). The fat fraction is defined as a function of fat and water content, as previously described [32] and calculated as follows:

$$Fatfraction[\%] = \frac{Fat}{Fat + Water} \times 100.$$

6.2.6. STATISTICAL ANALYSIS

A Jarque-Bera test was used to test each data set for normality. All data sets were found not to be normally distributed. Therefore, the estimated physiological parameters were calculated as median values and the variation was represented as minimum and maximum values. A nonparametric Wilcoxon rank-sum test was used to perform inferential statistics, to compare the effects of probe pressure on DRS determined blood and fat fraction data sets. Confidence intervals of the physiological parameters derived from the fitting model were calculated in order to estimate the statistical errors of the fit parameters according to the method described previously by Amelink et al. [33]. Thus, the confidence interval range provides an indication of the signal to noise ratio and thereby the quality of the DRS measurements. Normalization of the spectra was applied at 1200 nm, in order to qualitatively compare spectral recordings during animal sacrifice. The significance value was set to 0.01.

6.3. RESULTS

An illustration of an anterior breach is presented in Fig. 6.2. The initial position of the fiber-optic K-wire in cancellous bone shows a median blood content of 28.9% [min 21.4 - max 51.3] and median fat fraction of 26.4% [min 11.9 - max 50.0]. The transition of the fiber-optic K-wire from cancellous bone to Pre-cortical zone (PCZ) led to a drop in fat fraction to 5.3% [min 0 - max 17.3], while the median blood content remained at 28.8%. However, the blood content in the PCZ showed high variability (min 21.0% - max 100%). As the fiber-optic K-wire progressed into the cortical bone, the median blood content declined to 19.4% [min 18.9 - max 20.5] and median fat fraction dropped to 0% [min 0 - max 0.1]. Finally, as the fiber-optic K-wire breached the cortical bone boundary, both the median blood content, 48.9% [min 48.1- max 49.6] and median fat fraction, 11.2% [min 10.9 - max 11.4] showed a sharp increase respectively.

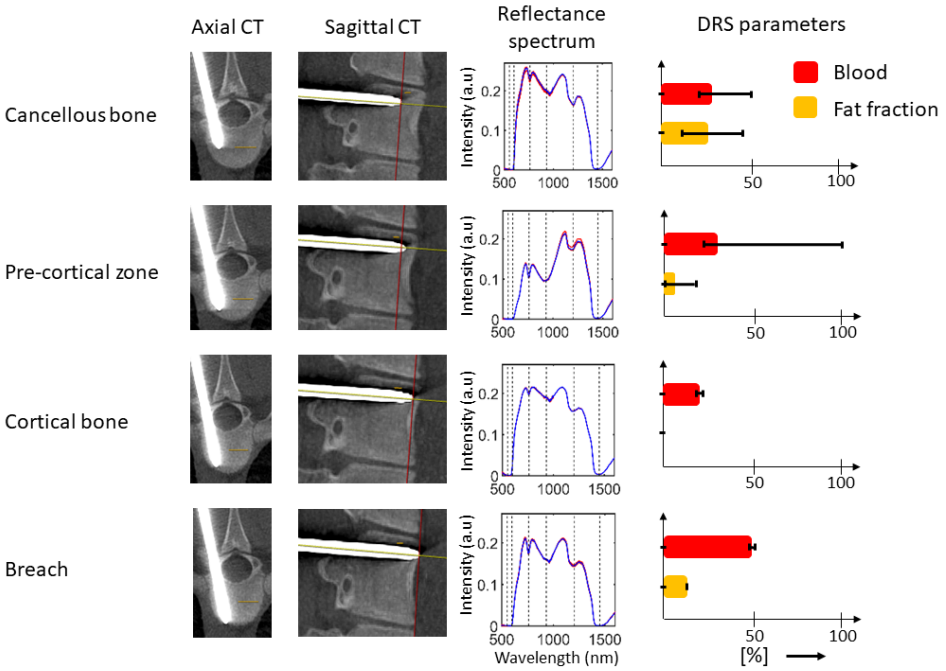

Figure 6.2: Example of an insertion into a porcine vertebra *in vivo*. DRS readings and associated imaging of an anterior fiber-optic K-wire breach. First and second column depict axial and sagittal computed tomographies of each position, respectively. The third column depicts the measured spectra at each position in red and corresponding fitted spectra in blue. The fourth column shows the median values of blood content and fat fraction with error bars indicating min and max values.

The amount of locally sampled blood content is found to be significantly higher during retracted probe condition as compared to low and high pressure probe conditions ($p<0.01$). This blood content was also found to differ between low and high pressure probe conditions ($p<0.01$) as shown in Fig. 6.3a.

Meanwhile, the amount of locally sampled fat fraction in front of the probe tip was

found to be constant during low and high pressure probe conditions (p= 0.65), as shown in Fig. 6.3b. Whereas, the amount of fat fraction was found to be significantly lower during retracted probe condition as compared to both low and high pressure probe conditions (p<0.01).

Blood content and fat fraction estimated for low and high pressure probe handling conditions have a limited relationship between each other as indicated by the low regression values in Fig 6.3c. Nevertheless, the range of 95% confidence interval [1.5-3.2%] indicates a high confidence of the estimation of fat fraction values for low and high pressure probe conditions from the DRS spectra as depicted in Fig.6.3d.

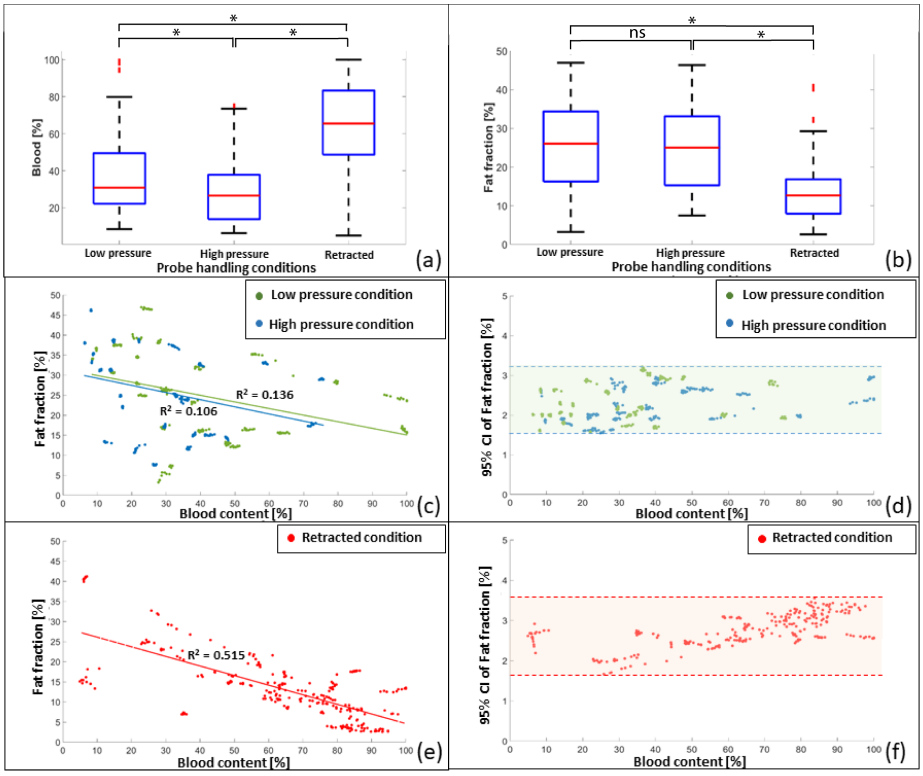

Figure 6.3: Effect of probe handling conditions on DRS based physiological parameters. (a), (b) Box plots depicting effect of probe handling conditions on blood and fat fraction. (c), (e) Scatter plot depicting distribution of blood and fat fraction due to various probe handing conditions. (d), (f) 95% confidence interval of fat fraction determination due to various probe handling conditions.

However, the retracted probe condition does indicate a trend towards a decrease in fat fraction as the locally probed blood content increases (R^2 = 0.515) as shown in Fig.6.3e. The narrow 95% confidence interval range [1.7-3.6%] indicates a high reliability of estimated values from the DRS spectra (Fig. 6.3f).

Blood content in the vertebral body decreased from 18.9% to 8.1% during 70 minutes from the time of cardiac arrest of the animal as depicted in Fig.6.4a. However, the fat

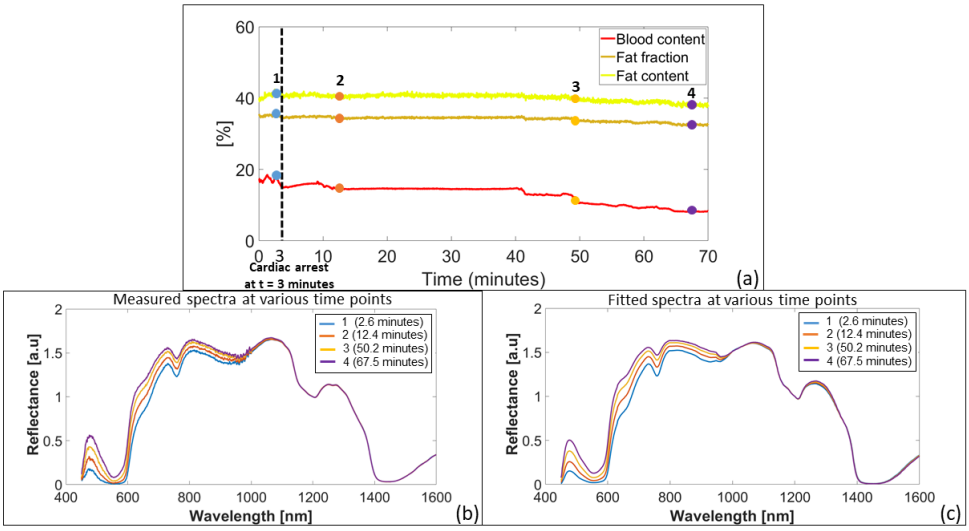

Figure 6.4: (a) Temporal changes in blood, fat fraction and fat during animal sacrifice. (b,c) Normalized spectra at 1200 nm shown at various time points for measured and fitted spectra respectively.

fraction and fat content remained relatively stable with a decrease from 35.5% to 32.3% and from 41.5% to 37.7%, respectively.

6.4. DISCUSSION

In the present study, we investigated the reliability of fat fraction measurements as a breach detection signal during different tissue perfusion and probe handing conditions using a fiber-optic K-wire inserted in porcine vertebrae in a minimally invasive *in vivo* setting. Optical fibers integrated into a K-wire were inserted into the vertebrae under image guidance while DRS measurements were recorded at various positions of the probe. The results of this study confirm that a breach can be detected in an *in vivo* setting. Sufficient contact between probe and perfused vertebral tissue ensures reliable DRS measurements. Moreover, changes in probe-handling conditions had a minor impact on the quality of the DRS measurements. Continuous DRS measurements during sacrifice of the animal indicated that the main discriminating parameter for breach detection, namely fat fraction, is largely unsusceptible to changes in tissue perfusion. A fiber-optic K-wire approaching the cortical bone boundary showed a sharp drop in DRS-based fat fraction during the transition of the probe from cancellous bone to PCZ and cortical bone (Fig. 6.2). This finding agrees with previous publications on human cadavers [17, 18]. However, a high variability of blood content and fat fraction in cancellous bone and PCZ regions within the vertebra was found as represented by the error bars in Fig. 6.2. A possible reason for such variation in the locally sampled blood and fat fraction can be attributed to the heterogeneity within the tissue due to the random distribution of vascular structures and triglyceride storage sites [17, 34, 35]. This finding is supported by the fact that cancellous bone is known to house red and yellow bone marrow within

its organic matrix for erythropoiesis and fat storage, respectively [36]. Another possible cause for the high variability in blood content can be attributed to the filling of the bone cavity from a prior retracted probe measurement condition, influencing subsequent measurements.

The relatively low blood content in cortical bone as compared to cancellous bone is in correspondence with previously published data [34, 35]. Another important aspect that was investigated, was the effect of tissue perfusion on the fat fraction and blood content measurements due to varying probe handling conditions. A significantly higher blood content was measured when the probe was retracted within the vertebrae (Fig. 6.2a). This finding makes intuitive sense since a void at the tip of the probe is expected to be created and blood tends to flow into the void space due to the temporary retraction of the probe. The fact that fat fraction significantly drops during the retracted probe condition further strengthens this claim as the composition of this bony void would mainly be a blood-filled pool (Fig. 6.3b and Fig. 6.3e). The implication of the dependence of blood and fat fraction values on retracted handling conditions is clinically relevant since it provides an indication of the directionality of the probe within the vertebrae. Since a high blood content and low fat fraction measurement most likely indicates that the probe has been retracted. Such information, derived from quantifying blood content primarily from the visible wavelength range of 450-600 nm, can be important for the surgeon for intraoperative guidance of the fiber-optic K-wire during pedicle screw placement.

Lower blood content was measured when high pressure was exerted as compared to low probe pressure. This finding is in line with previously published studies which show an inverse dependence of probe contact pressure and local hemodynamics due to the decrease in local blood volume under focal pressure [20, 24]. Similar fat fraction measurements were observed during low and high pressure probe conditions ($p = 0.65$) indicating that manual probe handling changes (i.e. using manual pressure, hammer or drill) do not affect the fat fraction measurements as long as there is a direct contact between the probe tip and the bone surface (Fig. 6.3b). Cugmas et al. [20] observed an inverse dependence of exerted probe pressure and water content in the 950 – 1600 nm wavelength window. In the present study, the effect on fat and water content was minor. The main cause of discrepancy may be attributed to the relatively lower probe pressure induced local deformation of vertebral bone, due to its higher mechanical strength (Young's modulus), as compared to human skin.

The estimation of signal quality or the signal to noise ratio of the spectra recorded during varying probe handling conditions was also important to quantify in order to avoid spurious fat fraction measurements. The 95% confidence intervals of determining fat fraction varied in a relatively narrow range of 1.5 – 3.6% under three probe handling conditions (Fig. 6.3d and Fig. 6.3f). This finding implies that tissue perfusion does not significantly affect the quality of the DRS spectra. Thus, the fat fraction determined from the fitting model can be considered to reliably reflect the local tissue composition despite the inevitable presence of blood around the probe tip.

The fact that the fat fraction signal remained almost unaffected during decreased blood circulation within the porcine specimen further points towards the reliability of fat fraction as a breach detection signal (Fig. 6.4). This finding also further validates previous cadaveric studies which investigated the use of intraoperative fat fraction measure-

ments in order to detect breaches during pedicle screw placement procedures [17, 18, 37] . The stable nature of the fat fraction signal during continuous DRS measurement within the vertebral body, 70 minutes after the time of cardiac arrest, indicates the relative independence of fat and fat fraction measurements as compared to blood content measurements. After cardiac arrest, DRS measurements show a gradual decrease in vertebral blood content (time points 1-4, fig 6.4a). In line with this, the measured reflectance spectral intensity increases in the wavelength range of 530-580 nm (Fig6.4b), the wavelength band know to be the region of maximum absorptivity of blood chromophore derivatives [38]. This phenomenon may be explained by the gradual settling of blood, livor mortis, once circulation ceases [39]. However, it is known that the fat and water chromophores are mainly sensitive to light in the near infrared wavelength range between 1000-2200 nm [32]. Fig. 6.4b indicates that the normalized reflectance intensity in the range of 1000-1600 nm for various time points showed a complete overlap after normalizing the spectra around the wavelength of 1200 nm. Fig. 6.4c depicting the reflectance spectra derived from the fitting model showed a similar trend. Thus, confirming that DRS determined blood and fat fraction values independently reflect the locally probed tissue composition. The noise within the fat and fat fraction signals in Fig. 6.4a can be attributed to the assumptions made in the fitting model.

It must be noted that the blood content defined in this study was based on the average haemoglobin concentration of a normal human. It is known that the average haemoglobin concentration of a pig is lower [40]. However, this aspect is expected to have a minor effect on the findings since relative trends rather than absolute values are of interest.

The configuration of the fiber optic K-wire allows integration into different surgical instruments. For example, it can be integrated into a manual pedicle probe (gear shift) or into a drill for quick and safe pedicle cannulation and K-wire placement.

Previously, an electrical conductivity based device has been investigated as a breach detection tool [41]. It has the drawback that the quality of the feedback is susceptible to probe handling conditions [15]. The method of breach detection applied in this study presents the possibility of measuring the local blood content and fat fraction. A combination of those has the potential to serve as a reliable feedback during pedicle screw placement procedures. However, further investigations are required to verify this claim.

6.5. CONCLUSIONS

This study investigated the reliability of fat fraction measurement as a breach detection method during tissue perfusion and different probe handling conditions. We have demonstrated that fat fraction quantification for intraoperative pedicle screw breach detection is reliable, irrespective of changes in tissue perfusion and probe handling conditions.

REFERENCES

[1] R. W. Gaines Jr, "The use of pedicle-screw internal fixation for the operative treatment of spinal disorders," *JBJS*, vol. 82, no. 10, p. 1458, 2000.

[2] L. Balabaud, S. Pitel, I. Caux, C. Dova, B. Richard, P. Antonietti, and C. Mazel, "Lumbar spine surgery in patients 80 years of age or older: morbidity and mortality," *European Journal of Orthopaedic Surgery & Traumatology*, vol. 25, no. 1, pp. 205–212, 2015.

[3] J. Ma, S. Fan, and F. Zhao, "Intraoperative malposition of pedicle probe or screws: a potential cause of the acceleration of degeneration in superior adjacent intervertebral disc," *Medical hypotheses*, vol. 77, no. 6, pp. 1102–1104, 2011.

[4] N. E. Epstein, "A review of medicolegal malpractice suits involving cervical spine: what can we learn or change?," *Clinical Spine Surgery*, vol. 24, no. 1, pp. 15–19, 2011.

[5] F. M. Phillips, I. Cheng, Y. R. Rampersaud, B. A. Akbarnia, L. Pimenta, W. B. Rodgers, J. S. Uribe, N. Khanna, W. D. Smith, J. A. Youssef, *et al.*, "Breaking through the "glass ceiling" of minimally invasive spine surgery," 2016.

[6] V. M. Lu, P. Kerezoudis, H. E. Gilder, B. A. McCutcheon, K. Phan, and M. Bydon, "Minimally invasive surgery versus open surgery spinal fusion for spondylolisthesis: a systematic review and meta-analysis," *Spine*, vol. 42, no. 3, pp. E177–E185, 2017.

[7] A. Manbachi, R. S. Cobbold, and H. J. Ginsberg, "Guided pedicle screw insertion: techniques and training," *The Spine Journal*, vol. 14, no. 1, pp. 165–179, 2014.

[8] V. Kosmopoulos and C. Schizas, "Pedicle screw placement accuracy: a meta-analysis," *Spine*, vol. 32, no. 3, pp. E111–E120, 2007.

[9] N.-F. Tian, Q.-S. Huang, P. Zhou, Y. Zhou, R.-K. Wu, Y. Lou, and H.-Z. Xu, "Pedicle screw insertion accuracy with different assisted methods: a systematic review and meta-analysis of comparative studies," *European Spine Journal*, vol. 20, no. 6, pp. 846–859, 2011.

[10] I. D. Gelalis, N. K. Paschos, E. E. Pakos, A. N. Politis, C. M. Arnaoutoglou, A. C. Karageorgos, A. Ploumis, and T. A. Xenakis, "Accuracy of pedicle screw placement: a systematic review of prospective in vivo studies comparing free hand, fluoroscopy guidance and navigation techniques," *European Spine Journal*, vol. 21, no. 2, pp. 247–255, 2012.

[11] V. E. Staartjes, A. M. Klukowska, and M. L. Schröder, "Pedicle screw revision in robot-guided, navigated, and freehand thoracolumbar instrumentation: a systematic review and meta-analysis," *World neurosurgery*, vol. 116, pp. 433–443, 2018.

[12] P. A. Helm, R. Teichman, S. L. Hartmann, and D. Simon, "Spinal navigation and imaging: history, trends, and future," *IEEE transactions on medical imaging*, vol. 34, no. 8, pp. 1738–1746, 2015.

[13] Y.-S. Bai, Y.-F. Niu, Z.-Q. Chen, X.-D. Zhu, L. K. P. Gabriel, H. K. Wong, and M. Li, "Comparison of the pedicle screws placement between electronic conductivity device and normal pedicle finder in posterior surgery of scoliosis," *Clinical Spine Surgery*, vol. 26, no. 6, pp. 316–320, 2013.

[14] T. N. Pajewski, V. Arlet, and L. H. Phillips, "Current approach on spinal cord monitoring: the point of view of the neurologist, the anesthesiologist and the spine surgeon," *European Spine Journal*, vol. 16, no. 2, pp. 115–129, 2007.

[15] P. T. Guillen, R. G. KnoPPeR, J. KRoGeR, N. D. Wycliffe, O. A. Danisa, and W. K. Cheng, "Independent assessment of a new pedicle probe and its ability to detect pedicle breach: a cadaveric study," *Journal of Neurosurgery: Spine*, vol. 21, no. 5, pp. 821–825, 2014.

[16] C.-H. Lee, H.-W. Kim, H. R. Kim, C.-Y. Lee, J.-H. Kim, and F. Sala, "Can triggered electromyography thresholds assure accurate pedicle screw placements? a systematic review and meta-analysis of diagnostic test accuracy," *Clinical Neurophysiology*, vol. 126, no. 10, pp. 2019–2025, 2015.

[17] A. Swamy, G. Burström, J. W. Spliethoff, D. Babic, C. Reich, J. Groen, E. Edström, A. E. Terander, J. M. Racadio, J. Dankelman, *et al.*, "Diffuse reflectance spectroscopy, a potential optical sensing technology for the detection of cortical breaches during spinal screw placement," *Journal of biomedical optics*, vol. 24, no. 1, p. 017002, 2019.

[18] G. Burström, A. Swamy, J. W. Spliethoff, C. Reich, D. Babic, B. H. Hendriks, H. Skulason, O. Persson, A. E. Terander, and E. Edström, "Diffuse reflectance spectroscopy accurately identifies the pre-cortical zone to avoid impending pedicle screw breach in spinal fixation surgery," *Biomedical Optics Express*, vol. 10, no. 11, pp. 5905–5920, 2019.

[19] J. W. Spliethoff, W. Prevoo, M. A. Meier, J. de Jong, H. M. Klomp, D. J. Evers, H. J. Sterenborg, G. W. Lucassen, B. H. Hendriks, and T. J. Ruers, "Real-time in vivo tissue characterization with diffuse reflectance spectroscopy during transthoracic lung biopsy: a clinical feasibility study," *Clinical cancer research*, vol. 22, no. 2, pp. 357–365, 2016.

[20] B. Cugmas, M. Bregar, M. Bürmen, F. Pernuš, and B. Likar, "Impact of contact pressure–induced spectral changes on soft-tissue classification in diffuse reflectance spectroscopy: problems and solutions," *Journal of biomedical optics*, vol. 19, no. 3, p. 037002, 2014.

[21] M. Bregar, B. Cugmas, P. Naglic, D. Hartmann, F. Pernuš, B. Likar, and M. Bürmen, "Properties of contact pressure induced by manually operated fiber-optic probes," *Journal of biomedical optics*, vol. 20, no. 12, p. 127002, 2015.

[22] W. Chen, R. Liu, K. Xu, and R. K. Wang, "Influence of contact state on nir diffuse reflectance spectroscopy in vivo," *Journal of Physics D: Applied Physics*, vol. 38, no. 15, p. 2691, 2005.

[23] L. Lim, B. S. Nichols, N. Rajaram, and J. W. Tunnell, "Probe pressure effects on human skin diffuse reflectance and fluorescence spectroscopy measurements," *Journal of biomedical optics*, vol. 16, no. 1, p. 011012, 2011.

[24] Y. Ti and W.-C. Lin, "Effects of probe contact pressure on in vivo optical spectroscopy," *Optics express*, vol. 16, no. 6, pp. 4250–4262, 2008.

[25] G. Burström, R. Nachabe, O. Persson, E. Edström, and A. E. Terander, "Augmented and virtual reality instrument tracking for minimally invasive spine surgery: a feasibility and accuracy study," *Spine*, vol. 44, no. 15, pp. 1097–1104, 2019.

[26] A. Elmi-Terander, G. Burström, R. Nachabe, H. Skulason, K. Pedersen, M. Fagerlund, F. Ståhl, A. Charalampidis, M. Söderman, S. Holmin, *et al.*, "Pedicle screw placement using augmented reality surgical navigation with intraoperative 3d imaging: a first in-human prospective cohort study," *Spine*, vol. 44, no. 7, p. 517, 2019.

[27] E. Edström, G. Burström, R. Nachabe, P. Gerdhem, and A. Elmi Terander, "A novel augmented-reality-based surgical navigation system for spine surgery in a hybrid operating room: design, workflow, and clinical applications," *Operative Neurosurgery*, 2019.

[28] R. Nachabe, B. H. Hendriks, A. E. Desjardins, M. van der Voort, M. B. van der Mark, and H. J. Sterenborg, "Estimation of lipid and water concentrations in scattering media with diffuse optical spectroscopy from 900 to 1600 nm," *Journal of biomedical optics*, vol. 15, no. 3, p. 037015, 2010.

[29] R. Nachabé, B. H. Hendriks, M. van der Voort, A. E. Desjardins, and H. J. Sterenborg, "Estimation of biological chromophores using diffuse optical spectroscopy: benefit of extending the uv-vis wavelength range to include 1000 to 1600 nm," *Biomedical optics express*, vol. 1, no. 5, pp. 1432–1442, 2010.

[30] T. M. Bydlon, R. Nachabé, N. Ramanujam, H. J. Sterenborg, and B. H. Hendriks, "Chromophore based analyses of steady-state diffuse reflectance spectroscopy: current status and perspectives for clinical adoption," *Journal of biophotonics*, vol. 8, no. 1-2, pp. 9–24, 2015.

[31] B. H. Hendriks, A. J. Balthasar, G. W. Lucassen, M. van der Voort, M. Mueller, V. V. Pully, T. M. Bydlon, C. Reich, A. T. van Keersop, J. Kortsmit, *et al.*, "Nerve detection with optical spectroscopy for regional anesthesia procedures," *Journal of translational medicine*, vol. 13, no. 1, p. 380, 2015.

[32] R. Nachabé, J. W. van der Hoorn, R. van de Molengraaf, R. Lamerichs, J. Pikkemaat, C. F. Sio, B. H. Hendriks, and H. J. Sterenborg, "Validation of interventional fiber optic spectroscopy with mr spectroscopy, mas-nmr spectroscopy, high-performance thin-layer chromatography, and histopathology for accurate hepatic fat quantification," *Investigative radiology*, vol. 47, no. 4, pp. 209–216, 2012.

[33] A. Amelink, D. J. Robinson, and H. J. Sterenborg, "Confidence intervals on fit parameters derived from optical reflectance spectroscopy measurements," *Journal of biomedical optics*, vol. 13, no. 5, p. 054044, 2008.

[34] I. McCarthy, "The physiology of bone blood flow: a review," *JBJS*, vol. 88, no. suppl_3, pp. 4–9, 2006.

[35] M. Brookes, "Blood flow rates in compact and cancellous bone, and bone marrow.," *Journal of anatomy*, vol. 101, no. Pt 3, p. 533, 1967.

[36] E. N. Marieb and K. Hoehn, *Human anatomy & physiology*. Pearson education, 2007.

[37] A. Swamy, G. Burström, J. W. Spliethoff, D. Babic, S. Ruschke, J. M. Racadio, E. Edström, A. Elmi-Terander, J. Dankelman, and B. H. Hendriks, "Validation of diffuse reflectance spectroscopy with magnetic resonance imaging for accurate vertebral bone fat fraction quantification," *Biomedical optics express*, vol. 10, no. 8, pp. 4316–4328, 2019.

[38] W. Zijlstra, A. Buursma, and W. Meeuwsen-Van der Roest, "Absorption spectra of human fetal and adult oxyhemoglobin, de-oxyhemoglobin, carboxyhemoglobin, and methemoglobin," *Clinical chemistry*, vol. 37, no. 9, pp. 1633–1638, 1991.

[39] M. Buchan and G. Anderson, "Time since death: a review of the current status of methods used in the later postmortem interval," *Canadian Society of Forensic Science Journal*, vol. 34, no. 1, pp. 1–22, 2001.

[40] S. Bhattarai and J. P. Nielsen, "Association between hematological status at weaning and weight gain post-weaning in piglets," *Livestock Science*, vol. 182, pp. 64–68, 2015.

[41] C. Bolger, M. O. Kelleher, L. McEvoy, M. Brayda-Bruno, A. Kaelin, J.-Y. Lazennec, J.-C. Le Huec, C. Logroscino, P. Mata, P. Moreta, *et al.*, "Electrical conductivity measurement: a new technique to detect iatrogenic initial pedicle perforation," *European Spine Journal*, vol. 16, no. 11, pp. 1919–1924, 2007.

7

GENERAL DISCUSSION

In this thesis we have described the results of various preclinical studies in order to evaluate the application of Diffuse Reflectance Spectroscopy (DRS) for the detection of cortical breaches during spinal screw fixation procedures. We integrated the DRS technique into the instruments used by spine surgeons within the current clinical workflow. We also described the challenges faced, scope for improvements and future research directions.

In the **Chapter 1** we validated the clinical need for spinal instrumentation such as screws and rods to maintain spinal stability and ensure faster recovery time after surgical treatment of various spinal disorders. The challenges associated with the free-hand technique for screw fixation are highlighted. Due to the complex spinal anatomy, the procedure is known to be technically demanding with a long learning curve. Adding to the complexity of these procedures is the rise in minimally invasive approaches as reduced surgical site exposure offers several benefits to the patient such as shorter hospital stays and faster recovery times. The technically demanding nature of the procedure is reflected in literature in terms of high accuracy variability in screw placement. The risk of neurological complications associated with pedicle screw fixation is rare albeit, as serious as paraplegia and death. Moreover, malpositioned screws without clinical symptoms can cause screw loosening leading to improper fusion which could result in spinal instability. In the worst case scenario, a revision surgery might become necessary.

In order to tackle these challenges and prevent adverse patient outcomes, several imaging and non-imaging based guidance devices and systems have been developed and entered the clinical setting. These technological advances have been able to improve screw placement accuracy but often at the expense of high radiation exposure especially to the surgeon or high costs associated with purchase, installation and servicing of such systems. However, it also important to note that high acquisition and maintenance costs of such imaging-based technologies can be offset by equally high reoperation costs due to symptomatic misplaced screws. Thus, cost-effectiveness of such advanced imaging-based technologies increases especially when such surgeries are performed in high numbers [1].

PediGuard® probe seems to be one of the promising non-imaging based cost-effective solutions that is under clinical use. However, the sensitivity of the device is known to be affected by applied pressure changes, resulting in difficulties while interpreting the breach detection signal by the surgeon.

To this end, DRS is proposed as a potential alternative technique for intraoperative breach detection and pedicle screw guidance due to its capability of spectral acquisition and visualization within a second which allows for intraoperative decision making. Morever, its relatively simple optical components and the small diameters associated with the optical fibers, makes the technique readily integratable into existing surgical tools and workflows. It is known that several screws are placed per patient and multiple verification steps are required before a screw is safely fixated. The DRS technique could potentially help shorten the workflow by avoiding these additional screw verification steps while maintaining or improving patient safety. Moreover, the use of harmless non-ionising radiation belonging to the visible and near-infrared wavelength range makes the technique safe in the clinical environment.

In the **Chapter 2** we studied the possibility of DRS for breach detection by investigating the spectral and physiological differences between cancellous and cortical bone within a 400-1600 nm wavelength window. Optical properties of cancellous and cortical bone for breach detection were first determined by performing surface measurements of the bone types on vertebral cross-sections via visual inspection. It was shown that blood, fat and photon scattering were significantly different between the tissue types. However, significant variation of these properties were found within the vertebral body of cancellous bone indicating the heterogeneous nature of the tissue. Cortical bone thickness was also calculated and found in the median range of 1.5 - 2.8 mm. Previous studies which used CT-imaging to measure the cortical thickness confirmed our findings [2, 3]. However, Ritzel et al. [4] used a bone staining approach, found a lower range (0.15-0.40 mm) of cortical thickness. The discrepancy is most likely related to the specimen preparation and the staining approach. Moreover, the group found a 15% decrease in cortical thickness in the osteoporotic group as compared to the control group. Thus, the effect on cortical bone boundary thickness due to degenerative and other bone related diseases cannot be ignored.

A Monte-Carlo simulation was then performed in order to simulate an optical probe penetrating through different layers of tissue by reducing the thickness in steps. A drop in fat content of more than 1 mm before the optical probe came in contact with the cortical boundary was found. A turn by turn insertion of a custom-built optical screw probe into a cadaveric vertebra showed a similar drop indicating the possibility of breach detection and anticipation. However, higher variation and a more gradual drop in the fat signal was found as the image-guided optical probe approached the cortical bone boundary which can be linked to the heterogeneous nature of cancellous bone.

In order to better understand this variation in the fat signal during cancellous bone penetration, diffuse reflectance based fat fraction (DRFF) was first compared to proton density fat fraction (PDFF) measured via the MRI technique in **Chapter 3**. This was performed since MRI is one of the most common techniques used to quantitatively assess fat concentration in vertebral tissues. DRFF measurements were invasively determined by inserting an optical screw probe into the cancellous bone of the vertebral body. These

values were found to be highly correlated (P = 0.960) to the PDFF values determined non-invasively via the MRI technique.

Given that DRS and MRI techniques showed good agreement in fat fraction measurements, insights were drawn about the fat fraction distributions from MRI literature. Published *in vivo* human studies show that the PDFF variation within the vertebral body depends upon age, gender, vertebral level and diseases. Moreover, variation in PDFF between two patient cohorts that undergo spinal fusion surgery (older adults and adolescents) also exists. Thus, the DRS technique would have to accommodate for such variation in fat fraction in order for it to be used as a reliable breach detection tool.

In **Chapter 4**, this variation of fat fraction is further investigated across the spinal column by defining zones within the vertebrae in the MR images of the six cadavers. Also, in order to further study the drop in fat fraction between cancellous and cortical bone boundary, an additional zone was defined namely the pre-cortical zone (PCZ) in consultation with physicians. Results showed that the PDFF distribution of the cortical bone boundary was lower than that of cancellous bone across cervical to lumbar vertebral levels, barring a few exceptions. Moreover, the aggregate PDFF distributions of the various zones for the six cadavers showed a gradual drop in median PDFF from cancellous, PCZ and towards cortical bone boundary. However, a large spread in the distributions were observed. One of the cadavers (Cadaver5) showed unusually low PDFF across the spinal column. This cadaver was known to previously suffer from a malignant neoplasm of the esophagus thus making it an unlikely candidate for spinal fusion. The other outliers can also be attributed to altered anatomy due to underlying malignancies within specific vertebrae. The most common cohort that undergo spinal fusion surgery are the older adults who often suffer from various degenerative disorders which make them susceptible to bone-related diseases. Hence, these comorbidities and their relationship to fat fraction as a breach detection signal cannot be ignored and must be further investigated in future studies.

The image guided insertion performed using the optical screw probe with integrated optical fibers in **Chapter 2** was further investigated in **Chapter 5** by performing various clinically relevant breach scenarios. A total of 45 pedicle screw breaches were performed and categorised as anterior, inferior, medial and lateral based on the direction of the breach relative to the location of cortical bone boundary. Moreover, the PCZ between cancellous and cortical bone was given special interest since its detection would warn the surgeon of an impending breach. In all breach scenarios a drop in fat fraction from cancellous bone to PCZ and cortical bone boundary was found. After breaching a sharp rise in fat fraction for all breach scenarios was observed except in case of a medial breach. The aggregated dataset showed a statistically significant drop in fat fraction between all consecutive tissues ($p<0.01$). In addition to fat fraction, collagen content was also computed using the fitting model. It was found that the collagen content increased from cancellous to PCZ and continued to remain high during the transition to cortical bone in all breach scenarios. Moreover, the collagen distribution of PCZ showed dichotomous behavior with its binomially distributed peaks correlating well with either cancellous or cortical bone (see Figure 5.7a).

The annotated dataset was also used to train a support vector machine (SVM) classification model in order to classify cancellous from cortical bone. The model achieved a

sensitivity, specificity and accuracy of 98.1%,98.9% and 98.7% respectively, when using fat fraction and collagen content as inputs. Moreover, a Leave One Out (LOO) cross validation method was also applied to further test the reliability of the SVM model. The LOO method confirmed the high discriminatory power of fat fraction and collagen in classifying the two bone types and thereby in detecting breaches. However, it is important to note that for intra-operative breach detection and decision making, tissue classification would have to be performed in real-time. This poses several additional challenges that might have an impact on the reliability of the model. For example, in **Chapter 3** it was found that the variation of fat fraction in vertebral bones is a function of patient parameters such as a age, gender, vertebral levels and diseases. Given that fat fraction is one of the strongest discriminatory parameters, a training dataset based on patient parameters such as age, gender, vertebral levels and diseases might be necessary. Thereby, with every new patient case, the classification model can be trained on the appropriate patient parameters thereby maximizing the reliability of breach detection.

A breach scenario that must be given special attention is when the direction of the probe is parallel to the cortical bone boundary. In such a breach scenario, there is a low probability of a forward-looking DRS probe to detect the cortical border parallel to its path. A screw with a larger diameter following such a trajectory might lead to the perforation of the spinal canal leading to a risk of neural injury. In order to reliabily detect such breaches, developing a sideways-looking probe might be a way forward as demonstrated previously [5, 6].

Another challenge of intraoperative breach detection is related to the risk of misclassification during varying probe handling conditions in a clinically applicable *in vivo* setting where blood perfusion becomes apparent unlike previous *ex vivo* investigations. In **Chapter 6**, an *in vivo* porcine model was used to study the effect of tissue perfusion and probe handling conditions on the reliability of fat fraction measurements. Moreover, a minimally invasive workflow was adopted by introducing a Jamshidi needle through a skin incision under image guidance. The Jamshidi needle was guided by DRS sensing at the tip of a K-wire with integrated optical fibers. During an anterior breach scenario, a similar drop in fat fraction was observed as seen in previous chapters even within perfused vertebra. Moreover, fat fraction measurements were not affected by low and high probe pressure changes as compared to blood content. This finding was further validated by the high confidence in estimation of the fat fraction values indicated by the narrow range of 95% confidence intervals [1.5-3.2]%.

Additionally, retraction of the probe showed a significant increase in blood content and a decrease in fat fraction which was an intuitive finding linked to the formation of a blood pool upon retraction. This dependence of blood content and fat fraction can be clinically relevant as it provides an indication of the directionality of the probe during an insertion. However, it is highly likely that this indication of directionality will not be able to guide the surgeon towards the correct screw trajectory. The surgeon would have to rely on his/her experience and/or use imaging to plan the next steps for accurate screw placement and confirmation.

Feedback from the clinically adopted electrical conductivity based device (PediGuard® probe [7]) is known to be susceptible to these probe handling changes [8]. These effects on signal quality due to probe handling conditions such as during the re-

traction of the probe can be most likely attributed to the filling of blood around the probe tip. Thus, resulting in increase in local electrical conductivity measured by the device even when the probe is in cancellous bone. We demonstrate that using the DRS technique these changes can be detected. The surgeon can thus be warned during insufficient probe contact pressure thereby mitigating the risks of misclassification and false alarms. Therefore, the use of the visible wavelength window range in quantifying blood content seems valuable as it serve as an additional independent parameter reflecting the locally probed tissue composition. This information can thereby be used to maintain or improve the reliability of the intraoperative breach detection algorithm.

Another aspect to consider while using the DRS determined physiological parameters for breach detection is the assumptions made in Farrell model which was adopted to calculate fat, water, blood, collagen and photon scattering from spectra. The model holds when the reduced scattering is greater than the absorption. Also the fiber-to-fiber distance should be greater than scattering length. Morever, the tissue medium should be homogeneous [9]. The latter assumption is most likely to be violated especially when the DRS probe is in cancellous bone. These assumptions contribute towards the signal to noise ratio of the physiological parameters. However, given that the DRS determined fat fraction measurements correlated well with MRI measurements in cancellous bone (**Chapter 3**), model validity does not seem to be effected.

7.1. FUTURE PERSPECTIVE

Overall, the preclinical studies described in this thesis have demonstrated that the DRS technique has the potential to be used for intraoperative breach detection and thereby reduce the risk of malpositioned instrumentation. However, for it to be a cost-effective, clinically adoptable solution, several additional challenges need to be addressed. The hardware components such as the optical spectrometers, light source and the computer interface for processing and spectral visualization have a relatively large size. These components should be miniaturized as much as possible, ideally fitting into the handle of screw probe or the Jamshidi needle. It is expected that the reduction in the size of these components might have an effect on the quality of the DRS spectra and thereby on the physiological parameters derived. Thus, future studies should find a trade-off between the optimal wavelength detection window and size of the components desired.

Moreover, the type of feedback or alarm should be designed such that the cognitive load to the surgeon for intraoperative decision making during a breach scenario is minimized. In other words, the alarm or feedback should be easily understandable and actionable. An important reason behind the PediGuard® probe in being clinically adopted can be attributed to its seamless integration into the clinical workflow due to its small size while maintaining accuracy of breach detection [10]. The DRS-probe also has the potential to be a useful stand-alone aid in developing countries especially in low-resource setting environments where advanced technical equipment is scarce and unaffordable.

Other possible areas where DRS could add value is by improving the accuracy of existing 3D computer assisted navigation and robotics technologies [11–14]. Since navigation and robotics help improve instrument path planning and spatial orientation, DRS sensing at the tip of the surgical instruments could serve as an adjunct to these technolo-

gies by providing a warning when there is a tissue change. Such technological advances have the potential to increase MIS workflow adoptions.

In order to further understand the effects of degenerative conditions such as osteoporosis and other diseases on breach transition profiles, development of a bone phantom might be necessary. This might require a physical model development consisting of the organic blood, fat, water and collagen within an inorganic hydroxyapatite matrix. An alternative approach might be to simulate such a bone phantom in a Monte-Carlo model by incorporating the heterogeneity within cancellous bone. Burying fat and blood optical properties into the inorganic trabecular structure derived from microCT data might be a way forward. Initial studies in this direction by previous groups can provide a start point [15–17]. Another resource comes from Dominik and his group [18], who have further improved the Monte-Carlo model of Wang et al.[19] by creating an open-source model that has the capability of building 3D layers along with photon path tracing and visualization.

An analytical model was used in this thesis to describe light transport in tissues based on diffusion theory and *a priori* knowledge of chromophores present in vertebral bones [9, 20]. This approach allowed us to directly extract meaningful physiological parameters such as blood and fat from the probed tissue volume. The high interpretability of the signals allowed us to gather insights even with limited data. However, as more spectral data becomes available using advanced empirical approaches of feature extraction such as reinforcement learning and artificial neural networks might help uncover new features for breach detection.

In this thesis, the DRS sensing was integrated into an optical screw probe used in an open surgical workflow as well as into a K-wire used in a minimally invasive workflow. Identification of which of the existing surgical tools and workflows would most benefit from spectral sensing using DRS should be further carried out by conducting more detailed surgical workflow analysis and gathering clinical feedback. Furthermore, the influence of instrument feed rate and DRS sampling frequency on the breach detection signals is also currently being investigated.

REFERENCES

[1] N. Dea, C. G. Fisher, J. Batke, J. Strelzow, D. Mendelsohn, S. J. Paquette, B. K. Kwon, M. D. Boyd, M. F. Dvorak, and J. T. Street, "Economic evaluation comparing intraoperative cone beam ct-based navigation and conventional fluoroscopy for the placement of spinal pedicle screws: a patient-level data cost-effectiveness analysis," *The Spine Journal*, vol. 16, no. 1, pp. 23–31, 2016.

[2] M. Yusof, L. Ming, and M. Abdullah, "Computed tomographic measurement of cervical pedicles for transpedicular fixation in a malay population," *Journal of Orthopaedic Surgery*, vol. 15, no. 2, pp. 187–190, 2007.

[3] P. Chanplakorn, C. Kraiwattanapong, K. Aroonjarattham, P. Leelapattana, G. Keorochana, S. Jaovisidha, and W. Wajanavisit, "Morphometric evaluation of subaxial cervical spine using multi-detector computerized tomography (md-ct) scan: the consideration for cervical pedicle screws fixation," *BMC musculoskeletal disorders*, vol. 15, no. 1, p. 125, 2014.

[4] H. Ritzel, M. Amling, M. Pösl, M. Hahn, and G. Delling, "The thickness of human vertebral cortical bone and its changes in aging and osteoporosis: A histomorphometric analysis of the complete spinal column from thirty-seven autopsy specimens," *Journal of Bone and Mineral Research*, vol. 12, no. 1, pp. 89–95, 1997.

[5] U. Utzinger and R. R. Richards-Kortum, "Fiber optic probes for biomedical optical spectroscopy," *Journal of Biomedical Optics*, vol. 8, no. 1, pp. 121–148, 2003.

[6] C. Reich, B. H. W. Hendriks, W. C. J. Bierhoff, T. M. Bydlon, V. Parthasarathy, S. Stoffelen, and F. M. A. M. Van Gaal, "Side-looking lung biopsy device," Sept. 10 2019. US Patent 10,405,838.

[7] M. Senn, *DSG Technology*, (accessed May, 2020). https://www.spineguard.com/dynamic-surgical-guidance-technology/.

[8] P. T. Guillen, R. G. KnoPPeR, J. KRoGeR, N. D. Wycliffe, O. A. Danisa, and W. K. Cheng, "Independent assessment of a new pedicle probe and its ability to detect pedicle breach: a cadaveric study," *Journal of Neurosurgery: Spine*, vol. 21, no. 5, pp. 821–825, 2014.

[9] R. Nachabe, B. H. Hendriks, A. E. Desjardins, M. van der Voort, M. B. van der Mark, and H. J. Sterenborg, "Estimation of lipid and water concentrations in scattering media with diffuse optical spectroscopy from 900 to 1600 nm," *Journal of biomedical optics*, vol. 15, no. 3, p. 037015, 2010.

[10] D. Dixon, B. Darden, J. Casamitjana, K. A. Weissmann, S. Cristobal, D. Powell, and D. Baluch, "Accuracy of a dynamic surgical guidance probe for screw insertion in the cervical spine: a cadaveric study," *European Spine Journal*, vol. 26, no. 4, pp. 1149–1153, 2017.

[11] G. Burström, R. Nachabe, O. Persson, E. Edström, and A. E. Terander, "Augmented and virtual reality instrument tracking for minimally invasive spine surgery: a feasibility and accuracy study," *Spine*, vol. 44, no. 15, pp. 1097–1104, 2019.

[12] M. J. Tormenti, D. B. Kostov, P. A. Gardner, A. S. Kanter, R. M. Spiro, and D. O. Okonkwo, "Intraoperative computed tomography image–guided navigation for posterior thoracolumbar spinal instrumentation in spinal deformity surgery," *Neurosurgical focus*, vol. 28, no. 3, p. E11, 2010.

[13] A. Elmi-Terander, G. Burström, R. Nachabe, H. Skulason, K. Pedersen, M. Fagerlund, F. Ståhl, A. Charalampidis, M. Söderman, S. Holmin, *et al.*, "Pedicle screw placement using augmented reality surgical navigation with intraoperative 3d imaging: a first in-human prospective cohort study," *Spine*, vol. 44, no. 7, p. 517, 2019.

[14] D. P. Devito, L. Kaplan, R. Dietl, M. Pfeiffer, D. Horne, B. Silberstein, M. Hardenbrook, G. Kiriyanthan, Y. Barzilay, A. Bruskin, *et al.*, "Clinical acceptance and accuracy assessment of spinal implants guided with spineassist surgical robot: retrospective study," *Spine*, vol. 35, no. 24, pp. 2109–2115, 2010.

[15] E. Margallo-Balbás and P. J. French, "Shape based monte carlo code for light transport in complex heterogeneous tissues," *Optics express*, vol. 15, no. 21, pp. 14086–14098, 2007.

[16] L. V. Wang, R. E. Nordquist, and W. R. Chen, "Optimal beam size for light delivery to absorption-enhanced tumors buried in biological tissues and effect of multiple-beam delivery: a monte carlo study," *Applied optics*, vol. 36, no. 31, pp. 8286–8291, 1997.

[17] G. W. Lucassen, W. Verkruysse, M. Keijzer, and M. J. van Gemert, "Light distributions in a port wine stain model containing multiple cylindrical and curved blood vessels," *Lasers in Surgery and Medicine: The Official Journal of the American Society for Laser Medicine and Surgery*, vol. 18, no. 4, pp. 345–357, 1996.

[18] D. Marti, R. N. Aasbjerg, P. E. Andersen, and A. K. Hansen, "Mcmatlab: an open-source, user-friendly, matlab-integrated three-dimensional monte carlo light transport solver with heat diffusion and tissue damage," *Journal of biomedical optics*, vol. 23, no. 12, p. 121622, 2018.

[19] L. Wang, S. L. Jacques, and L. Zheng, "Mcml—monte carlo modeling of light transport in multi-layered tissues," *Computer methods and programs in biomedicine*, vol. 47, no. 2, pp. 131–146, 1995.

[20] T. J. Farrell, M. S. Patterson, and B. Wilson, "A diffusion theory model of spatially resolved, steady-state diffuse reflectance for the noninvasive determination of tissue optical properties in vivo," *Medical physics*, vol. 19, no. 4, pp. 879–888, 1992.

ACKNOWLEDGEMENTS

First and foremost i would like to thank my promotors Prof. Benno Hendriks and Prof. Jenny Dankelman for their valuable support and feedback all these years. It was a great pleasure knowing and working with you Benno. You introduced me to the fascinating world of tissue optics and its application in spine surgery. Apart from your scientific bent of mind, I always admired your work ethic and calm approach to pressure situations. As my daily supervisor, you made it a point to find time for me. You gave me freedom and responsibility when required. Conducting experiments with you at Philips, Radbound and Cincinnati Children's hospital was a challenging but an exciting learning experience. Your scientific yet pragmatic approach to problem solving gave me a direction during my PhD work which was driven by your passion for bringing the potential of Diffuse Reflectance Spectroscopy (DRS) to clinical practice. I thank you again for your valuable guidance and support throughout these years.

Jenny, I still remember the day I walked into your office during the first year of my Master studies looking for new projects for my thesis. You laid the first seed in my PhD journey by putting me in touch with Benno. I deeply appreciate your constant support and patience with me all these years. Apart from giving me valuable feedback and guidance with respect to the scientific process of my work, you helped me immensely in overcoming hurdles and challenges during my studies. Despite your busy schedule, you always maintained an open door culture and provided a welcoming environment for sharing updates. I would like to extend my sincere thanks to you for showing your patience with me. I hope we can continue to collaborate in the near future.

My PhD project would not have materialized without the support of my manager at Philips research namely, Dr. Michel Van Bruggen. All these years you continued to provide guidance and mentorship. I always looked forward to our meetings. You took the time to think along with me while providing critical feedback. You always made me feel part of your group at Philips. I also enjoyed the group outings which made me feel like home in Eindhoven. Thank you for continuing to believe in me and supporting me all these years.

Dear Dr. Drazenko Babic, your influence on my thinking especially during the initial years has been instrumental in my PhD project. Together with Benno, you conceived the idea, which led to the first experiment in Cincinnati investigating the possibility of applying the DRS technique for spine applications. You taught me how to think from a clinical perspective. Our coffee corner discussions at the High Tech Campus were always stimulating and led me in taking a broader perspective on my PhD project. I always considered you as a mentor and will continue to do so in the future.

To my Karolinska Institute colleagues Dr. Adrian Elmi-Terander, Dr. Gustav Burström and Dr. Erik Edström, working with you was a privilege as it brought the important clinical perspective of the end user, the surgeon, into my PhD project. Your clinical feedback and involvement helped improve the quality and relevance of the work immensely.

I want to thank the members of my PhD committee Prof. Dick Sterenborg, Prof. Theo Ruers, Prof. Sjoerd Stallinga, Prof. Ronald Dekker for their valuable time and effort devoted to reviewing this thesis.

Thank you Dr. John Racadio, Nicole Hilvert and all other Cincinnati Children's hospital colleagues that made it possible for us to conduct all the crucial pre-clinical studies. John, your kind hospitality at Cincinnati was much appreciated.

I sincerely thank Dr. Stefan Ruschke and Dr. Diana Lindquist for your contribution and expert advice during the data acquisition process of quanititative MR images.

Thanks Jarich for guiding me in my PhD journey. It was a pleasure working with you. You have been instrumental in shaping my research work. Right from all the technical discussions, planning and performing DRS experiments to manuscript reviewing. The long days in the Cincinnati hospital lab working tirelessly to get everything right and to get the data we needed was one of most interesting and challenging time of my project. The shared experiences together with our Philips, Karolinska and Cincinnati colleagues over beers only made things even more special.

To Joanneke, Henk, Gerald, Frank, Christian and all other Philips colleagues I have worked with over the years, it was a pleasure working with you all. Special thanks to Wilma for patiently dealing with my administrative requests and for regularly correcting my Dutch.

Marco, my dear friend and desk mate. As you already know, I consider you as part of my family in Eindhoven. Having your constant support has been of great value. Another PhD colleague who I cannot thank enough is my dear friend Saskia. You have always patiently helped me throughout my PhD journey whether it is debugging code or help with the scientific writing process. The board game nights and making Hutspot together during cold winter days made everything feel better. I would also like to thank the PhD and intern community at Philips for hosting technical events, lunches and post work meet-ups. I especially enjoyed the after lunch walks with you all around the beautiful High Tech Campus in Eindhoven.

My colleagues at the TU Delft played a valuable role in my PhD journey as well. Thanks Karen for always being there as a friend right from our Master's days. Thanks you Dr. Dimitra Dodou, Sara, Ingmar, Costanza and Merle for the stimulating discussions and support.

I would also like to thank the Master and Bachelor students while being involved in guiding their graduation projects. Matthijs, Floris, Bram, Karel, Pim, Joram and Teun. It was an energizing experience working with you all.

Lastly, I would like to thank my family. My brother has been my mentor from the very beginning of my school days always guiding me through life. Dear Tuabhya, your strong engineering and scientific mind-set has always inspired me. Thanks ma and dad for your unconditional love and support. I am extremely grateful to have you both behind me through thick and thin.

Curriculum Vitæ

Akash Swamy was born on the 28th of January 1992 in Bangalore, India. He completed his schooling at several different cities across India. After graduating high school in 2010, Akash moved to a university town of Manipal to study Mechanical Engineering at the Manipal Institute of Technology. While pursuing his bachelor studies, he encountered a hospital across the street where he witnessed a chaotic environment with a large number of people waiting to be treated for various illnesses. Inspired also by his teacher Dr. Vasanth Kamath and classmate Siddhant Gupta, he developed an interest towards solving engineering challenges in order to improve quality of healthcare provided by care givers. As an extracurricular project, he worked with a physiotherapist to design a prototype serving to help patients with limited lung function. For his bachelor thesis project, he collaborated with a dentist to estimate the fatigue life of dental implants by simulating biting forces on the implants using a finite element modelling method.

Akash obtained his Bachelor's degree in 2014, after which he travelled to Delft, Netherlands to pursue his Masters in Biomedical Engineering within the Medical Instruments and Bio-Inspired design group. In the 2nd year, he travelled to Eindhoven to pursue his internship at Philips research and wrote his master thesis focusing on applying an optical-based tissue sensing technique namely Diffuse Reflectance Spectroscopy (DRS) in order to detect bone tissue boundaries within vertebrae. Next to his studies, Akash contributed as a member of a volunteer-run local music community in Eindhoven. As a drummer hobbyist, he performed in various live cover bands and jam sessions.

After receiving his Master's degree in 2016, Akash started working as a PhD candidate at the TU Delft. In collaboration with Philips research, he was given the opportunity to expand his research work by focusing on investigating the applicability of DRS for intraoperative instrument guidance and breach detection during pedicle screw placement procedures.

PUBLICATIONS

A. Swamy, Burström G, Spliethoff J.W, Babic D, Reich C, Groen J, Edström E, Elmi-Terander A, Racadio J.M, Dankelman J and Hendriks B.H.W, *Diffuse reflectance spectroscopy, a potential optical sensing technology for the detection of cortical breaches during spinal screw placement*, Journal of Biomedical Optics **24**, 1 (2019).

A. Swamy, Burström G, Spliethoff J.W, Babic D, Ruschke S, Racadio J.M, Edström E, Elmi-Terander A, Dankelman J and Hendriks B.H.W, *Validation of diffuse reflectance spectroscopy with magnetic resonance imaging for accurate vertebral bone fat fraction quantification*, Biomedical Optics Express **10**, 8 (2019).

G Burstrom, Swamy A, Spliethoff J.W, Reich C, Babic D, Hendriks B.H.W, Skulason H, Persson O, Elmi-Terander A and Edström E, *Diffuse reflectance spectroscopy accurately identifies the pre-cortical zone for breach detection during spinal fixation surgery*, Biomedical Optics Express **10**, 11 (2019).

A. Swamy, Spliethoff J.W, Burström G, Babic D, Reich C, Groen J, Edström E, Elmi-Terander A, Racadio J.M, Dankelman J and Hendriks B.H.W, *Diffuse Reflectance Spectroscopy for breach detection during pedicle screw placement: An early stage in vivo investigation in a porcine model.*, Biomedical Engineering OnLine,**19**, 1 (2020).

CONFERENCE CONTRIBUTIONS

A. Swamy, Hendriks B.H.W, Dankelman J, *Intraoperative surgical instrument guidance for spinal screw placement procedures using Diffuse Reflectance Spectroscopy (Oral presentation)*, Advanced Biomedical and Clinical Diagnostic and Surgical Guidance Systems XVIII, International Society for Optics and Photonics, SPIE Photonics West, February 2020, San Francisco, USA.

A. Swamy, Hendriks B.H.W, Dankelman J, *Towards real-time in ivvo intraoperative surgical instrument guidance using Diffuse Reflectance Spectroscopy furing spinal implant placement procedures (Oral presentation)*, The International Society for Medical Innovation and Technology , Nov 2019, Heilbron, Germany.

A. Swamy, Hendriks B.H.W, Dankelman J, *Diffuse reflectance spectroscopy, a potential optical sensing technology for the detection of cortical breaches during spinal screw placement (Oral presentation)*, European Optical Society, October 2018, Delft, The Netherlands.

A. Swamy, Hendriks B.H.W, Dankelman J, *Correlation of fat fraction derived from verte-*

bral bones using Diffuse Reflectance Spectroscopy and Magnetic Resonance Imaging (Poster presentation), Biophotonics summer school, June 2019, Island of Ven, Sweden.

A. Swamy, Hendriks B.H.W, Dankelman J, *in vivo pedicle screw breach detection during spine surgery using diffuse reflectance spectroscopy (Poster presentation)*, Dutch BioPhysics, October 2019, Veldhoven, The Netherlands.